


# A Study of Nine Compact Triply Eclipsing Triples

S. A. Rappaport<sup>1</sup> \*, T. Borkovits<sup>2,3,4,5,6</sup>, R. Gagliano<sup>7</sup>, T. L. Jacobs<sup>8</sup>, A. Tokovinin<sup>9</sup>, T. Mitnyan<sup>3</sup>, R. Komžík<sup>10</sup>, V. B. Kostov<sup>11,12</sup>, B. P. Powell<sup>11</sup>, G. Torres<sup>13</sup>, I. Terentev<sup>14</sup>, M. Omohundro<sup>14</sup>, T. Pribulla<sup>10</sup>, A. Vanderburg<sup>1</sup>, M. H. Kristiansen<sup>15</sup>, D. Latham<sup>13</sup>, H. M. Schwengeler<sup>14</sup>, D. LaCourse<sup>16</sup>, I. B. Bíró<sup>2,3</sup>, I. Csányi<sup>2</sup>, D. R. Czaivalinga<sup>3</sup>, Z. Garai<sup>5,6,10</sup>, A. Pál<sup>4,17</sup>, J. E. Rodriguez<sup>18</sup>, D. J. Stevens<sup>19</sup>

<sup>1</sup> Department of Physics, Kavli Institute for Astrophysics and Space Research, M.I.T., Cambridge, MA 02139, USA

<sup>2</sup> Baja Astronomical Observatory of University of Szeged, H-6500 Baja, Szegedi út, Kt. 766, Hungary

<sup>3</sup> ELKH–SZTE Stellar Astrophysics Research Group, H-6500 Baja, Szegedi út, Kt. 766, Hungary

<sup>4</sup> Konkoly Observatory, Research Centre for Astronomy and Earth Sciences, H-1121 Budapest, Konkoly Thege Miklós út 15-17, Hungary

<sup>5</sup> ELTE Eötvös Loránd University, Gothard Astrophysical Observatory, Szent Imre h. u. 112, 9700 Szombathely, Hungary

<sup>6</sup> MTA-ELTE Exoplanet Research Group, H-9700 Szombathely, Szent Imre h. u. 112, Hungary

<sup>7</sup> Amateur Astronomer, Glendale, AZ 85308

<sup>8</sup> Amateur Astronomer, 12812 SE 69th Place Bellevue, WA 98006, USA

<sup>9</sup> Cerro Tololo Inter-American Observatory | NSF’s NOIRLab, Casilla 603, La Serena, Chile

<sup>10</sup> Astronomical Institute, Slovak Academy of Sciences, 05960 Tatranská Lomnica, Slovakia

<sup>11</sup> NASA Goddard Space Flight Center, 8800 Greenbelt Road, Greenbelt, MD 20771, USA

<sup>12</sup> SETI Institute, 189 Bernardo Avenue, Suite 200, Mountain View, CA 94043, USA

<sup>13</sup> Center for Astrophysics | Harvard & Smithsonian, 60 Garden St., Cambridge, MA 02138, USA

<sup>14</sup> Citizen Scientist, c/o Zooniverse, Dept. of Physics, University of Oxford, Denys Wilkinson Building, Keble Road, Oxford, OX1 3RH, UK

<sup>15</sup> Brorfelde Observatory, Observator Gyldenkernes Vej 7, DK-4340 Tølløse, Denmark

<sup>16</sup> Amateur Astronomer, 7507 52nd Place NE Marysville, WA 98270, USA

<sup>17</sup> Kavli Institute for Astrophysics and Space Research, M.I.T., Cambridge, MA 02139, USA

<sup>18</sup> Department of Physics and Astronomy, Michigan State University, East Lansing, MI 48824, USA

<sup>19</sup> University of Minnesota Duluth, Duluth, MN 55812, USA

Accepted XXX. Received YYY; in original form ZZZ

## ABSTRACT

In this work we report the independent discovery and analysis of nine new compact triply eclipsing triple star systems found with the *TESS* mission: TICs 47151245, 81525800, 99013269, 229785001, 276162169, 280883908, 294803663, 332521671, and 356324779. Each of these nine systems exhibits distinct third-body eclipses where the third (‘tertiary’) star occults the inner eclipsing binary (EB), or vice versa. We utilize a photodynamical analysis of the *TESS* photometry, archival photometric data, *TESS* eclipse timing variations of the EBs, available archival spectral energy distribution curves (SED), and, in some cases, newly acquired radial velocity observations, to solve for the parameters of all three stars, as well as most of the orbital elements. From these analyses we find that the outer orbits of all nine systems are viewed nearly edge on (i.e., within  $\lesssim 4^\circ$ ), and 6 of the systems are coplanar to within  $5^\circ$ ; the others have mutual inclination angles of  $20^\circ$ ,  $41^\circ$ , and possibly  $179^\circ$  (i.e., a retrograde outer orbit). The outer orbital periods range from 47.8 days to 604 days, with eccentricities spanning 0.004 to 0.61. The masses of all 18 EB stars are in the range of  $0.9\text{--}2.6 M_\odot$  and are mostly situated near the main sequence. By contrast, the masses and radii of the tertiary stars range from  $1.4\text{--}2.8 M_\odot$  and  $1.5\text{--}13 R_\odot$ , respectively. We make use of the system parameters from these 9 systems, plus those from a comparable number of compact triply eclipsing triples published previously, to gain some statistical insight into their properties.

**Key words:** binaries:eclipsing – binaries:close – stars:individual: TIC 47151245, TIC 81525800, TIC 99013269, TIC 229785001, TIC 276162169, TIC 280883908, TIC 294803663, TIC 332521671, TIC 356324779

## 1 INTRODUCTION

Triply eclipsing triple star systems have a number of characteristics in common with ordinary eclipsing binaries (EBs),

\* E-mail: sar@mit.edu

but can be far richer astrophysically. For example, detection of a sequential set of one type of outer eclipse, such as the primary outer eclipses, immediately determines the outer orbital period,  $P_{\text{out}}$ . Detection of both types of outer eclipses (primary and secondary) leads to a value of  $e_{\text{out}} \cos \omega_{\text{out}}$  for the outer orbit, by analogy with how this quantity is determined in regular eclipsing binaries (EBs) based on the spacing of the two types of eclipses (Stern 1939). As is the case for an ordinary EB, an eccentric outer triple’s orbit, coupled with an outer inclination angle  $i_{\text{out}} < 90^\circ$ , may allow for only a single eclipse per orbit, typically nearer to periastron. For simple EBs there is also a relation between the eclipse durations and  $e \sin \omega$  (Kopal 1959); while for triples this is much more difficult to apply, but should also hold approximately<sup>1</sup> when averaged over many outer eclipses. In principle, if the radius of the tertiary star,  $R_B$ , is a substantial fraction of the outer semi-major axis,  $a_{\text{out}}$ , then this may result in ellipsoidal light variations (ELVs) raised on the tertiary star. Additionally, the tertiary star may be brought into corotation with the orbit, by analogy with ordinary binaries, in which case starspots can corotate with the outer orbit producing additional periodic modulations. For circular orbits in flat triples (i.e., with zero mutual inclination angle,  $i_{\text{mut}}$ , between the inner EB plane and the outer orbital plane), the eclipse depths are still proportional to the surface brightness of the two stars involved in the eclipses.

Several additional features are also possible in triply eclipsing triples that have no counterpart in ordinary EBs. The very presence of the tertiary star will cause the orbital period of the inner binary to become longer (see, e.g. Rappaport et al. 2013; Borkovits et al. 2015). The time-varying nature of this effect leads to a very useful ‘dynamical delay’ in the eclipse timing of the EB when at least one of the two orbits is eccentric, or if the two orbits are inclined (see, e.g., Borkovits et al. 2011). The presence of the tertiary can cause driven apsidal motion in the inner binary, and will lead to orbital plane precession – at least to the extent that the two planes are not aligned. If the mutual inclination angle,  $i_{\text{mut}}$  is large enough, i.e.,  $\gtrsim 39^\circ$ , this can lead to Zeipel-Lidov-Kozai (ZLK) cycles (von Zeipel 1910; Lidov 1962; Kozai 1962; see also the review by Borkovits (2022) for a discussion of these and other dynamical effects in multi-stellar systems).

Another important way that triply eclipsing triples are astrophysically richer than simple EBs is that the dynamical interactions among the stars, as well as the geometrical information from the inner and outer eclipses, are often sufficient to extract the system masses, radii,  $T_{\text{eff}}$ ’s, and ages with considerable accuracy, as well as the detailed architecture of the orbits (see, e.g., Borkovits et al. 2019a, 2020b, 2022a; Rappaport et al. 2022).

When one of the stars in a binary evolves, it can begin to transfer mass to the other star. The effects of the mass loss on the orbit, and on the mass-losing, as well as the mass-accreting, stars have been widely studied for many decades, and are relatively well understood (Bhattacharya & van den Heuvel 1991; Eggleton 2006; Tauris & van den Heuvel 2023).

In the case of triple systems, if the tertiary star evolves first it will start to transfer mass to the binary. This transfer may be stable or unstable, and the latter might lead to something analogous to a common envelope scenario for binary stars. In the case where one of the EB stars evolves first, any mass ejected from the binary will encounter the tertiary star on its way out of the system. These processes are more varied and more complex than in the binary case, and have received considerable scrutiny over the past decade, in particular (see, e.g., Tauris & van den Heuvel 2014; de Vries et al. 2014; Sabach & Soker 2015; Hillel et al. 2017; Comerford & Izzard 2020; Muñoz et al. 2020; Soker & Bear 2021; Glanz & Perets 2021; Hamers et al. 2022).

The *Kepler* (Borucki et al. 2010), *K2* (Howell et al. 2014), and *TESS* (Ricker et al. 2015) missions, with their long-term, wide field, precision photometry from space, have made it much easier to discover triply eclipsing triple star systems. They are typically identified when an extra, isolated pair of eclipses appears in the lightcurve of an ordinary eclipsing binary, or a long exotically-shaped extra eclipse appears that cannot be produced in a simple binary (see the recent extensive review of Borkovits 2022).

In a number of recent papers (e.g., Kristiansen et al. 2022; Rappaport et al. 2022) we discussed how we have found 52 new triply eclipsing triple systems in the *TESS* data. Of those systems, we were able to find the outer orbital period of 20 of them using archival ground-based photometry.<sup>2</sup> In Rappaport et al. (2022) we reported on six of these triply eclipsing triples, and provided a full set of stellar and orbital parameters for each. In this work we report on 9 of the remaining systems.

In Section 2 we discuss how the third body events are discovered in *TESS* data, and we present plots of the third body events with fitted models. We mention in Section 3 other contemporaneous detections of the triple-nature of a number of the nine systems which are studied in this work. In Section 4 we discuss fits to the archival spectral energy distributions (SED) and make first estimates of the stellar properties – masses, radii, and effective temperatures. In Section 5 we demonstrate how archival photometric data from a number of ground-based surveys were utilized to determine the outer orbital period of most of the triples via the detection of third-body eclipses. We discuss in Section 6 several sources of input to the system analysis other than the *TESS* photometry, archival photometry, and SED curves. The detailed photodynamical model by which we jointly analyze the photometric lightcurves, eclipse timing variations, and spectral energy distributions, is reviewed in Section 7. Tables of system parameters, including extracted masses, radii, and effective temperatures, as well as the orbital parameters for both the inner and outer orbits, are given in Section 8 for each of the nine triple systems. We summarize our results in Section 9 where we also discuss some of the more important findings from this and some of our recent related studies of triply eclipsing triples.

<sup>1</sup> Use of the word “approximately” in this context acknowledges the fact that the exact shape and duration of outer eclipses do not repeat precisely due to the fact that these depend on the phasing of the inner binary at the times of the outer conjunctions.

<sup>2</sup> Discovering one outer eclipse with *TESS*, or even two of them separated by a couple of years, is insufficient to determine the outer period.

## 2 DISCOVERY OF TRIPLY ECLIPSING TRIPLES WITH *TESS*

Our ‘Visual Survey Group’ (VSG; Kristiansen et al. 2022) has continued its search for multi-stellar systems in the *TESS* photometric lightcurves. Thus far, we estimate that we have visually surveyed about 9 million lightcurves from *TESS* full-frame images (FFI) of anonymous stars down to *TESS* magnitude  $T \lesssim 15$ . In addition, we have also visually inspected somewhat more than 1 million lightcurves of preselected eclipsing binaries. The latter were found in the *TESS* data via machine learning (ML) searches (see Powell et al. 2021) of some 120 million lightcurves in Sectors 1-48 *TESS* FFI lightcurves. We have found that the visual and ML searches (see, e.g., Powell et al. 2021; Kostov et al. 2021, 2022) are an excellent complement to each other. ML is certainly faster, by orders of magnitude, but more limited than the human brain in terms of what unexpected things it can find.

For the bulk of our visual searches, the lightcurves are displayed with Allan Schmitt’s *LcTools* and *LcViewer* software (Schmitt et al. 2019), which allows for an inspection of a typical lightcurve in just few seconds. The 9 million lightcurves of ‘anonymous’ stars came from the following sources: Science Processing Operations Center (SPOC, Jenkins et al. 2016); the Difference Imaging Pipeline (Oelkers & Stassun 2018); the PSF-based Approach to *TESS* High quality data Of Stellar clusters (PATHOS, Nardiello et al. 2019); the Cluster Difference Imaging Photometric Survey (CDIPS, Bouma et al. 2019); the MIT Quick Look Pipeline (QLP, Huang et al. 2020); the *TESS* Image CALibrator Full Frame Images (TICA, Fausnaugh et al. 2020); and the Goddard Space Flight Center (GSFC, see Sect. 2, Powell et al. 2021).

These visual plus ML searches have led to numerous discoveries which are summarized in Kristiansen et al. (2022). Among other things, this has led to a catalog of 97 quadruple star systems (Kostov et al. 2022). We note here, in passing, that about half of the quadruple systems of our catalog were found by visually surveying anonymous FFI lightcurves, while the other half were the result of visual searches through the set of pre-selected EBs (which were themselves found by a ML algorithm).

In our searches for triply eclipsing triples we look for an eclipsing binary lightcurve with an additional extra eclipse that is typically strangely shaped and of longer duration than the EB eclipses, or a rapid succession of isolated eclipses. Once such ‘extra’ eclipses, or ‘third body’ events are found, there is usually very little doubt that they are due to a tertiary star eclipsing the EB or vice versa.

From searches through lightcurves obtained from the first three full years of *TESS* observations, we have found more than 52 of these triply eclipsing triples. Twenty of these 52 systems were found in the set of 9 million ‘anonymous’ FFI lightcurves, while the remaining 32 were found among the sample of only 1 million preselected EB lightcurves. This statistic is discussed in Rappaport et al. (2022).

Of these 52 triply eclipsing triples, we have determined the outer orbital period for 20 of them via a combination of *TESS* and archival ground-based photometry. We have previously reported four of these 20 systems in Borkovits et al. (2020b) and Borkovits et al. (2022a), and six more in Rappaport et al. (2022). One additional triple among the 20 was found to have an unreliable outer period. Here we present the discovery

and analysis of the remaining 9 new triply eclipsing triples from among this set. The TIC numbers and basic cataloged data (e.g., coordinates, magnitudes, distance, etc.) are given in Table 1. The sectors in which they were observed and in which third-body events were found are given in Table 2.

Seven of the nine systems reported in this work were observed only in FFIs from *TESS* with either 30-min or 10-min cadence. The two remaining triples, TICs 99013269 and 276162169 in some particular sectors were also observed in 2-min cadence mode. Segments from the *TESS* lightcurves exhibiting third-body eclipses are shown in Fig. 1 for all nine sources. The sources were observed for a minimum of a single sector for one of the triples and a maximum of 23 sectors for another target (which is near the ecliptic pole), with an average of a few sectors per source. For 5 of the 9 triples only a single third-body eclipse was detected, while at the other extreme 3 and 4 outer eclipses were seen for two other triples. In most cases, even when more than one outer eclipse were detected, they were in *TESS* sectors that were too far apart in time to make a unique determination of the outer period.

Given that the sectors are only approximately a month long, and the outer orbital periods range from 48 to 604 days, it is not surprising that we observed just 16 third body events out of a total of 48 observing sectors. Based on the third-body events detected with *TESS*, (i) we cannot generally determine the outer orbital period from the *TESS* data alone, and (ii) the photodynamical fits to these systems will typically not include both types of outer eclipses (i.e., primary and secondary). Nonetheless, with the use of ground-based archival data, we were able to determine the outer orbital period for 7 of the 9 systems, as well as the parameter  $e_{\text{out}} \cos \omega_{\text{out}}$  (from the relative separations of the outer eclipses) for 5 of the 9 systems.

## 3 OTHER DETECTIONS OF THESE NINE SYSTEMS

Four of the nine systems we report here were noticed previously in the quadruples catalog by Zasche et al. (2022) as triply eclipsing triples and were correctly reported as such. The outer orbital periods were given but no other information about the systems was presented—either the orbital or stellar parameters. These sources are itemized in Table 3 along with the outer periods found by Zasche et al. (2022).

With the release of Gaia DR3 (Babusiaux et al. 2022; Gaia Collaboration 2022) are included about half a million orbits measured by Gaia in a number of difference ways (e.g., astrometric, spectroscopic, eclipsing, etc.). The epochal data on which these orbital determinations were made are not given, nor is any further analysis made of any other system parameters (in particular, the properties of the stars, including the tertiary and those of the inner binary). A check of the Gaia DR3 data set shows that four of the systems we report on have measured orbital parameters, and those are also listed in Table 3. For a fifth system (TIC 332521671) Gaia has a completely different outer period listed for nearby TIC 332521670, and we conclude that this latter binary is unrelated to our triple system.

In the same Table (3) we also preview our final results and list the outer period, eccentricity, and argument of periastron,

**Table 1.** Main properties of the nine triple systems from different catalogs

Parameter	47151245	81525800	99013269	229785001 <sup>†</sup>	276162169	280883908	294803663	332521671	356324779
RA J2000	17:13:43.81	06:09:18.45	20:21:04.69	18:54:44.67	20:13:25.79	04:29:21.01	14:51:09.97	12:00:01.3	04:31:15.65
Dec J2000	-33:04:06.99	27:43:28.55	29:30:38.14	68:46:50.90	32:55:27.06	69:43:12.75	-63:35:08.82	-53:14:15.74	57:45:01.11
$T^a$	10.27 ± 0.02	13.10 ± 0.01	8.90 ± 0.03	11.34 ± 0.01	11.68 ± 0.06	10.26 ± 0.01	11.22 ± 0.02	9.60 ± 0.01	12.68 ± 0.01
$G^b$	10.34 ± 0.00	13.60 ± 0.01	9.55 ± 0.00	11.85 ± 0.01	12.06 ± 0.00	11.01 ± 0.00	12.02 ± 0.00	10.15 ± 0.00	13.01 ± 0.00
$G_{BP}^b$	10.44 ± 0.01	13.99 ± 0.01	10.10 ± 0.00	12.03 ± 0.00	12.39 ± 0.00	11.69 ± 0.00	12.73 ± 0.00	10.58 ± 0.01	13.27 ± 0.00
$G_{RP}^b$	10.15 ± 0.01	13.04 ± 0.01	8.81 ± 0.00	11.27 ± 0.00	11.56 ± 0.00	10.19 ± 0.00	11.18 ± 0.00	9.55 ± 0.00	12.58 ± 0.00
$B^c$	10.50 ± 0.07	14.56 ± 0.17	10.87 ± 0.05	12.63 ± 0.36	12.91 ± 0.14	12.69 ± 0.17	13.59 ± 0.08	11.19 ± 0.07	13.65 ± 0.11
$V^c$	10.33 ± 0.01	13.81 ± 0.17	9.92 ± 0.01	11.95 ± 0.03	12.24 ± 0.09	11.57 ± 0.02	12.62 ± 0.06	10.37 ± 0.01	13.09 ± 0.08
$J^d$	10.00 ± 0.02	12.33 ± 0.02	7.87 ± 0.03	10.83 ± 0.02	10.90 ± 0.02	9.11 ± 0.04	9.92 ± 0.02	8.80 ± 0.02	12.04 ± 0.02
$H^d$	9.96 ± 0.02	12.05 ± 0.02	7.38 ± 0.03	10.56 ± 0.02	10.76 ± 0.02	8.51 ± 0.03	9.33 ± 0.02	8.37 ± 0.04	11.95 ± 0.03
$K^d$	9.88 ± 0.02	11.97 ± 0.02	7.25 ± 0.02	10.50 ± 0.02	10.68 ± 0.02	8.35 ± 0.02	9.14 ± 0.02	8.26 ± 0.03	11.85 ± 0.03
$W1^e$	9.74 ± 0.02	11.97 ± 0.02	7.10 ± 0.05	10.38 ± 0.02	10.68 ± 0.02	8.25 ± 0.02	9.01 ± 0.02	8.19 ± 0.02	11.81 ± 0.02
$W2^e$	9.80 ± 0.02	11.97 ± 0.02	7.22 ± 0.02	10.42 ± 0.02	10.71 ± 0.02	8.33 ± 0.02	9.04 ± 0.02	8.23 ± 0.02	11.84 ± 0.02
$W3^e$	9.72 ± 0.08	11.54 ± NA	7.18 ± 0.02	10.35 ± 0.04	10.90 ± 0.18	8.27 ± 0.02	8.95 ± 0.03	8.16 ± 0.02	11.68 ± 0.24
$W4^e$	7.96 ± 0.31	...	7.17 ± 0.08	...	...	8.43 ± 0.31	...	8.10 ± 0.19	...
$T_{\text{eff}} [K]^b$	8192 ± 275	5374 ± 250	4806 ± 110	6277 ± 1300	5750 ± 180	4402 ± 333	4362 ± 125	5201 ± 110	6362 ± 780
$T_{\text{eff}} [K]^a$	...	6340 ± 124	6249 ± 122	6016 ± NA	9660 ± 900	...	5734 ± 122	5455 ± 123	8379 ± 124
Radius [ $R_{\odot}$ ] <sup>b</sup>	...	4.23 ± 0.35	17.8 ± 0.9	...	5.19 ± 0.36	...	14.3 ± 0.8	7.82 ± 0.67	8.41 ± 2.0
Radius [ $R_{\odot}$ ] <sup>a</sup>	...	3.75 ± NA	16.5 ± NA	1.23 ± NA	4.41 ± 0.20	...	13.5 ± NA	7.67 ± NA	7.36 ± NA
Distance [pc] <sup>f</sup>	1023 ± 20	1979 ± 81	805 ± 31	780 ± 200	1552 ± 25	3072 <sup>+2200</sup> <sub>-900</sub>	1770 ± 55	748 ± 9.5	3245 ± 150
$E(B - V)^a$	0.46 ± 0.02	0.24 ± 0.02	0.45 ± 0.04	...	0.63 ± 0.08	...	0.56 ± 0.02	0.091 ± 0.001	0.41 ± 0.02
$\mu_{\alpha}$ [mas/yr] <sup>b</sup>	-0.35 ± 0.03	-0.55 ± 0.02	-0.37 ± 0.04	-5.33 ± 0.38	-0.44 ± 0.01	+4.31 ± 0.11	-6.05 ± 0.01	-6.66 ± 0.02	0.97 ± 0.02
$\mu_{\delta}$ [mas/yr] <sup>b</sup>	-4.26 ± 0.02	-3.29 ± 0.02	-3.58 ± 0.05	-14.07 ± 0.49	-0.98 ± 0.01	-2.62 ± 0.13	-3.61 ± 0.02	-0.33 ± 0.02	-1.23 ± 0.01
$\text{RUWE}^{b,g}$	0.749	0.957	4.20	29.5	0.916	9.83	1.43	1.13	0.948
$P_{\text{binary}}^h$ [d]	1.202	1.649	6.534	0.929	2.550	5.248	2.246	1.247	3.477
$P_{\text{triple}}^h$ [d]	284.90	47.85	604.05	165.25	117.10	184.35	153.14	48.50	86.65

*Notes.* General: "NA" in this table indicates that the value is not available. (a) *TESS* Input Catalog (TIC v8.2) (Paegert et al. 2021). (b) Gaia EDR3 (Gaia collaboration 2021); the uncertainty in  $T_{\text{eff}}$  and  $R$  listed here is 1.5 times the geometric mean of the upper and lower error bars cited in DR2. Magnitude uncertainties listed as 0.00 are  $\lesssim 0.005$ . (c) AAVSO Photometric All Sky Survey (APASS) DR9, (Henden et al. 2015), <http://vizier.u-strasbg.fr/viz-bin/VizieR?-source=II/336/apass9>. (d) 2MASS catalog (Skrutskie et al. 2006). (e) WISE point source catalog (Cutri et al. 2013). (f) Bailer-Jones et al. (2021). (g) The Gaia Renormalized Unit Weight Error (RUWE) is the square root of the normalized  $\chi^2$  of the astrometric fit to the along-scan observations. Values in excess of about unity are sometimes taken to be a sign of stellar multiplicity. (h) Binary and outer orbital periods from this work; given here for reference purposes. (i) 2+1+1 quadruple.

**Table 2.** *TESS* Observation Sectors for the Triples<sup>a</sup>

Object	Sectors Observed	Third Body Events
TIC 47151245	S12 & S39	S39
TIC 81525800	S43-S45	S43 & S44
TIC 99013269	S14-S15, S41, S55	S41
TIC 229785001	23 sectors in S14-S55	S16, S22, S40 & S52
TIC 276162169	S14-15, S41, S54-S55	S14, S55
TIC 280883908	S25-S26 & S52-S53	S25-S26 & S53
TIC 294803663	S11-S12 & S38-S39	S12
TIC 332521671	S10 & S37	S37
TIC 356324779	S19	S19

*Notes.* (a) At least six of these sources will also be observed in later *TESS* sectors.

for comparison to the Gaia results and the periods found by Zasche et al. (2022).

#### 4 PRELIMINARY SED ANALYSIS

When we first discover a triply eclipsing triple, we make an initial analysis of its composite spectral energy distribution (SED). This provides us with preliminary estimates of the nature of the three stars in the system. We make use of the VizieR (Ochsenbein et al. 2000; A.-C. Simon & T. Boch: <http://vizier.unistra.fr/vizieR/sed/>) SED database which, in turn, utilizes the extensive sky coverage of surveys such as Skymapper (Wolf et al. 2018), Pan-STARRS (Chambers et al. 2016), SDSS (Gunn et al. 1998), 2MASS (Skrutskie et al. 2006), WISE (Cutri et al. 2013), and in some cases Galex (Bianchi et al. 2017). These typically provide ~18-25 flux values over the range 0.12-0.40  $\mu\text{m}$  to 21  $\mu\text{m}$ .

For this initial SED analysis, we assume that the three stars

in the system have evolved in a coeval manner since their formation as a triple system. We also assume that no mass transfer has previously occurred among the three stars, in particular between the binary stars. With these preliminary working hypotheses, there are only four parameters that need to be fitted in a Markov chain Monte Carlo analysis (see, e.g., Ford 2005; Rappaport et al. 2021):  $M_{Aa}$ ,  $M_{Ab}$ ,  $M_B$ , and the age of the system, where  $Aa$  and  $Ab$  denote the stars in the inner binary, while  $B$  refers to the tertiary star in the outer orbit. We utilize *MIST* stellar evolution tracks (Paxton et al. 2011, 2015, 2019; Dotter 2016; Choi et al. 2016) for an assumed solar composition of the three stars<sup>3</sup>, and the stellar atmosphere models from Castelli & Kurucz (2003). If these four parameters can be determined, then we automatically find the stellar radii and effective temperature of all three stars from evolution tracks.

To fit the SED curve, we typically need an accurate distance to the source as well as the corresponding interstellar extinction,  $A_V$ . For typical objects of comparable brightness and distance to those of our 9 systems Gaia (Gaia collaboration 2021) has a cataloged distance with better than 5% accuracy. Information on the extinction to the target can be found from a variety of sources (e.g., Bayestar19; Green et al. 2019). Thus, in principle, it is not necessary to fit for these parameters. However, because the systems we are observing are not single stars, and the Gaia distances may in some cases be adversely affected, we add these two quantities (distance and  $A_V$ ) to the fitted MCMC parameters, but with priors that are limited to  $\approx \pm 4$  times their listed uncertainties.

<sup>3</sup> This particular assumption is for the preliminary SED analysis only. See Sect. 7 for a description of the more comprehensive photodynamical analysis.

**Table 3.** Other Detections of the Triples<sup>a</sup>

Object	This Work <sup>b</sup>	Gaia DR3 Orbits <sup>b,c</sup>	Zasche et al. <sup>b,d</sup>
	( $P_{\text{out}}$ , $e_{\text{out}}$ , $\omega_{\text{out}}$ )	( $P_{\text{out}}$ , $e_{\text{out}}$ , $\omega_{\text{out}}$ )	
TIC 47151245	284.90 d; 0.480; 219°	...	285 d
TIC 81525800	47.85 d; 0.614; 201°	...	...
TIC 99013269	604.05 d; 0.463; 271°	Astr.: 609.5 d; 0.458; ...	...
TIC 229785001	165.25 d; 0.458; 31°	Spect.: 166.0 d; 0.493; 16°	165.3 d
TIC 276162169	117.10 d; 0.268; 243°	...	...
TIC 280883908	184.35 d; 0.260; 146°	Spect.: 184.1 d; 0.258; 142°	...
TIC 294803663	153.14 d; 0.030; 313°	Spect.: 153.1 d; 0.047; 252°	153.1 d
TIC 332521671	48.50 d; 0.004; 311°	...	...
TIC 356324779	86.65 d; 0.284; 144°	...	86.7 d

*Notes.* (a) Six of the nine triply eclipsing systems were spotted in prior broad surveys, but no quantitative analysis of the system parameters (especially of the constituent stars) was undertaken. Four of them have outer orbits reported by Gaia, but no third body eclipses were reported by Gaia. Four of the systems had third body eclipses detected by [Zasche et al. \(2022\)](#), and the outer period could be deduced from those extra eclipses. (b) Where available, we show for each source, the period, eccentricity, and argument of periastron of the outer orbit, separated by semicolons. (c) The Gaia orbital solutions are marked as either astrometric or spectroscopic; [Babusiaux et al. \(2022\)](#); [Gaia Collaboration \(2022\)](#) (d) [Zasche et al. \(2022\)](#).

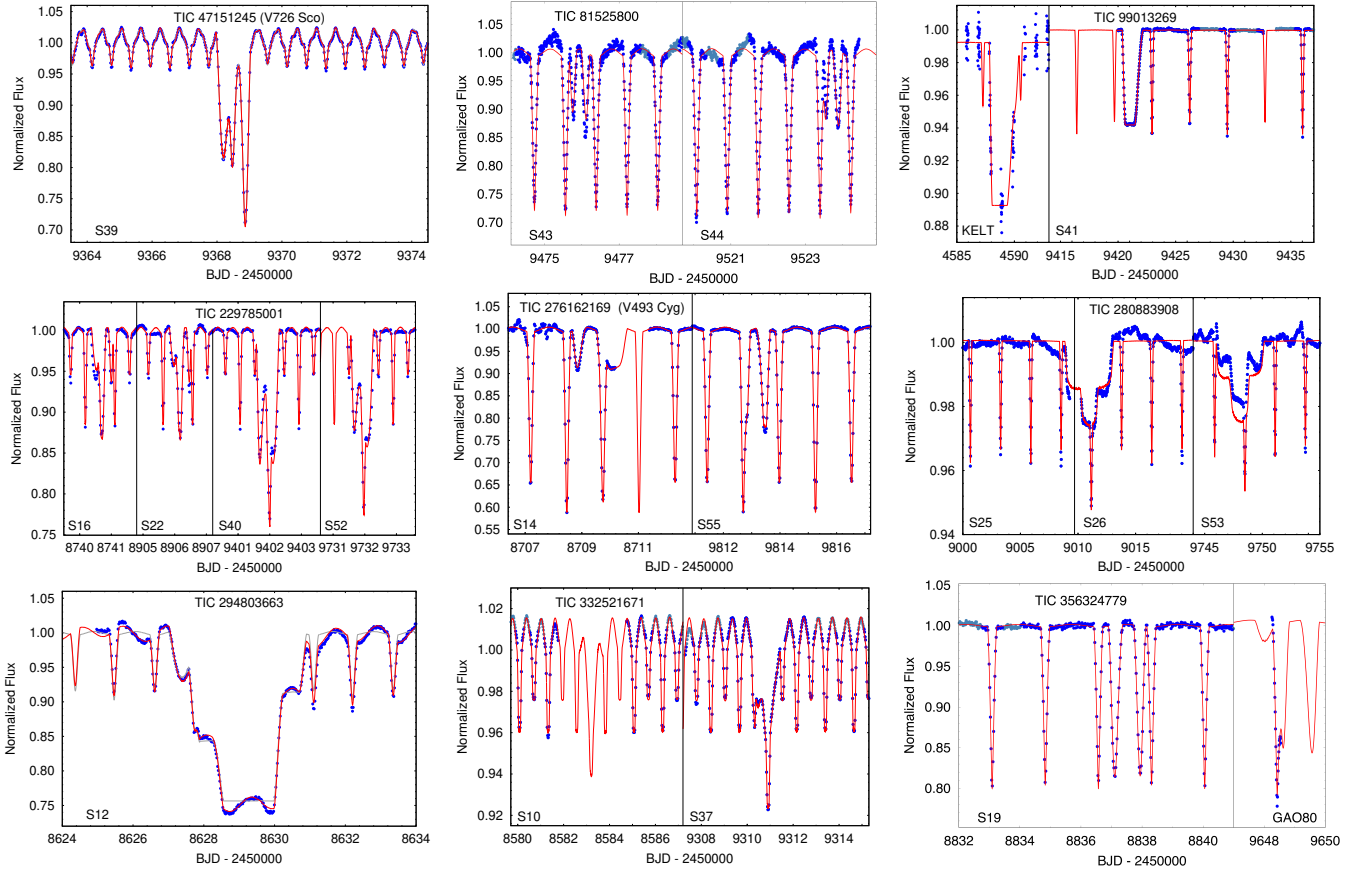


**Figure 1.** *TESS* third body lightcurves. We present a portion of a sector’s lightcurve for each source containing the third body event that led to their discoveries. For most of the sources there is only a single third body event that was detected. The overplotted model lightcurves are discussed in Sect. 7. The lighter blue points in the out-of-eclipse region were omitted from the photodynamical fits to save computation time. Note, in the case of TICs 47151245 and 294803663 the light gray lines represent the pure triple-star model, without the contributions of the stellar oscillations.

Even though we have 18-25 SED data points, and only  $\simeq 6$  MCMC parameters to fit for, that is often insufficient for a robust solution. The reasons include the facts that (i) the wavelength spacing between SED points is too close to have them represent truly independent wavelengths, and (ii) most

SED curves can be fit with a non-physical function containing no more than 4 or 5 parameters which define the characteristic shape. We therefore find it extremely useful to add a number of supplementary constraints in the MCMC fit. For this set of systems, we used five additional constraints. The

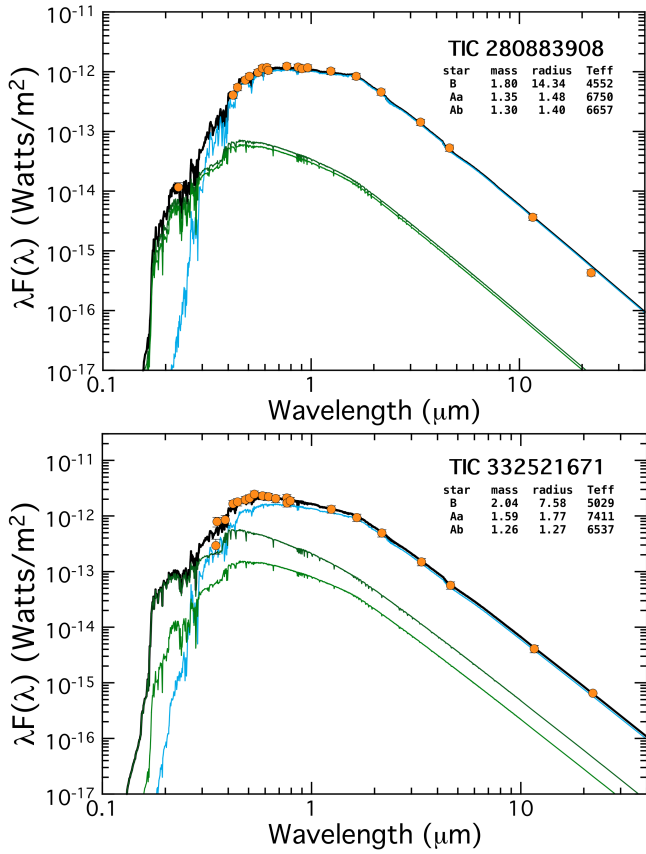


**Figure 2.** SED fits for two triply eclipsing triples of the nine discussed in this work. The cyan curve represents the model spectrum of the tertiary star (B) while the green curves are for the EB stars (Aa and Ab). The sum of the three model spectra is given by the heavy black curve. The fits for the three stellar masses, radii, and  $T_{\text{eff}}$ 's were made using only the measured SED points, and five simple crude constraints enumerated in the text. We make the explicit assumption that the three stars have evolved in a coeval manner without mass transfer.

first three of the following stem from the fact that in most cases, the tertiary star tends to dominate the system light either because (in 4 cases) it is substantially evolved off the main sequence, or because (in 7 of 9 cases) it is the most massive star. In only one case (TIC 276162169) is neither of these true, in which case we forgo the preliminary SED fit. For the other 8 systems we adopt the following: (i)  $M_B > 1.1 M_{Aa}$  and  $> 1.1 M_{Ab}$ , to be certain that the tertiary would be evolved substantially more than the EB stars. (ii)  $R_B$  equals the average of the values given in the *TESS* Input Catalog (TIC v8.2) and by Gaia DR2  $\pm 4\sigma$  of those measurements. (iii) Same as (ii) but for  $T_{\text{eff},B}$ . See Table 1 for the values of  $R_B$  and  $T_{\text{eff},B}$  (from Gaia and the TIC) based on the composite system light. (iv) The temperature ratio of the two EB stars can be estimated approximately from the ratio of their eclipse depths. Finally, (v) we take the luminosity of the primary EB star ( $L_{Aa}$ ) to have a fraction of the system luminosity that is greater than the primary eclipse depth.

With just this basic information, we fit the SED for all the properties of the stars in 8 of our 9 systems. Here, since there are nine of them, and plots of the fits are not highly illu-

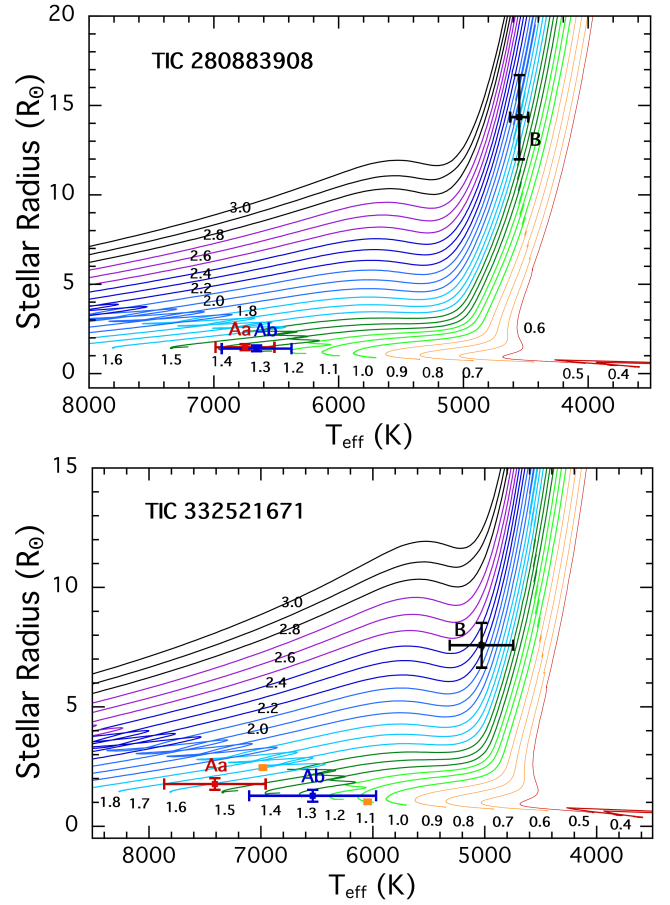


**Figure 3.** The locations of the three stars in two triple systems of the nine in this work, shown superposed on the MIST stellar evolution tracks for stars of solar composition. The numbers next to the tracks are the stellar masses in  $M_{\odot}$ . The locations of the stars in this diagram were taken from the SED fits whose results are given in Fig. 2. More accurate stellar parameters are tabulated in Sect. 7 based on the full photodynamical analyses. The parameters given here for the three stars in TIC 280883908 and for star B in TIC 332521671 are in excellent agreement with those we find from the full photodynamical analysis in Sect. 7. However, stars Aa and Ab in the latter triple are off by about  $1\sigma$  in  $T_{\text{eff}}$  and  $1-3\sigma$  in radius from the more comprehensive analysis (shown with small orange markers), which is not atypical when the constraints are limited.

minating, we show only two illustrative examples—for TIC 280883908 and TIC 332521671 (see Fig. 2). The measured SED points (orange circles) have been corrected for interstellar extinction. The continuous cyan curve represents the model fit for the tertiary while the green curves are for the stars in the EB. The total flux from all three stars is represented by the heavy black curve. For these two triples the tertiary dominates the system light, contributing 91% and 72%, respectively. These first estimates of the stellar parameters provide some very quick insight into what kinds of stars we are working with, and can be utilized as the initial input guesses to the photodynamical analysis (see Sect. 7).

We can also utilize the system parameters for the stars found from this preliminary SED analysis to show the locations of the stars superposed on the MIST evolution tracks.

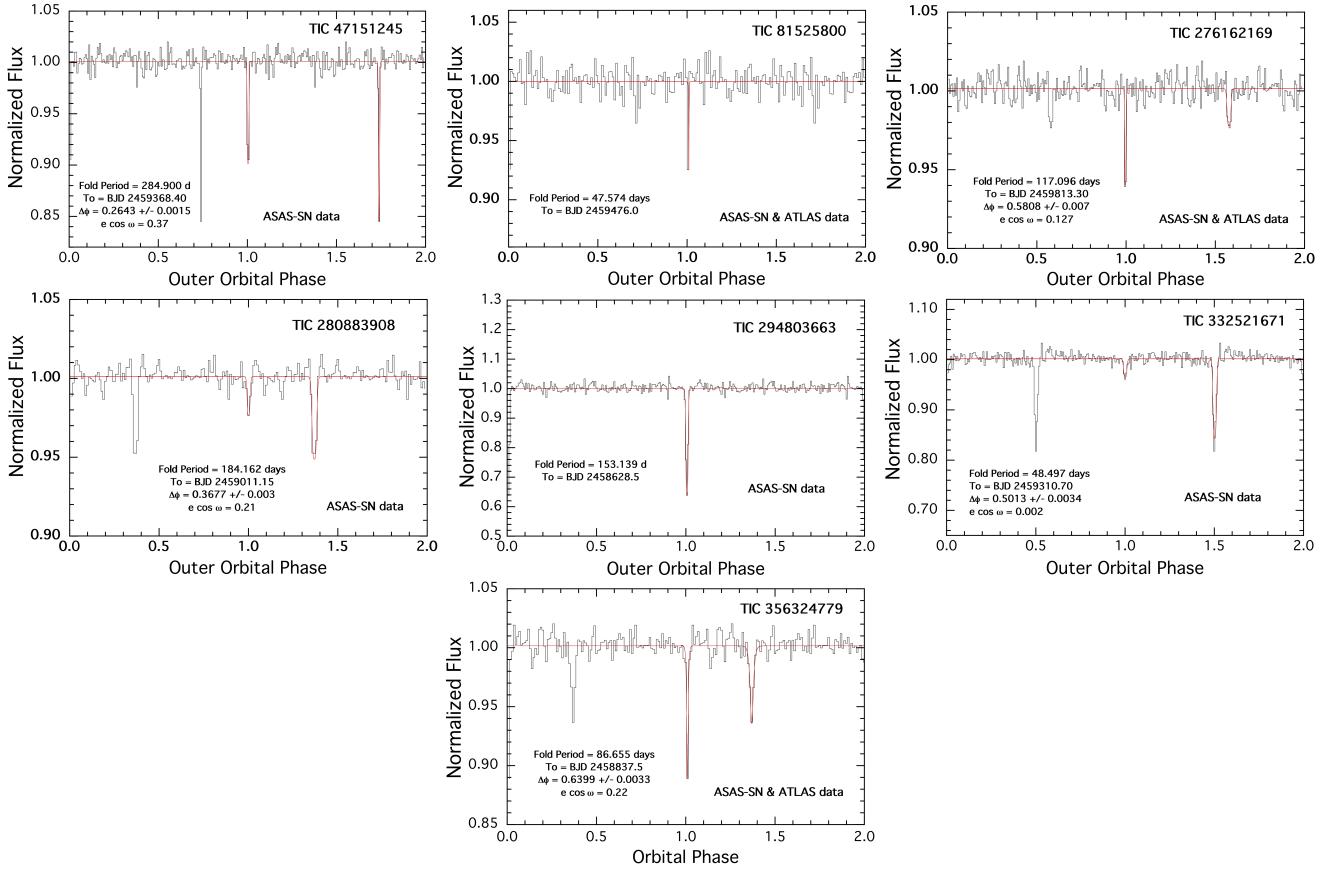


**Figure 4.** Folded, binned, and averaged lightcurves for the outer orbits of seven triply eclipsing triple systems. These were found using archival data from ASAS-SN and ATLAS (see Sect. 5 for details). Each panel lists the fold period, the reference time of phase zero (based on the *TESS* detection of an outer eclipse), the orbital phase difference between the primary and secondary outer eclipses (for five of the systems), and the inferred value of  $e \cos \omega_{\text{out}}$  (if both types of outer eclipses are seen). The red curve is a fit to the one or two outer eclipses during the second plotted orbital cycle only, and are used to determine the orbital phase difference between the two eclipses.

Again, we show only two illustrative examples of this type of visualization of the stars’ evolutionary state in Fig. 3 (also for TIC 280883908 and TIC 332521671). Note how both tertiaries are evolved substantially off the main sequence while the EB stars are both still quite near the MS.

## 5 OUTER ORBITAL PERIODS FOUND FROM ARCHIVAL DATA

Following the discovery of a triply eclipsing triple system with *TESS*, and after determining the basic parameters of the constituent stars via an SED fit, we would most like to know the nature of its outer orbit, especially  $P_{\text{out}}$  and, if possible, the eccentricity,  $e_{\text{out}}$ . In this aspect of our work, we have most often made use of the ASAS-SN (Shappee et al. 2014; Kochanek et al. 2017) and ATLAS (Tonry et al. 2018; Smith et al. 2020) archival data sets. The ASAS-SN data covers the entire sky and typically contains some  $\sim 1800$ - $3000$  photometric measurements of a given star, while the ATLAS archives (covering above declinations of  $-30^\circ$ ) often have approximately 2000 photometric measurements. The ATLAS data go somewhat deeper than the ASAS-SN data, but they tend to saturate more quickly on brighter stars. The two data sets complement each other nicely, and can quite often be median normalized

to each other and co-added for greater statistical precision. We also routinely check for KELT (Pepper et al. 2007, 2012), WASP (Pollacco et al. 2006), HAT (Bakos et al. 2002) and MASCARA data (Talens et al. 2017) to see whether they are available for a particular system.

For all of the 9 sources, there were ASAS-SN archival data available. For four of the sources there were also non-saturated ATLAS data. With these data we were able to obtain a robust period for the outer orbit for 7 of the 9 systems, and they were also very useful in determining the long-term average EB periods. We also obtained KELT data for one of our targets, TIC 99013269. However, opposite to the other archival data, whose use is described in this section, the KELT dataset was found to be extremely helpful at the final stage of the photodynamical analysis, hence, it will be discussed there in Sect. 8.1.3.

We analyze the archival photometric data by doing a Box Least Squares transform (Kovács et al. 2002) (BLS) in a search for the outer eclipses (either outer primary or outer secondary eclipse, or both). We prepare the archival data for a BLS search by (i) removing obvious outlier points, (ii) median normalizing data from different filter bands, and (iii) subtracting out the lightcurve of the inner EB by Fourier means (as described in Powell et al. 2021). In the process

of the latter operation we remove between 5 and 100 orbital harmonics depending on the sharpness of the eclipses in the lightcurve of the EB. This cleaning process requires knowing the orbital period of the EB very accurately. In turn, we determine the long-term average binary period from the *TESS* data and/or from the archival data.

The results of the outer period search for 7 of our 9 triply eclipsing triple stars are shown in Fig. 4. Each panel shows a folded, binned, and averaged lightcurve of the archival data about the period which corresponds to the most significant peak in the BLS transform. The time of the third-body eclipse observed in the *TESS* data is taken to be zero phase for the outer orbit fold in each panel. For 5 of these triples, both the primary and secondary outer eclipses are securely detected. For those systems, the outer period of the triple as well as the value of  $e_{\text{out}} \cos \omega_{\text{out}}$  are accurately determined. For the remaining two triples only one of the outer eclipses is determined, thereby leading to an accurate measure of  $P_{\text{out}}$ , but not for  $e_{\text{out}} \cos \omega_{\text{out}}$ . Two of the systems have quite short outer periods of 47.6 days (TIC 81525800) and 48.5 days (TIC 332521671).

## 6 OTHER SOURCES OF INFORMATION

In addition to the *TESS* photometry and archival photometry (typically from ASAS-SN and ATLAS), for our analysis we used other kinds of photometric and spectroscopic datasets, as well. First of all we derived eclipse timing data from the *TESS* observations. We list these eclipse timing variation (‘ETV’) curves as distinct from the *TESS* photometric lightcurves even though the ETVs are, in fact, derived from the *TESS* photometry. In the photodynamics code (see Sect. 7) the  $\chi^2$  contribution found from fitting the modeled eclipse times to the measured ones is separate and distinct from the contribution computed from fitting the modeled lightcurves to the measured *TESS* photometry. All of the systems have ETV curves that the photodynamical analyses utilize. For all but one of the systems, the ETV data carried useful auxiliary information and, moreover, for at least 3 of the systems the ETV points were particularly helpful in constraining the system parameters.

To supplement the ETVs that were derived from the *TESS* data, we also organized ground-based photometric and/or spectroscopic follow up observations for some of our systems. In this way, we observed photometrically a total of eight further regular eclipses from three of the nine EBs, and also a part of an additional third body eclipse in one case. Importantly, we also obtained radial velocity (RV) data for five of the nine systems. Note that we incorporated into the joint photodynamical analyses not only the ETV points determined from these follow up observations, but also the eclipsing lightcurves themselves. Finally, note that Gaia orbital parameters are also available for four of our systems. In some cases we also used Gaia periods to find reliable initial-guess parameters for the photodynamical fit.

We tabulate all the RV and ETV data in Tables A1–A4 and B1–B9 for RVs and ETVs, respectively. Moreover, below we show separately the fits to the RV and ETV points for those systems where it provides substantial supplemental information, and mention when there are also Gaia solutions.

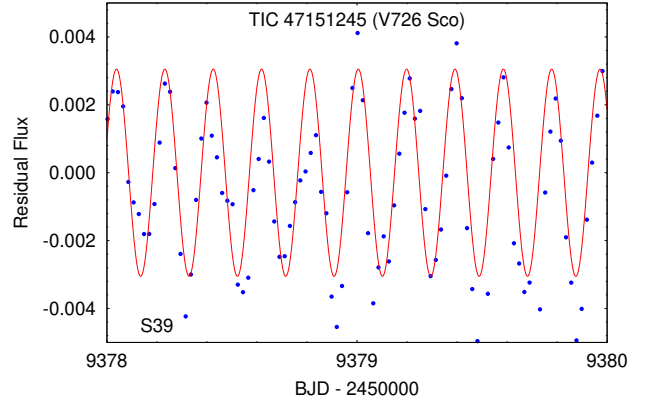


**Figure 5.** Stellar oscillations in TIC 47151245, and the Fourier fit. The dominant pulsation period is 0.1933 d.

### 6.1 TIC 47151245: Archival Data

TIC 47151245 is the only one of our nine triples which has no Gaia orbit, no useful ETV curve, and no RV data. In spite of this we have derived a quite meaningful system solution. Part of the reason for this success is the fact that this system has arguably one of our two best outer orbital folds from the ASAS-SN archival data. In this lightcurve we detect clearly the primary and secondary outer eclipses, and thereby measure precisely both the outer period and the value of  $e_{\text{out}} \cos \omega_{\text{out}}$  (see Fig. 4).

Interestingly, we also see a strong oscillation from one of the three hot stars ( $\sim 8500$  K). The residuals to the model fit are shown in Fig. 5, along with a Fourier fit which yields only a single period of 0.1933 days. Unfortunately, we cannot use this pulsation to aid in the mass determination, in part because we do not know which star it comes from.

### 6.2 TIC 81525800: ETVs

The ETV curve for TIC 81525800 is shown in Figure 6. It covers Sectors 43, 44 and 45 of the *TESS* data as well as followup ground-based observations made by the 80-cm RC telescope of Baja Astronomical Observatory (BAO80 – see Borkovits et al. 2022a for technical details), Hungary on the night of 21/22 March 2022. The ETV curve is dominated by the dynamical delay due to the short outer orbital period of only 47.8 days<sup>4</sup> and the high outer eccentricity of 0.61. The outer orbit of 47.8 days is well mapped out by the ETV points after only two sectors of *TESS* data.

### 6.3 TIC 99013269: RVs, ETVs, and Gaia results

This system exhibited only one, but quite remarkable, extra eclipsing event at the very beginning of the Sector 41 observations. Despite the brightness of the EB, the archival data were found to be unusable for determining the outer orbital

<sup>4</sup> Note that the outer period of this triple is listed in Table 6 as 49.75 d. The latter is the instantaneous osculating period in this very close and highly eccentric binary. Hence the apparent discrepancy with the eclipsing period cited here and listed in Fig. 4



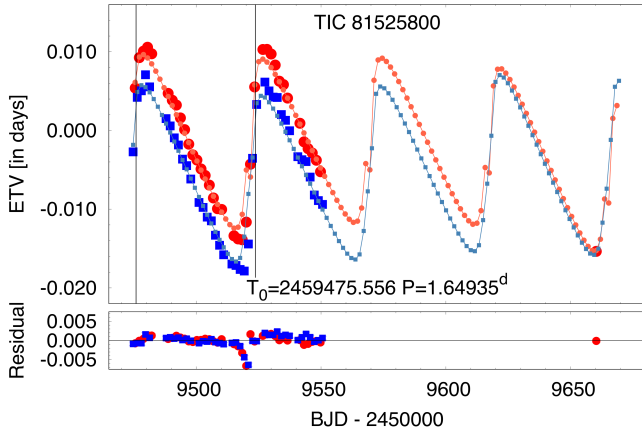


**Figure 6.** Eclipse timing data and its photodynamical model for TIC 81525800. Here, and also for the forthcoming ETV curves, larger red and blue filled circles represent observed primary and secondary eclipses, respectively, while the smaller symbols stand for the model ETV points. These latter points have been connected with straight line segments. Small apparent discontinuities in the model ETV points around the periastron passages in this highly eccentric outer orbit are noticeable. They arise from the discontinuous sampling of the continuous period variations which are dominated by dynamical, third-body perturbations instead of the pure and much smoother LTTE. The vertical lines show the locations of the third-body eclipses observed with *TESS*. The earlier points are from Sectors 43, 44, and 45 of the *TESS* observations, while the last point is from a ground-based follow-up measurement with the BAO80 instrument.

period. There was weak evidence for a  $\sim 303$ -day outer period, but with the assumption of that period, we were unable to find any realistic and physically stable solution. Therefore, we initiated a long-term spectroscopic follow up for obtaining RV data, and planned to postpone the detailed study of this EB to a later time.

For the spectroscopic follow up we used three different instruments. 16 of the 20 RV points were obtained with the fibre-fed ACE spectrograph attached to the 1-m RCC telescope of Konkoly Observatory at Piszkes-tető, Hungary. Three points were acquired with a fibre-fed Échelle spectrograph mounted on the 1.3-m Nasmyth-Cassegrain telescope of Skalnate Pleso Observatory, Slovakia. Finally, one RV measurement was taken with the ESpeRo spectrograph (Bonev et al. 2017) mounted on the 2m RCC telescope of the Rozhen National Astronomical Observatory (NAO), Bulgaria.

After Gaia’s third data release, however, we immediately realized that this system is tabulated in the Gaia DR3 non-single stars (NSS) catalog (Babusiaux et al. 2022; Gaia Collaboration 2022) as an astrometric binary with a period of  $P_{\text{astr}} = 609.5$  d. Hence, we initiated some preliminary photodynamical runs, using *TESS* Sector 14, 15 and 41 data, the ETV curves determined from these data, and the first set of our RV data that was available at that time. From those inputs we found a consistent and astrophysically reliable solution. This photodynamical run was reiterated and refined when the Sector 55 *TESS* observations were released. The RV and ETV curves with the best-fit joint photodynamical solution are plotted in Fig. 7, top and bottom panels, respectively. Our outer period and eccentricity are  $604.05 \pm 0.01$  days and

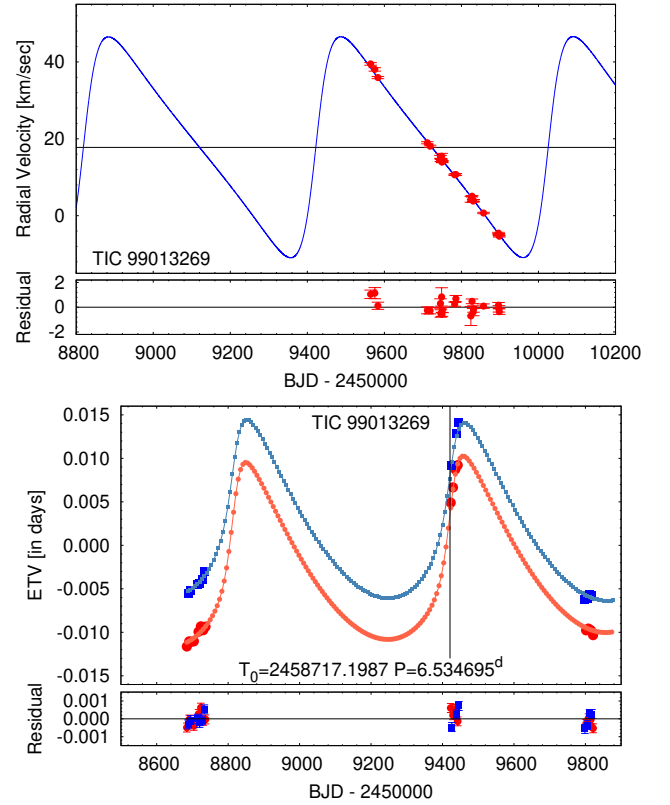


**Figure 7.** Radial velocity and eclipse timing data for TIC 99013269. The RV data were gathered with the 1-m Piszkestető (Hungary), 1.3-m Skalnate Pleso (Slovakia) and 2m Rozhen (Bulgaria) telescopes, while the ETV data are from *TESS* Sectors 14, 15, 41 and 55. The outer period is  $604.05 \pm 0.01$  d.

$0.463 \pm 0.005$ , compared to Gaia’s values of  $609.5 \pm 2$  days and  $0.46 \pm 0.03$ , so in fairly decent agreement to within the larger Gaia uncertainties. Of course, Gaia provides no information about the stellar constituents of the triple.

#### 6.4 TIC 229785001: ETVs and Gaia results

This system is located in the northern continuous viewing zone (NCVZ) of *TESS* and, hence, it was observed almost continuously during years 2 and 4 of the prime and extended missions of the spacecraft. The ETVs in Fig. 8 clearly indicate a longer time-scale variation in addition to the 165-day outer orbit of the triple. Therefore, for a satisfactory modeling of the lightcurve features (mainly the locations and morphologies of the third-body eclipses) we assumed that TIC 229785001 is indeed at least a quadruple stellar system with a hierarchy type of  $(2+1)+1$ . Hence, we added a fourth, distant star to the triple system revolving on a wider orbit about the center of mass of the inner triple subsystem. The relatively short observing window of *TESS* did not make it possible to determine the parameters of this outermost orbit with satisfactory precision or, even, uniquely. Thus, the parameters of the outermost orbit given later in Table 7 should not to be taken too seriously, and may be substantially revised after future observations.

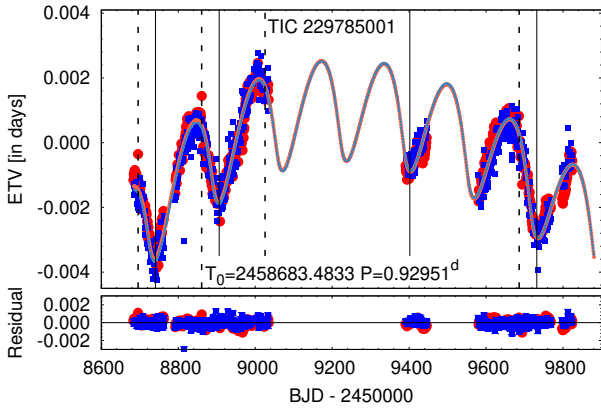


**Figure 8.** Eclipse timing data for TIC 229785001. The ETV data are from *TESS* Sectors 14-16, 17-26, 40-41, 47-53, and 55. Solid and dashed vertical lines represent the locations of the primary and secondary third-body eclipses, respectively.

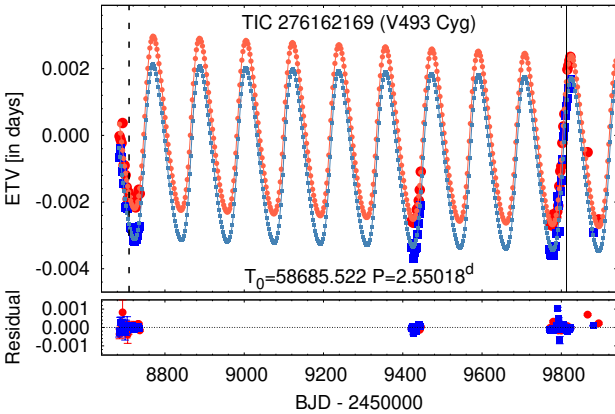


**Figure 9.** Eclipse timing data for TIC 276162169. The majority of the ETV data are from *TESS* Sectors 14-15, 41, 54-55, while the last three points are obtained during our follow up observations with the GAO80 instrument.

Gaia gives an outer orbital period of 166.0 days compared to our value of 165.25 days, and the corresponding outer eccentricities are 0.49 vs. 0.46, respectively. Thus, these are in basic agreement.

### 6.5 TIC 276162169: ETVs

The ETV curve shown in Figure 9 samples the outer orbit of 117 days relatively well over *TESS* sectors 14-15, 41, and 54-55, and also includes three points from ground-based observations with the 80-cm RC telescope of Gothard Astrophysical Observatory, Szombathely, Hungary (GAO80 – see, again, Borkovits et al. 2022a for technical details). In this case the dynamical and light-travel time effect (LTTE) delays give quite similar contributions to the ETV curve, which in fact strongly constrains the orbital and dynamical properties of the triple system.

Note, this is the only system in our sample for which for-

mer, ground-based eclipse-timing observations are available. The Lichtenknecker Database of the BAV<sup>5</sup> lists 26 times of eclipse between 1935 and 2017. However, due to their large uncertainties (which substantially exceed the full amplitude of the ETVs induced by the third-body), we have decided not to use these data.

### 6.6 TIC 280883908: RVs, ETVs, and Gaia results

We obtained 19 RV points with the Tillinghast Reflector Echelle Spectrograph (TRES) on the 1.5m reflector at the Fred Lawrence Whipple Observatory, Arizona, USA. The two most recent points were obtained after our final photodynamical analysis and, hence, were not used in the model fit. We obtained one additional point with the 2m Rozhen telescope. In order to keep the homogeneity of the RV measurements, however, we did not use this latter point for the analysis. Figure 10 (top panel) shows all but the latest RV point for TIC 280883908 together with the photodynamical solution curve.

The ETV points taken from the *TESS* observations are shown in the bottom panel of Figure 10. In spite of the fact that the ETV points cover just two *TESS* sectors of  $\sim 50$  days, or a little more than a quarter of the outer orbit, they are a useful complement to the RV data since the ETV points measure the motion of the EB, while the RVs follow the tertiary star.

Gaia gives an outer orbital period of 184.1 days compared to our value of 184.35 days, and the corresponding outer eccentricities are essentially the same at 0.26. So, again, these are in good agreement.

### 6.7 TIC 294803663: RVs, ETVs, Gaia results, and pulsations

We obtained six RV data points from the CHIRON spectrometer mounted on the 1.5 m SMARTS telescope at CTIO in Chile (Tokovinin et al. 2013). Spectra with a resolution of 25,000 were taken in the service mode and processed by the standard pipeline (Paredes et al. 2021). RVs of the slowly-rotating tertiary component were derived by cross-correlation with a binary mask based on the solar spectrum. Broad lines of the EB components are not detectable.

This target was observed by *TESS* during two pairs of consecutive sectors (11-12 & 38-39), separated by two years. The ETV curve (Fig. 11) during each of the two  $\sim 50$ -day intervals covers two different phases of the outer orbit. While this ETV curve would be insufficient to determine a unique orbit by itself, it is valuable as a supplement to the full orbital solution.

In addition to the eclipses in this system, we find a strong and nearly periodic signal (see Fig. 12), which we attribute to stellar oscillations in the giant tertiary star. Four periods are required to fit the oscillations: 1.211 d, 2.427 d, 9.98 d, and 13.56 d. The latter two periods are likely associated with the *TESS* instrument. while the first is just the higher harmonic of the second.

<sup>5</sup> Bundesdeutsche Arbeitsgemeinschaft für Veränderliche Sterne – <https://www.bav-astro.eu/index.php/veroeffentlichungen/lichtenknecker-database/lkdb-b-r>

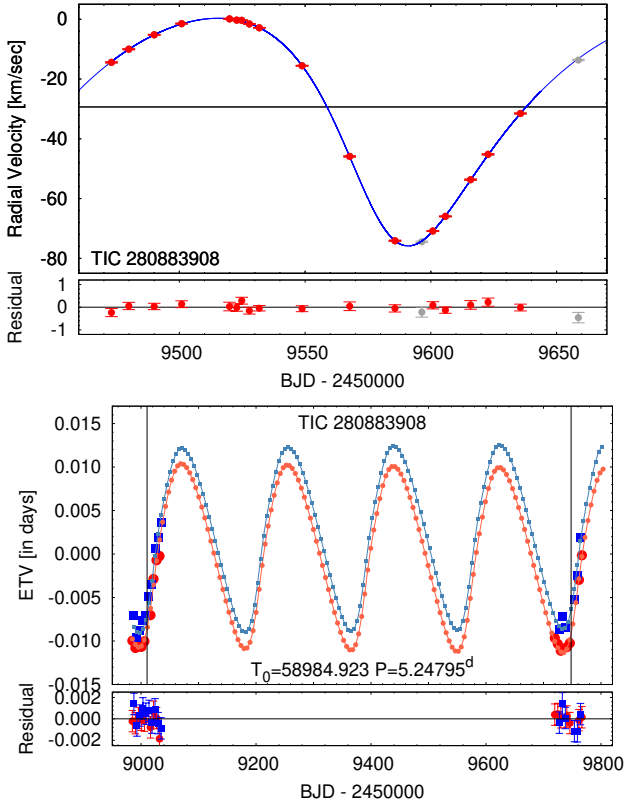


**Figure 10.** Radial velocity and eclipse timing data for TIC 280883908. All but one RV data points are from TRES and make this the best sampled of any of our RV curves. The two RV points shown as gray dots were not used for the photodynamical analysis (see text). Furthermore, note that the very last TRES RV point, obtained about 260 days later than the previous one, was not plotted to avoid a large decrease in the horizontal resolution of the plot. The ETV data are from two pairs of *TESS* Sectors 25-26 and 52-53, which are separated by two years. Each pair of *TESS* observations samples nearly the same part of the outer orbit of 184 days.

### 6.8 TIC 332521671: RVs and ETVs

The radial velocity and eclipse timing data for TIC 332521671 are shown in Fig. 13. The RV data are from the CHIRON spectrometer (Tokovinin et al. 2013). The complementary ETV data are from *TESS* Sectors 10 and 37. The RV curve hints at a rather circular outer orbit, which indeed turns out to be the case for the 48.6-day outer orbit system. The ETV curve is rather incomplete, but the full photodynamical model suggests that the inner binary might be undergoing forced apsidal precession with a rather short period of  $\sim 4$  years. We will discuss, however, in Sect. 8.1.8 that this effect most probably is not real, but only a pure numerical consequence of the two year-long gap between the Sector 10 and 37 ETV points, where nothing constrains our integrator.

### 6.9 TIC 356324779: ETVs

The ETV curve for TIC 356324779 is shown in Figure 14. It covers the Sector 19 *TESS* data as well as six followup

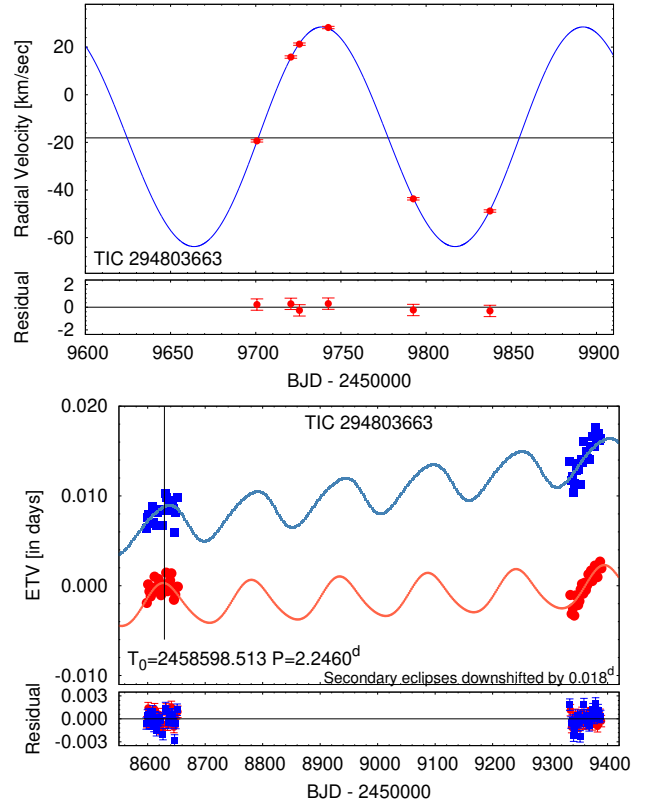


**Figure 11.** Radial velocity and eclipse timing data for TIC 294803663. The RV data are from CHIRON at CTIO. The model fits are the superposed smooth curves. Red and blues points (and curves) represent primary and secondary eclipses of the inner eclipsing binary, respectively. Vertical line represents the location of the third-body eclipse event observed by *TESS*. Note, for a better visibility the secondary ETV curve is downshifted by  $0.018^d$ .

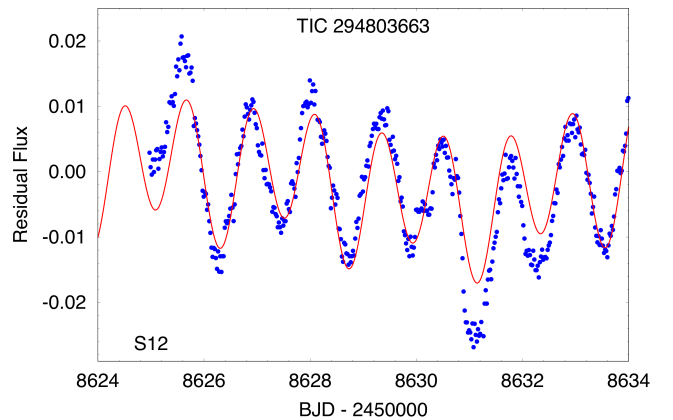


**Figure 12.** Oscillations from the giant tertiary star in TIC 294803663, and Fourier fit.

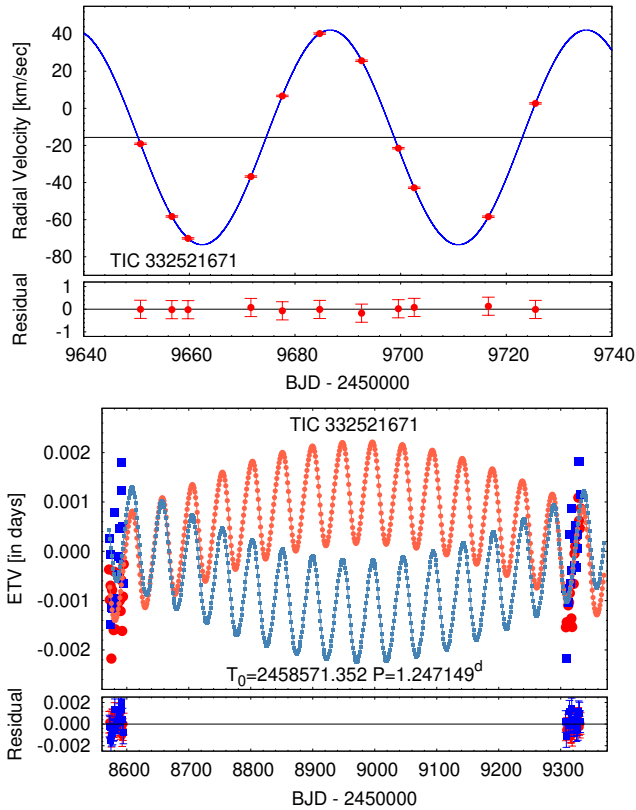


**Figure 13.** Radial velocity and eclipse timing data for TIC332521671. The RV data are from CHIRON at CTIO, while the ETV data are from *TESS* Sectors 10 and 37.

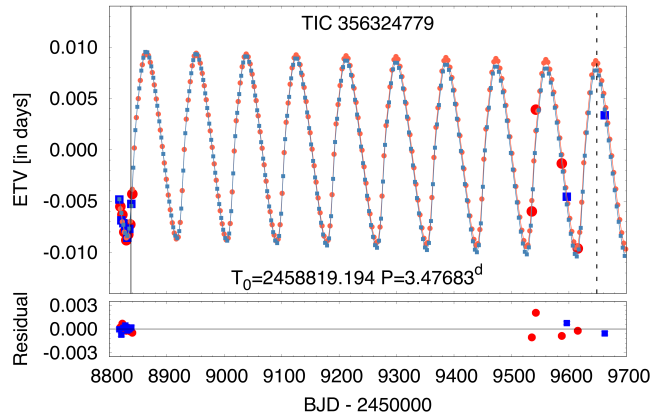


**Figure 14.** Eclipse timing data for TIC 356324779. The earlier points are from Sector 19 of the *TESS* observations, while the later points are ground-based followup measurements with BAO80 and GAO80 telescopes.

ground-based inner EB eclipse observations with the BAO80 and GAO80 instruments. Note, besides the regular inner EB eclipses, one additional GAO80 observation serendipitously caught a section of a third-body eclipse (see the very last panel of Fig. 1).

## 7 PHOTODYNAMICAL ANALYSIS FOR THE SYSTEM PARAMETERS

We have carried out a photodynamical analysis of all nine of our triply eclipsing triples. For this phase of the analysis of the system parameters, we utilize the software package LIGHTCURVEFACTORY (see, e.g. Borkovits et al. 2019a, 2020a, and references therein). As described in a number of previous papers, the code contains (i) emulators for the *TESS* lightcurve, the corresponding ETVs, and radial velocity curve (where available), (ii) a built-in numerical integrator to calculate the perturbed three-body coordinates and velocities of the three stars in the triple; and (iii) an MCMC-based search routine for finding the best-fit system parameters. The latter utilizes an implementation of the generic Metropolis-Hastings algorithm (see, e.g., Ford 2005). The development, implementation, and use of LIGHTCURVEFACTORY, as well as the steps involved in the analysis process, have been explained in detail as the code was applied to a wide range of multistellar systems (Borkovits et al. 2018, 2019a,b, 2020a,b, 2021; Mityan et al. 2020). LIGHTCURVEFACTORY has been used successfully to study compact and wider triple systems (with and without outer eclipses), as well as quadruple systems with either a 2+2 or 2+1+1 configuration.

Virtually all of the specifics of how this code was used to analyze compact triply eclipsing triples found with *TESS*, were described in Rappaport et al. (2022). Therefore, we will provide a high-level overview here, highlighting inputs to the code and the parameters that are either determined or constrained by the MCMC fit. In all, there are 26 system parameters that are output from the analysis. Specifically, these are all the stellar parameters (including mass, radius,  $T_{\text{eff}}$ ), all of the elements of the inner and outer orbits, the system metallicity and age, as well as the distance to the source and the interstellar extinction.

The ‘input’ information that is used by the code to determine these 26 system parameters can be divided into two basic categories. First, there are the ‘input data’. These include the *TESS* lightcurve which contains (i) EB eclipse profiles, (ii) the third-body eclipse profile(s), (iii) the times of the EB eclipses which are distinct from the shape and depths of eclipses, (iv) archival SED values, (v) radial velocities (available only for four of the systems), and (vi) the outer orbital period and possibly  $e_{\text{out}} \cos \omega_{\text{out}}$  determined from ASAS-SN, ATLAS, and other ground-based archival data. Second, we utilize PARSEC model stellar evolution tracks and isochrones as well as model stellar atmospheres (Bressan et al. 2012). The former enables us to relate stellar mass to radius and  $T_{\text{eff}}$  for a given age and metallicity, while the latter allows us to compute magnitudes in different bands to fit the SED. The available input information for each of the nine triples is summarized in Table 4.

The *TESS* lightcurves that we used for the photodynamical analysis were taken from the full-frame images (‘FFI’) where the photometry was done with the FITSH package (Pál 2012). To save computational time we binned the 10-min cadence data to 30-min cadence, and in the case of seven of the nine current systems, dropped out the out-of-eclipse sections of these lightcurves, retaining only the  $\pm 0.15$  phase-domain regions around the binary eclipses themselves. However, during sections of the data containing the third-body (i.e., ‘outer’) eclipses, we kept the data for an entire binary

**Table 4.** Input Information for the System Analysis<sup>a</sup>

Object	<i>TESS</i> 3rd-Body Eclipse(s) <sup>a</sup>	<i>TESS</i> EB Lightcurve <sup>a</sup>	Archival Outer Eclipses <sup>b</sup>	SED Points <sup>c</sup>	ETV Curve <sup>d</sup>	RV Data <sup>e</sup>	Gaia Orbit <sup>f</sup>
TIC 47151245	✓	✓	✓	✓			
TIC 81525800	✓	✓	✓	✓	✓		
TIC 99013269	✓	✓		✓	✓	✓	✓
TIC 229785001	✓	✓		✓	✓		✓
TIC 276162169	✓	✓	✓	✓	✓		
TIC 280883908	✓	✓	✓	✓	✓	✓	✓
TIC 294803663	✓	✓	✓	✓	✓	✓	✓
TIC 332521671	✓	✓	✓	✓	✓	✓	
TIC 356324779	✓	✓	✓	✓	✓		

Notes. (a) See Fig. 1. (b) See, e.g., Fig. 4. (c) See, e.g., Fig. 2. (d) See Figs. 6, 7, 8, 9, 10, 11, 13, and 14. (e) See Fig. 7, 10, 11, and 13. (f) Babusiaux et al. (2022); Gaia Collaboration (2022)

**Table 5.** Definitions of Triple System Parameters in Tables 6–10

Parameter <sup>a</sup>	Definition
$t_0$	Epoch time for osculating elements
$P$	Orbital period
$a$	Orbital semimajor axis
$e$	Orbital eccentricity
$\omega$	Argument of periastron (of secondary)
$i$	Orbital inclination angle
$\mathcal{T}_0^{\text{inf/sup}}$	Time of conjunction of the secondary <sup>b</sup>
$\tau$	Time of periastron passage
$\Omega$	Longitude of the node relative to inner orbit
$i_{\text{mut}}$	Mutual inclination angle <sup>c</sup>
$q$	Mass ratio (secondary/primary)
$K_{\text{pri}}$	“K” velocity amplitude of primary
$K_{\text{sec}}$	“K” velocity amplitude of secondary
$R/a$	Stellar radius divided by semimajor axis
$T_{\text{eff}}/T_{\text{eff,Aa}}$	Temperature relative to EB primary
fractional flux	Stellar contribution in the given band
$m$	Stellar mass
$R$	Stellar radius
$T_{\text{eff}}$	Stellar effective temperature
$L_{\text{bol}}$	Stellar bolometric luminosity
$M_{\text{bol}}$	Stellar absolute bolometric magnitude
$M_V$	Stellar absolute visual magnitude
$\log g$	log surface gravity (cgs units)
$[M/H]$	log metallicity abundance to H, by mass
$E(B - V)$	Color excess in B-V bands
extra light, $\ell_4$	Contaminating flux in the given band
$(M_V)_{\text{tot}}$	System absolute visual magnitude
distance	Distance to the source

Notes. (a) The units for the parameters are given in Tables 6–10. (b) The superscript of “inf/sup” indicates inferior vs. superior conjunctions. (c) More explicitly, this is the angle between the orbital planes of the inner binary and the outer triple orbit.

period both before and after the first and last contacts of the given third-body eclipse.

We note that the *TESS* lightcurves of TICs 47151245 and 294803663 needed some extra care. As was mentioned above, these lightcurves exhibit large stellar oscillations. We modeled these oscillations simultaneously with the triple star lightcurve modeling, fitting harmonic functions to the residual lightcurves in each trial step. In the case of the former system we used a single frequency, while in the latter system, four<sup>6</sup> frequencies were required. While the frequencies were

kept fixed, the corresponding coefficients of the sine and cosine terms were obtained via matrix inversion. Then the  $\chi_{\text{LC}}^2$  value was calculated for this mixed lightcurve, and used for the acceptance or rejection of the given trial step. More details of this procedure can be found in Borkovits et al. (2018).

The system parameters that are derived from the photodynamical analyses are tabulated in Tables 6 through 10. The tables include 7 basic parameters describing the inner and the outer orbits, and their relative orientations; several relative values (e.g.,  $R/a$ ,  $T_B/T_{Aa}$ ); the properties of all three stars (including  $M$ ,  $R$ ,  $T_{\text{eff}}$ ,  $L$ , and  $M_V$ ); and 6 global system parameters such as distance,  $[M/H]$ , and  $E(B - V)$ . The definitions of all the parameters listed in Tables 6 through 10 are given first in Table 5.

## 8 STELLAR AND ORBITAL PARAMETERS FOR THE NINE TRIPLES

### 8.1 Individual Triples

In this section we briefly discuss the bigger-picture results for each of the nine triply eclipsing triples. Before looking at the results for the individual systems, we present a pictorial overview of all the binary orbits in Fig. 15. These are what the orbits would look like to a distant observer viewing the systems from the poles of the outer orbital planes. The parameters used to generate this figure, as well as those we refer to in the discussion of each system, are taken from Tables 6 to 10 and are based on the photodynamical fits (unless otherwise specifically indicated).

#### 8.1.1 TIC 47151245 = V726 Sco

The TIC 47151245 system was formerly classified as a likely detached EB with a 1.202-day-period (see, e.g., Avvakumova et al. 2013). Our results confirm these findings. In the absence of any RV data we were able to determine the stellar masses only with a moderate accuracy of 8–10%. To within this limiting accuracy we found that the primary and tertiary stars have similar masses ( $m_{Aa} = 2.03 \pm 0.17 M_{\odot}$  and  $m_B = 2.11 \pm 0.21 M_{\odot}$ , respectively), while the secondary of the EB is a bit less massive  $m_{Ab} = 1.78 \pm 0.17 M_{\odot}$ .

tion and its harmonic, while the other two lower frequencies were used to model some likely instrumental effects.

<sup>6</sup> From these four frequencies, only two belong to a physical pulsa-

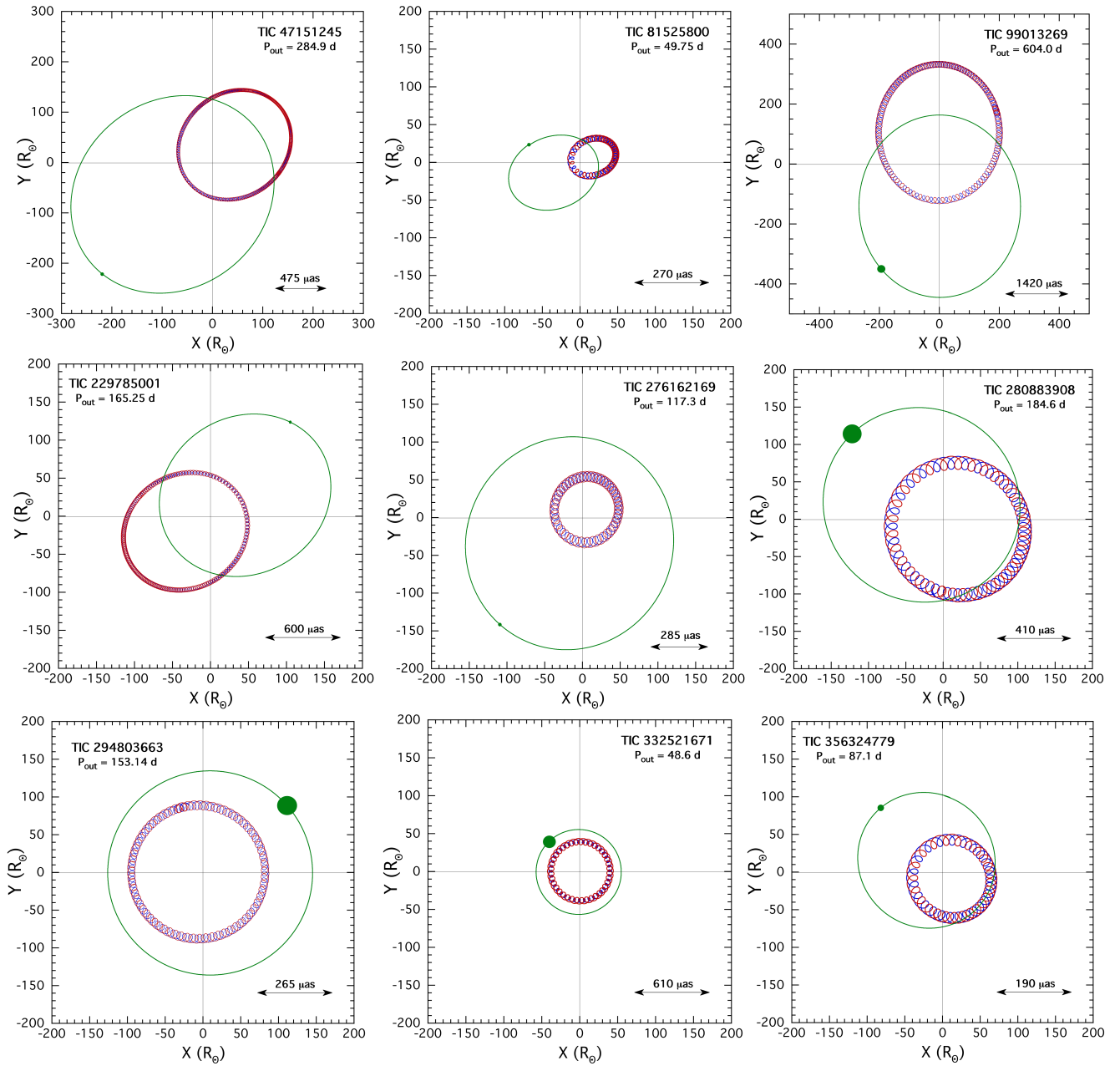


**Figure 15.** The outer orbits of the nine triply eclipsing systems seen from above the orbital plane. The stars are all moving counter-clockwise except for the tertiary in TIC 276162169 which is moving clockwise (i.e., in a retrograde fashion). The observer is at  $y \rightarrow -\infty$ . Red and blue tracks are for the primary and secondary stars in the EB, respectively, while the green track is that of the tertiary star. The heavy filled green circle represents the size of the tertiary to scale on the plot.

Note, however, that despite the weaker accuracy on the masses, their ratios are constrained much better, and we find  $q_{\text{in}} = 0.88 \pm 0.02$  and  $q_{\text{out}} = 0.55 \pm 0.01$  for the inner and outer subsystems, respectively. The triple system is less ‘tight’ (defined as small period ratios  $P_{\text{out}}/P_{\text{in}}$ ) since in this system  $P_{\text{out}}/P_{\text{in}} = 284.3/1.203 = 236.3$ . Hence, we cannot expect strong, and short-timescale dynamical perturbations. Despite this, what makes this triple extraordinarily interesting is that, in contrast to the previously investigated, almost flat triply eclipsing triple systems, here we have found an unusually high mutual inclination of  $i_{\text{mut}} = 41^\circ \pm 1^\circ$ .

While, at the first sight, this result seems to be unexpected, an expert glance at the *TESS* lightcurve (upper left panel of Fig. 1) offers an immediate, qualitative justification of the significant non-alignment of the inner and outer orbits. As one can see, the depths of the regular eclipses of the inner EB are similar in amplitude to the strong ellipsoidal light variations of the out-of-eclipse sections of the lightcurve. This fact clearly reveals that the low amplitude of the inner eclipses cannot be explained with light dilution caused by the contaminating flux of a dominant tertiary object. The only explanation for a similar amplitude ellipsoidal light variation and

**Table 6.** Orbital and astrophysical parameters of TIC 47151245 and TIC 81525800 from the joint photodynamical *TESS*, ETV, SED and PARSEC isochrone solution. Note that the orbital parameters are instantaneous, osculating orbital elements and are given for epoch  $t_0$  (first row). Therefore, the orbital periods, in particular, cannot be used for predicting the times of future eclipses; see Table 11 for the latter, and Kostov et al. (2021) for a more general discussion.

	TIC 47151245			TIC 81525800		
	orbital elements					
	subsystem			subsystem		
	Aa–Ab	A–B		Aa–Ab	A–B	
$t_0$ [BJD - 2400000]	58626.5			59474.0		
$P$ [days]	$1.202508^{+0.000070}_{-0.000062}$	$284.374^{+0.491}_{-0.568}$		$1.6131^{+0.0043}_{-0.0065}$	$49.75^{+0.36}_{-0.14}$	
$a$ [ $R_\odot$ ]	$7.42^{+0.16}_{-0.22}$	$329.0^{+5.9}_{-9.8}$		$8.16^{+0.07}_{-0.09}$	$91.8^{+0.8}_{-1.0}$	
$e$	$0.0022^{+0.0018}_{-0.0012}$	$0.480^{+0.027}_{-0.035}$		$0.0202^{+0.00231}_{-0.0012}$	$0.614^{+0.017}_{-0.006}$	
$\omega$ [deg]	$269^{+21}_{-198}$	$218.6^{+5.7}_{-5.7}$		$144.1^{+4.2}_{-3.9}$	$201.0^{+1.2}_{-3.7}$	
$i$ [deg]	$64.43^{+0.62}_{-1.11}$	$90.318^{+0.039}_{-0.046}$		$90.63^{+2.17}_{-3.50}$	$87.55^{+0.34}_{-0.17}$	
$\mathcal{T}_0^{\text{inf}}$ [BJD - 2400000]	$58627.4569^{+0.0007}_{-0.0006}$	$59368.6719^{+0.0061}_{-0.0054}$		$59475.5227^{+0.0025}_{-0.0047}$	$59475.924^{+0.010}_{-0.012}$	
$\tau$ [BJD - 2400000]	$58626.648^{+0.759}_{-0.374}$	$59355.011^{+0.941}_{-0.882}$		$59474.966^{+0.018}_{-0.018}$	$59473.713^{+0.037}_{-0.034}$	
$\Omega$ [deg]	0.0			0.0		
$i_{\text{mut}}$ [deg]	$40.88^{+0.91}_{-0.96}$			$4.99^{+1.57}_{-3.77}$		
mass ratio [ $q = m_{\text{sec}}/m_{\text{pri}}$ ]	$0.881^{+0.021}_{-0.018}$	$0.546^{+0.010}_{-0.006}$		$0.969^{+0.057}_{-0.021}$	$0.498^{+0.016}_{-0.008}$	
$K_{\text{pri}}$ [ $\text{km s}^{-1}$ ]	$131.9^{+2.7}_{-4.1}$	$23.4^{+0.7}_{-0.5}$		$126.5^{+1.8}_{-1.7}$	$39.5^{+0.9}_{-0.9}$	
$K_{\text{sec}}$ [ $\text{km s}^{-1}$ ]	$149.7^{+2.7}_{-4.1}$	$42.7^{+1.4}_{-0.7}$		$130.5^{+1.5}_{-5.5}$	$78.5^{+1.2}_{-0.5}$	
	stellar parameters					
	Aa	Ab	B	Aa	Ab	B
	Relative quantities					
fractional radius [ $R/a$ ]	$0.3201^{+0.0063}_{-0.0073}$	$0.2458^{+0.0110}_{-0.0099}$	$0.00790^{+0.00018}_{-0.00018}$	$0.2274^{+0.0060}_{-0.0172}$	$0.2098^{+0.0169}_{-0.0069}$	$0.0192^{+0.0017}_{-0.0009}$
temperature relative to ( $T_{\text{eff}}$ ) <sub>Aa</sub>	1	$0.9689^{+0.013}_{-0.0142}$	$0.9963^{+0.0035}_{-0.0080}$	1	$0.9983^{+0.0018}_{-0.0032}$	$0.9999^{+0.0014}_{-0.0012}$
fractional flux [in <i>TESS</i> -band]	$0.3577^{+0.0109}_{-0.0154}$	$0.1959^{+0.0169}_{-0.0154}$	$0.4263^{+0.0207}_{-0.0203}$	$0.3395^{+0.0214}_{-0.0416}$	$0.2882^{+0.0517}_{-0.0186}$	$0.3132^{+0.0476}_{-0.0279}$
fractional flux [in $R_C$ -band]	–	–	–	$0.3441^{+0.0224}_{-0.0302}$	$0.3012^{+0.0570}_{-0.0293}$	$0.3301^{+0.0378}_{-0.0208}$
	Physical Quantities					
$m$ [ $M_\odot$ ]	$2.026^{+0.119}_{-0.173}$	$1.778^{+0.121}_{-0.170}$	$2.111^{+0.086}_{-0.212}$	$1.430^{+0.034}_{-0.093}$	$1.376^{+0.025}_{-0.019}$	$1.407^{+0.046}_{-0.078}$
$R$ [ $R_\odot$ ]	$2.026^{+0.119}_{-0.173}$	$1.833^{+0.100}_{-0.128}$	$2.586^{+0.078}_{-0.066}$	$1.864^{+0.050}_{-0.168}$	$1.723^{+0.106}_{-0.062}$	$1.763^{+0.157}_{-0.096}$
$T_{\text{eff}}$ [K]	$8569^{+206}_{-383}$	$8220^{+291}_{-297}$	$8563^{+207}_{-485}$	$6332^{+100}_{-112}$	$6326^{+100}_{-141}$	$6333^{+97}_{-114}$
$L_{\text{bol}}$ [ $L_\odot$ ]	$26.66^{+5.72}_{-5.10}$	$13.77^{+3.88}_{-3.00}$	$32.81^{+4.87}_{-8.01}$	$5.049^{+0.557}_{-1.149}$	$4.305^{+0.285}_{-0.299}$	$4.475^{+1.137}_{-1.674}$
$M_{\text{bol}}$	$1.21^{+0.23}_{-0.21}$	$1.92^{+0.27}_{-0.27}$	$0.98^{+0.30}_{-0.15}$	$3.01^{+0.28}_{-0.11}$	$3.19^{+0.08}_{-0.07}$	$3.14^{+0.18}_{-0.25}$
$M_V$	$1.19^{+0.20}_{-0.18}$	$1.89^{+0.27}_{-0.24}$	$0.97^{+0.27}_{-0.12}$	$2.99^{+0.30}_{-0.12}$	$3.17^{+0.08}_{-0.07}$	$3.12^{+0.19}_{-0.24}$
$\log g$ [dex]	$3.988^{+0.019}_{-0.016}$	$4.163^{+0.023}_{-0.027}$	$3.925^{+0.021}_{-0.025}$	$4.055^{+0.049}_{-0.019}$	$4.112^{+0.023}_{-0.062}$	$4.090^{+0.032}_{-0.060}$
	Global system parameters					
$\log(\text{age})$ [dex]	$8.859^{+0.130}_{-0.062}$			$9.388^{+0.082}_{-0.054}$		
$[M/H]$ [dex]	$-0.069^{+0.108}_{-0.111}$			$0.172^{+0.106}_{-0.052}$		
$E(B - V)$ [mag]	$0.115^{+0.026}_{-0.048}$			$0.278^{+0.024}_{-0.033}$		
extra light $\ell_4$ [in <i>TESS</i> -band]	$0.019^{+0.019}_{-0.014}$			$0.042^{+0.043}_{-0.030}$		
extra light $\ell_4$ [in $R_C$ -band]	...			$0.008^{+0.013}_{-0.006}$		
$(M_V)_{\text{tot}}$	$0.09^{+0.26}_{-0.16}$			$1.90^{+0.16}_{-0.12}$		
distance [pc]	$983^{+36}_{-52}$			$1718^{+61}_{-59}$		

eclipse depth is that the eclipses are nearly grazing, which, by itself, suggests that the inner orbit is being viewed far from a perfectly edge-on orientation. On the other hand, since the probability of outer eclipses decreases strongly with increasing separation (and hence outer orbital period) of the third component (see, e.g. Borkovits et al. 2022b, Appendix A), in order to detect third-body eclipses for such a relatively wide triple system<sup>7</sup>, one can expect that we have an almost edge-on view of the outer orbit. Hence, one can really justify the non-alignment of the two orbits even prior to making any quantitative analysis, or saying anything about the nature of the three stellar components.

Considering the consequences of this significant non-alignment of the two orbits, one should first realize that the observed mutual inclination is close to, but above, the well-known mutual inclination limit ( $i_{\text{mut}} = 39.23^\circ$ ) of the original, quadrupole, asymptotic ZLK theorem. In this particular

system, however, due to the strong tidal distortion of the inner binary stars (the fractional radii of the EB stars are  $r_{\text{Aa}} = 0.320 \pm 0.007$  and  $r_{\text{Ab}} = 0.246 \pm 0.011$ ), the tidal forces dominate the apsidal motion. Hence, the tidal damping prevents the inner pair from undergoing ZLK cycles, and enables the triple to remain stable in its present configuration for a very long time.

The only observable consequence of the large mutual inclination may reveal itself in the nodal precession of the orbital planes, which may lead to variations of the eclipse depths of both the inner and outer eclipses. The nodal period of the current system is  $P_{\text{node}} = 580 \pm 40$  years, which may seem to be quite a long time to wait for a dramatic change in the eclipse depths. However, the grazing nature of the eclipses makes their depths and durations very sensitive to even small variations of the EB's observable inclination ( $i_{\text{in}}$ ). Hence, a systematic monitoring of the regular eclipses in the forthcoming years or decades would be extremely useful.

Finally we also make some cautionary notes about the am-

<sup>7</sup> This triple has the second longest outer period in our sample.

**Table 7.** The same as in Table 6 above, but for TIC 99013269 and TIC 229785001.

	TIC 99013269			TIC 229785001			
	orbital elements						
	subsystem		A–B	subsystem		AB–C	
	Aa–Ab		Aa–Ab	A–B			
$t_0$ [BJD - 2400000]	58683.0		58683.0				
$P$ [days]	$6.534444^{+0.000016}_{-0.000014}$		$604.2425^{+0.0067}_{-0.0068}$	$0.929762^{+0.000016}_{-0.000015}$	$165.37^{+0.05}_{-0.05}$	$3254^{+136}_{-159}$	
$a$ [R $_{\odot}$ ]	$21.61^{+0.10}_{-0.09}$		$532.3^{+4.8}_{-2.7}$	$5.280^{+0.023}_{-0.023}$	$200.2^{+1.0}_{-1.0}$	$1573^{+47}_{-52}$	
$e$	$0.00742^{+0.00069}_{-0.00066}$		$0.4627^{+0.0052}_{-0.0053}$	$0.0005^{+0.0003}_{-0.0002}$	$0.458^{+0.020}_{-0.029}$	$0.14^{+0.04}_{-0.03}$	
$\omega$ [deg]	$259.3^{+0.8}_{-0.9}$		$270.6^{+0.6}_{-0.7}$	$84^{+64}_{-30}$	$31.1^{+2.7}_{-3.4}$	$121^{+10}_{-7}$	
$i$ [deg]	$90.13^{+0.07}_{-0.08}$		$92.33^{+0.08}_{-0.07}$	$87.72^{+0.39}_{-0.63}$	$89.23^{+0.04}_{-0.03}$	$102^{+6}_{-7}$	
$\tau_0^{\text{inf/sup}}$ [BJD - 2400000]	$58717.1942^{+0.0001}_{-0.0001}$		$59422.2041^{+0.0090}_{-0.0096}$	$58683.4709^{+0.0009}_{-0.0012}$	$58740.8480^{+0.0158*}_{-0.0148}$	...	
$\tau$ [BJD - 2400000]	$58716.998^{+0.014}_{-0.016}$		$58818.49^{+0.35}_{-0.34}$	$58682.973^{+0.100}_{-0.123}$	$58730.74^{+0.66}_{-0.64}$	$57817^{+56}_{-52}$	
$\Omega$ [deg]	0.0		$20.06^{+0.65}_{-0.56}$	0.0	$2.67^{+0.89}_{-1.23}$	$23^{+10}_{-15}$	
$i_{\text{mut}}$ [deg]		$20.17^{+0.65}_{-0.55}$			$3.13^{+0.83}_{-1.00}$	$28^{+10}_{-16}$	
mass ratio [ $q = m_{\text{sec}}/m_{\text{pri}}$ ]	$0.926^{+0.003}_{-0.003}$		$0.749^{+0.021}_{-0.009}$	$0.707^{+0.007}_{-0.007}$	$0.724^{+0.008}_{-0.009}$	$0.254^{+0.025}_{-0.021}$	
$K_{\text{pri}}$ [km s $^{-1}$ ]	$80.5^{+0.4}_{-0.4}$		$21.5^{+0.2}_{-0.2}$	$118.9^{+0.9}_{-0.9}$	$29.0^{+0.6}_{-0.6}$	$4.8^{+0.4}_{-0.3}$	
$K_{\text{sec}}$ [km s $^{-1}$ ]	$86.9^{+0.4}_{-0.3}$		$28.7^{+0.2}_{-0.1}$	$168.2^{+0.8}_{-0.9}$	$40.0^{+0.4}_{-0.6}$	$19.2^{+0.6}_{-0.8}$	
$\gamma$ [km s $^{-1}$ ]		$17.81^{+0.09}_{-0.09}$			...		
stellar parameters							
	Aa	Ab	B	Aa	Ab	B	
Relative quantities							
fractional radius [ $R/a$ ]	$0.0857^{+0.0005}_{-0.0005}$	$0.0762^{+0.0005}_{-0.0005}$	$0.0216^{+0.0004}_{-0.0006}$	$0.2508^{+0.0032}_{-0.0031}$	$0.1581^{+0.0018}_{-0.0018}$	$0.0085^{+0.0001}_{-0.0002}$	$0.00056^{+0.00006}_{-0.00005}$
temperature relative to ( $T_{\text{eff}}$ ) $_{\text{Aa}}$	1	$0.9666^{+0.0023}_{-0.0020}$	$0.6833^{+0.0054}_{-0.0073}$	1	$0.8178^{+0.0050}_{-0.0049}$	$1.1330^{+0.0126}_{-0.0126}$	$0.8494^{+0.0477}_{-0.0443}$
fractional flux [in <i>TESS</i> -band]	$0.0818^{+0.0010}_{-0.0010}$	$0.0585^{+0.0004}_{-0.0004}$	$0.8267^{+0.0191}_{-0.0325}$	$0.2544^{+0.0066}_{-0.0063}$	$0.0509^{+0.0013}_{-0.0012}$	$0.6271^{+0.0227}_{-0.0338}$	$0.0670^{+0.0227}_{-0.0214}$
Physical Quantities							
$m$ [M $_{\odot}$ ]	$1.646^{+0.022}_{-0.019}$	$1.525^{+0.021}_{-0.019}$	$2.371^{+0.108}_{-0.045}$	$1.337^{+0.018}_{-0.017}$	$0.945^{+0.014}_{-0.015}$	$1.650^{+0.032}_{-0.030}$	$0.999^{+0.096}_{-0.080}$
$R$ [R $_{\odot}$ ]	$1.852^{+0.011}_{-0.011}$	$1.648^{+0.014}_{-0.016}$	$11.509^{+0.287}_{-0.332}$	$1.324^{+0.022}_{-0.021}$	$0.835^{+0.013}_{-0.013}$	$1.707^{+0.037}_{-0.039}$	$0.890^{+0.109}_{-0.078}$
$T_{\text{eff}}$ [K]	$6995^{+163}_{-34}$	$6764^{+149}_{-29}$	$4798^{+35}_{-41}$	$6481^{+73}_{-48}$	$5305^{+63}_{-49}$	$7338^{+151}_{-112}$	$5516^{+323}_{-303}$
$L_{\text{bol}}$ [L $_{\odot}$ ]	$7.408^{+0.515}_{-0.200}$	$5.113^{+0.402}_{-0.156}$	$62.12^{+4.76}_{-2.40}$	$2.791^{+0.173}_{-0.154}$	$0.496^{+0.033}_{-0.028}$	$7.591^{+0.696}_{-0.531}$	$0.658^{+0.382}_{-0.219}$
$M_{\text{bol}}$	$2.60^{+0.03}_{-0.07}$	$2.99^{+0.03}_{-0.08}$	$0.29^{+0.04}_{-0.08}$	$3.66^{+0.06}_{-0.07}$	$5.53^{+0.06}_{-0.07}$	$2.57^{+0.08}_{-0.10}$	$5.22^{+0.44}_{-0.50}$
$M_V$	$2.53^{+0.03}_{-0.06}$	$2.94^{+0.04}_{-0.08}$	$0.66^{+0.03}_{-0.12}$	$3.63^{+0.06}_{-0.07}$	$5.70^{+0.08}_{-0.09}$	$2.50^{+0.08}_{-0.09}$	$5.33^{+0.54}_{-0.56}$
$\log g$ [dex]	$4.118^{+0.005}_{-0.005}$	$4.187^{+0.004}_{-0.004}$	$2.693^{+0.021}_{-0.020}$	$4.319^{+0.009}_{-0.009}$	$4.569^{+0.007}_{-0.007}$	$4.189^{+0.018}_{-0.013}$	$4.538^{+0.043}_{-0.060}$
Global system parameters							
$\log(\text{age})$ [dex]		$8.972^{+0.037}_{-0.087}$				$8.804^{+0.033}_{-0.052}$	
[ $M/H$ ] [dex]		$0.322^{+0.073}_{-0.120}$				$0.220^{+0.041}_{-0.063}$	
$E(B - V)$ [mag]		$0.166^{+0.028}_{-0.018}$				$0.229^{+0.030}_{-0.020}$	
extra light $\ell_4$ [in <i>TESS</i> -band]		$0.033^{+0.032}_{-0.017}$				–	
$(M_V)_{\text{tot}}$		$0.37^{+0.02}_{-0.11}$				$2.07^{+0.07}_{-0.07}$	
distance [pc]		$656^{+13}_{-17}$				$712^{+14}_{-13}$	

*Notes.*  $\tau_0^{\text{inf/sup}}$  denotes the moment of an inferior or superior conjunction of the secondary (Ab) and the tertiary (B) along their inner and outer orbits, respectively. Superior conjunctions are noted with \*.

biguity of our solution. Out of our nine currently investigated systems, TIC 47151245 is the only one where we had neither RV data nor a good ETV curve to better constrain the system configuration. The latter resulted from the large scatter of the ETV points due to the shallow, grazing eclipses observed with *TESS* (the scatter of the ETV points exceed the full amplitude of the model ETV curve.) Therefore, strictly speaking, we cannot even be certain about the type of the one observed outer eclipse, in particular, whether it occurred during an inferior or superior conjunction of the tertiary. (In other words, we cannot be certain whether the third star was the eclipser or, if it was eclipsed.) What makes this question more ambiguous is that the surface brightnesses of stars *Aa* and *B* are very similar, and even star *Ab* has only a slightly smaller surface brightness. Hence, regardless of whether star *Aa* eclipses star *B* or, vice versa, in the case of similar geometries the eclipses look very similar. Hence, it was not surprising that by assuming a superior outer star conjunction for the *TESS* observed third-body eclipse event, and adding  $180^\circ$  to  $\omega_{\text{out}}$  (i.e., virtually rotating the outer orbit by  $180^\circ$  to get very similar geometric conditions), we were able to obtain another, almost similarly good, solution as for the inferior conjunction case, which is tabulated in Table 6. The substantial difference, however, between the two solutions is that, in this second case, to correctly model the relative depths of

the three consecutive dips of the third-body eclipse, we had to reverse the revolution of the stars along either the inner or outer orbit. (As a practical matter, we have chosen the outer orbit, setting the outer node to be  $\Omega_{\text{out}} \approx 213^\circ$ .) As a consequence, this solution results in a *retrograde* solution, with a mutual inclination of  $i_{\text{mut}} \approx 139^\circ$ . While, these latter solutions were found to be statistically slightly weaker than the prograde solutions (Table 6), in order to make a secure choice between the two scenarios, radial velocity measurements will be critical.

### 8.1.2 TIC 81525800

With a mean third-body eclipsing period of 47.8 days, this is one of two quite short outer period systems in this set of 9 triples. It has, by far, the most eccentric outer orbit among the set with  $e = 0.61$ . The outer orbit is securely mapped out with the *TESS* ETV curve (see Fig. 6) which covers one and a half outer orbital cycles.

The inner binary has a period of 1.6 days, and the period ratio of  $\sim 30$ , puts this system quite near the dynamically unstable regime. From estimates of what constitutes a stable triple system, the ratio of orbital periods must satisfy

$$P_{\text{out}} \gtrsim 4.7 \left( \frac{M_{\text{AB}}}{M_{\text{B}}} \right)^{1/10} \frac{(1 + e_{\text{out}})^{3/5}}{(1 - e_{\text{out}})^{9/5}} P_{\text{in}} \quad (1)$$



**Table 8.** The same as in Table 6 above, but for TIC 276162169 and TIC 280883908.

	TIC 276162169			TIC 280883908		
	orbital elements					
	subsystem			subsystem		
	Aa-Ab	A-B		Aa-Ab	A-B	
$t_0$ [BJD - 2400000]	58683.0			58983.0		
$P$ [days]	$2.549807^{+0.000016}_{-0.000017}$	$117.27^{+0.06}_{-0.04}$		$5.241768^{+0.000191}_{-0.000104}$	$184.598^{+0.020}_{-0.021}$	
$a$ [ $R_\odot$ ]	$13.27^{+0.22}_{-0.28}$	$186.4^{+3.1}_{-2.7}$		$17.57^{+0.14}_{-0.19}$	$224.1^{+2.7}_{-3.3}$	
$e$	$0.00108^{+0.00008}_{-0.00008}$	$0.2682^{+0.0048}_{-0.0044}$		$0.0008^{+0.0006}_{-0.0003}$	$0.2596^{+0.0011}_{-0.0012}$	
$\omega$ [deg]	$306^{+3}_{-5}$	$243.4^{+1.0}_{-1.3}$		$200^{+41}_{-84}$	$146.4^{+0.3}_{-0.3}$	
$i$ [deg]	$89.85^{+0.33}_{-0.35}$	$90.20^{+0.07}_{-0.43}$		$89.78^{+0.48}_{-0.60}$	$88.97^{+0.53}_{-0.20}$	
$\mathcal{T}_0^{\text{inf/sup}}$ [BJD - 2400000]	$58685.5242^{+0.0006}_{-0.0006}$	$58709.4798^{+0.0128*}_{-0.0120}$		$58984.9144^{+0.0003}_{-0.0003}$	$59010.7402^{+0.0429*}_{-0.0564}$	
$\tau$ [BJD - 2400000]	$58683.234^{+0.040}_{-0.031}$	$58636.77^{+0.42}_{-0.29}$		$58983.897^{+0.603}_{-1.217}$	$58843.704^{+0.138}_{-0.132}$	
$\Omega$ [deg]	0.0	$179.62^{+1.48}_{-0.60}$		0.0	$-1.58^{+2.37}_{-3.32}$	
$i_{\text{mut}}$ [deg]	$179.18^{+0.37}_{-0.54}$			$2.25^{+2.78}_{-1.41}$		
mass ratio [ $q = m_{\text{sec}}/m_{\text{pri}}$ ]	$0.865^{+0.006}_{-0.005}$	$0.310^{+0.009}_{-0.008}$		$0.931^{+0.016}_{-0.019}$	$0.674^{+0.020}_{-0.026}$	
$K_{\text{pri}}$ [ $\text{km s}^{-1}$ ]	$122.1^{+1.9}_{-2.1}$	$19.7^{+0.2}_{-0.2}$		$81.6^{+1.2}_{-1.0}$	$25.60^{+0.93}_{-0.93}$	
$K_{\text{sec}}$ [ $\text{km s}^{-1}$ ]	$141.3^{+2.6}_{-3.5}$	$63.8^{+1.3}_{-1.7}$		$87.8^{+1.0}_{-1.1}$	$38.01^{+0.05}_{-0.05}$	
$\gamma$ [ $\text{km s}^{-1}$ ]	...			$-29.34^{+0.01}_{-0.01}$		
	stellar parameters					
	Aa	Ab	B	Aa	Ab	B
	Relative quantities					
fractional radius [ $R/a$ ]	$0.1835^{+0.0005}_{-0.0005}$	$0.1522^{+0.0008}_{-0.0007}$	$0.0079^{+0.0001}_{-0.0001}$	$0.0903^{+0.0021}_{-0.0017}$	$0.0785^{+0.0019}_{-0.0016}$	$0.0588^{+0.0017}_{-0.0015}$
temperature relative to $(T_{\text{eff}})_{\text{Aa}}$	1	$0.9252^{+0.0060}_{-0.0037}$	$0.6918^{+0.0211}_{-0.0157}$	1	$0.9766^{+0.0061}_{-0.0074}$	$0.7030^{+0.0077}_{-0.0058}$
fractional flux [in <i>TESS</i> -band]	$0.5677^{+0.0042}_{-0.0045}$	$0.3387^{+0.0013}_{-0.0013}$	$0.0863^{+0.0031}_{-0.0029}$	$0.0479^{+0.0029}_{-0.0027}$	$0.0335^{+0.0018}_{-0.0019}$	$0.9186^{+0.0027}_{-0.0028}$
	Physical Quantities					
$m$ [ $M_\odot$ ]	$2.585^{+0.134}_{-0.169}$	$2.234^{+0.110}_{-0.132}$	$1.490^{+0.051}_{-0.048}$	$1.374^{+0.026}_{-0.048}$	$1.273^{+0.035}_{-0.037}$	$1.781^{+0.100}_{-0.113}$
$R$ [ $R_\odot$ ]	$2.437^{+0.042}_{-0.054}$	$2.022^{+0.040}_{-0.047}$	$1.471^{+0.035}_{-0.041}$	$1.586^{+0.037}_{-0.036}$	$1.377^{+0.041}_{-0.034}$	$13.174^{+0.479}_{-0.467}$
$T_{\text{eff}}$ [K]	$10087^{+411}_{-517}$	$9334^{+347}_{-419}$	$6972^{+164}_{-145}$	$6688^{+49}_{-60}$	$6523^{+35}_{-34}$	$4704^{+35}_{-34}$
$L_{\text{bol}}$ [ $L_\odot$ ]	$55.12^{+11.74}_{-12.39}$	$27.91^{+5.50}_{-5.83}$	$4.593^{+0.687}_{-0.605}$	$4.496^{+0.344}_{-0.299}$	$3.090^{+0.213}_{-0.196}$	$76.28^{+3.78}_{-3.81}$
$M_{\text{bol}}$	$0.42^{+0.28}_{-0.21}$	$1.16^{+0.25}_{-0.20}$	$3.11^{+0.15}_{-0.15}$	$3.14^{+0.07}_{-0.08}$	$3.55^{+0.07}_{-0.07}$	$0.06^{+0.06}_{-0.05}$
$M_V$	$0.66^{+0.17}_{-0.13}$	$1.25^{+0.19}_{-0.13}$	$3.07^{+0.16}_{-0.16}$	$3.11^{+0.08}_{-0.08}$	$3.53^{+0.08}_{-0.08}$	$0.48^{+0.07}_{-0.06}$
$\log g$ [dex]	$4.076^{+0.008}_{-0.010}$	$4.174^{+0.008}_{-0.006}$	$4.275^{+0.010}_{-0.006}$	$4.172^{+0.013}_{-0.016}$	$4.263^{+0.013}_{-0.014}$	$2.446^{+0.020}_{-0.020}$
	Global system parameters					
$\log(\text{age})$ [dex]	$8.468^{+0.096}_{-0.078}$			$9.256^{+0.059}_{-0.028}$		
$[M/H]$ [dex]	$0.159^{+0.027}_{-0.024}$			$0.030^{+0.053}_{-0.073}$		
$E(B - V)$ [mag]	$0.648^{+0.024}_{-0.036}$			$0.277^{+0.015}_{-0.025}$		
$(M_V)_{\text{tot}}$	$0.09^{+0.18}_{-0.13}$			$0.33^{+0.06}_{-0.05}$		
distance [pc]	$1235^{+40}_{-52}$			$1183^{+40}_{-40}$		

Notes.  $\mathcal{T}_0^{\text{inf/sup}}$  denotes the moment of an inferior or superior conjunction of the secondary (Ab) and the tertiary (B) along their inner and outer orbits, respectively. Superior conjunctions are noted with \*.

where equation (1) is from Rappaport et al. (2013), which in turn is based on the work of Mardling & Aarseth (2001) and Mikkola (2008). The numerical value of the right hand side of this equation is 58. By comparison, both the outer eclipsing period of 47.8 and the formal osculating period given in Table 6 of 49.7 days are actually below the stability line. One should keep in mind however, that Eq. (1) is strictly valid only for point-mass systems, and the non-negligible tidal interactions between the two components of the inner pair may act to stabilize the system. Given that the system is 2 Gyr old, and is manifestly stable, it would be worthwhile to study this problem via long-term numerical integration.

The outer and inner orbits are viewed within a couple of degrees of edge on, and the mutual inclination angle is  $\simeq 5^\circ$ . So, this is a fairly flat system viewed nearly edge on.

The masses of all three stars are close to  $1.4 M_\odot$  F stars, and are just slightly evolved away from the main sequence.

The photometric distance that we calculate is  $1718 \pm 60$  pc compared to Gaia's distance of  $1979 \pm 80$  pc. This amounts to a 2.6- $\sigma$  discrepancy, which we do not consider alarming.

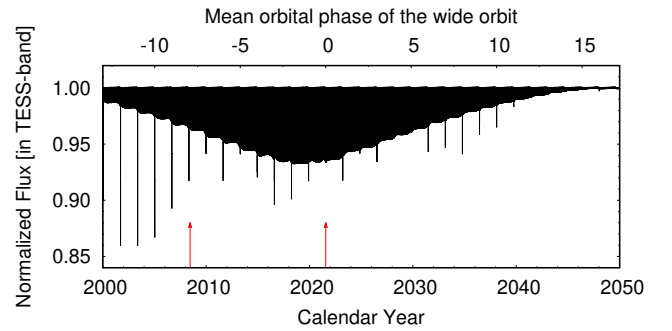


**Figure 16.** Photodynamical model lightcurve of TIC 99013269 for the epoch 2000-2050. The red arrows denote the position of the KELT and *TESS* third-body eclipses, respectively. See text for details.

### 8.1.3 TIC 99013269

This triple has the longest outer period in our current sample (604 days), and has the fifth longest outer period amongst

**Table 9.** The same as in Table 6 above, but for TIC 294803663 and TIC 332521671.

	TIC 294803663			TIC 332521671		
	orbital elements					
	subsystem			subsystem		
	Aa-Ab	A-B		Aa-Ab	A-B	
$t_0$ [BJD - 2400000]	58596.5			58571.0		
$P$ [days]	$2.245592^{+0.000008}_{-0.000006}$	$153.426^{+0.046}_{-0.047}$		$1.247934^{+0.000055}_{-0.000059}$	$48.5848^{+0.0062}_{-0.0038}$	
$a$ [ $R_\odot$ ]	$11.62^{+0.13}_{-0.10}$	$230.1^{+2.5}_{-2.0}$		$6.889^{+0.024}_{-0.025}$	$94.26^{+0.42}_{-0.47}$	
$e$	$0.0305^{+0.0019}_{-0.0018}$	$0.0299^{+0.0087}_{-0.0099}$		$0.0030^{+0.0021}_{-0.0016}$	$0.0041^{+0.0019}_{-0.0019}$	
$\omega$ [deg]	$127.1^{+3.4}_{-3.0}$	$313^{+9}_{-14}$		$229^{+17}_{-35}$	$311^{+34}_{-28}$	
$i$ [deg]	$86.10^{+0.88}_{-0.24}$	$88.65^{+0.08}_{-0.13}$		$87.85^{+0.48}_{-0.62}$	$85.43^{+0.31}_{-0.17}$	
$\mathcal{T}_0^{\text{inf/sup}}$ [BJD - 2400000]	$58598.5098^{+0.0003}_{-0.0003}$	$58629.0863^{+0.0132}_{-0.0131}$		$58571.3516^{+0.0003}_{-0.0002}$	$58583.3545^{+0.0571*}_{-0.1098}$	
$\tau$ [BJD - 2400000]	$58597.633^{+0.021}_{-0.019}$	$58493.1^{+3.2}_{-5.5}$		$58571.210^{+0.060}_{-0.120}$	$58568.5^{+4.7}_{-5.8}$	
$\Omega$ [deg]	0.0	$-0.05^{+2.77}_{-2.91}$		0.0	$-0.83^{+1.70}_{-1.67}$	
$i_{\text{mut}}$ [deg]	$3.07^{+1.58}_{-0.69}$			$2.80^{+0.84}_{-0.69}$		
mass ratio [ $q = m_{\text{sec}}/m_{\text{pri}}$ ]	$0.866^{+0.010}_{-0.010}$	$0.667^{+0.004}_{-0.006}$		$0.640^{+0.006}_{-0.006}$	$0.692^{+0.006}_{-0.007}$	
$K_{\text{pri}}$ [ $\text{km s}^{-1}$ ]	$121.3^{+1.6}_{-1.3}$	$30.4^{+0.4}_{-0.5}$		$109.0^{+0.7}_{-0.8}$	$39.99^{+0.38}_{-0.33}$	
$K_{\text{sec}}$ [ $\text{km s}^{-1}$ ]	$140.4^{+1.4}_{-1.6}$	$45.6^{+0.5}_{-0.4}$		$170.2^{+0.8}_{-1.0}$	$57.89^{+0.28}_{-0.13}$	
$\gamma$ [ $\text{km s}^{-1}$ ]	$-18.11^{+0.08}_{-0.08}$			$-15.63^{+0.04}_{-0.04}$		
	stellar parameters					
	Aa	Ab	B	Aa	Ab	B
	Relative quantities					
fractional radius [ $R/a$ ]	$0.2165^{+0.0037}_{-0.0042}$	$0.1705^{+0.0032}_{-0.0047}$	$0.0579^{+0.0010}_{-0.0008}$	$0.3615^{+0.0041}_{-0.0046}$	$0.1513^{+0.0019}_{-0.0017}$	$0.0888^{+0.0015}_{-0.0058}$
temperature relative to $(T_{\text{eff}})_{\text{Aa}}$	1	$0.9422^{+0.0065}_{-0.0061}$	$0.5694^{+0.0065}_{-0.0094}$	1	$0.8643^{+0.0074}_{-0.0073}$	$0.7091^{+0.0055}_{-0.0048}$
fractional flux [in <i>TESS</i> -band]	$0.1597^{+0.0034}_{-0.0034}$	$0.0863^{+0.0030}_{-0.0034}$	$0.7541^{+0.0027}_{-0.0027}$	$0.1984^{+0.0047}_{-0.0048}$	$0.0225^{+0.0006}_{-0.0005}$	$0.7006^{+0.0171}_{-0.0649}$
	Physical Quantities					
$m$ [ $M_\odot$ ]	$2.240^{+0.068}_{-0.067}$	$1.932^{+0.071}_{-0.047}$	$2.776^{+0.103}_{-0.088}$	$1.717^{+0.015}_{-0.024}$	$1.098^{+0.013}_{-0.012}$	$1.941^{+0.037}_{-0.035}$
$R$ [ $R_\odot$ ]	$2.520^{+0.047}_{-0.058}$	$1.975^{+0.065}_{-0.040}$	$13.36^{+0.19}_{-0.19}$	$2.490^{+0.029}_{-0.030}$	$1.043^{+0.015}_{-0.014}$	$8.371^{+0.165}_{-0.580}$
$T_{\text{eff}}$ [K]	$8694^{+98}_{-199}$	$8152^{+129}_{-117}$	$4902^{+91}_{-5.12}$	$6978^{+55}_{-44}$	$6039^{+41}_{-62}$	$4946^{+43}_{-33}$
$L_{\text{bol}}$ [ $L_\odot$ ]	$32.21^{+2.83}_{-3.26}$	$15.66^{+1.44}_{-1.38}$	$94.61^{+5.12}_{-6.52}$	$13.23^{+0.35}_{-0.39}$	$1.293^{+0.069}_{-0.064}$	$37.41^{+1.59}_{-3.38}$
$M_{\text{bol}}$	$1.00^{+0.12}_{-0.09}$	$1.78^{+0.10}_{-0.10}$	$-0.17^{+0.08}_{-0.06}$	$1.97^{+0.03}_{-0.03}$	$4.49^{+0.05}_{-0.06}$	$0.84^{+0.10}_{-0.05}$
$M_V$	$0.99^{+0.10}_{-0.08}$	$1.73^{+0.09}_{-0.09}$	$0.14^{+0.08}_{-0.06}$	$1.91^{+0.03}_{-0.03}$	$4.51^{+0.06}_{-0.06}$	$1.12^{+0.09}_{-0.05}$
$\log g$ [dex]	$3.987^{+0.014}_{-0.016}$	$4.129^{+0.013}_{-0.010}$	$2.631^{+0.015}_{-0.018}$	$3.878^{+0.012}_{-0.010}$	$4.441^{+0.007}_{-0.008}$	$2.881^{+0.053}_{-0.012}$
	Global system parameters					
$\log(\text{age})$ [dex]	$8.734^{+0.064}_{-0.056}$			$9.155^{+0.016}_{-0.013}$		
$[M/H]$ [dex]	$0.230^{+0.056}_{-0.081}$			$0.057^{+0.051}_{-0.042}$		
$E(B - V)$ [mag]	$0.631^{+0.018}_{-0.019}$			$0.088^{+0.025}_{-0.016}$		
extra light $\ell_4$ [in <i>TESS</i> -band]	...			$0.080^{+0.061}_{-0.020}$		
$(M_V)_{\text{tot}}$	$-0.43^{+0.09}_{-0.06}$			$0.66^{+0.06}_{-0.04}$		
distance [pc]	$1739^{+24}_{-26}$			$799^{+15}_{-47}$		

Notes.  $\mathcal{T}_0^{\text{inf/sup}}$  denotes the moment of an inferior or superior conjunction of the secondary (Ab) and the tertiary (B) along their inner and outer orbits, respectively. Superior conjunctions are noted with \*.

all the securely known triply eclipsing triples (see [Borkovits 2022](#), Table 1). Despite the fact that *TESS* observed only one outer eclipse, and our RV data cover only about half of a complete outer cycle, we were able to determine the outer period very robustly (with an accuracy of about 10 minutes). This is due to the fact that the KELT survey observed one third-body outer eclipse on three subsequent nights around 1st May 2008, i.e., eight outer orbital cycles earlier than the *TESS* third-body eclipse. Comparing the two third-body events (uppermost right panel of Fig. 1) one will readily note two substantial differences. First, the KELT third-body eclipse had a substantially longer duration than the *TESS* event. Second, despite the fact that both third-body eclipses have a flat bottom, i.e. they are total eclipses, the KELT event is far deeper, substantially exceeding the depths of the regular EB eclipses. By contrast, in the case of the *TESS* event, the depth of the extra dip is in between the eclipse depths of the inner EB's primary and secondary eclipses.

These changing outer eclipse properties can be explained by the fact that, during the KELT event, the giant tertiary star totally eclipsed both members of the inner EB, while in

the case of the *TESS* event, only the secondary component (star *Ab*) was eclipsed. This is a direct consequence of the remarkably inclined nature of the two orbital planes. Our results reveal robustly a mutual inclination of  $i_{\text{mut}} = 20^\circ \pm 0^\circ.6$  and, moreover, we obtained a relative position of the nodes ( $\Delta\Omega = \Omega_{\text{out}} = 20^\circ.1 \pm 0^\circ.6$ ) for the epoch of (the beginning of) the *TESS* observations, which leads to quite unequal eclipse probabilities for the two nearly equally massive inner stars, than for the  $\Delta\Omega \approx 0^\circ$  case.

The mutual inclination of  $i_{\text{mut}} = 20^\circ$  predicts an orbital plane precession with a period of  $P_{\text{node}} \sim 322 \pm 2$  years. We plot the *TESS*-band model lightcurve for the first half of the current century in Fig. 16. As one can see, at the very beginning of the new millennium the inner EB exhibited only very grazing eclipses, while in the same timeframe, the third-body eclipses reached their maximum depths and durations (these durations cannot be resolved in the figure). Then, the depths of the regular eclipses increased continuously until circa 2018, when the inner orbit was seen exactly edge-on. Currently both the inner and third-body eclipse depths show a decrease

**Table 10.** The same as in Table 6 above, but for TIC 356324779.

TIC 356324779			
orbital elements			
	subsystem		
	Aa–Ab	A–B	
$t_0$ [BJD - 2400000]	58816.0		
$P$ [days]	$3.47167^{+0.00013}_{-0.00009}$	$87.092^{+0.017}_{-0.018}$	
$a$ [ $R_\odot$ ]	$14.66^{+0.30}_{-0.23}$	$146.27^{+3.37}_{-2.68}$	
$e$	$0.00032^{+0.00012}_{-0.00012}$	$0.2836^{+0.0030}_{-0.0042}$	
$\omega$ [deg]	$66^{+9}_{-13}$	$143.9^{+0.5}_{-0.6}$	
$i$ [deg]	$90.08^{+0.50}_{-0.89}$	$89.28^{+0.13}_{-0.08}$	
$\tau_0^{\text{inf/sup}}$ [BJD - 2400000]	$58819.18605^{+0.00006}_{-0.00006}$	$58837.6027^{+0.0021*}_{-0.0021}$	
$\tau$ [BJD - 2400000]	$58817.213^{+0.086}_{-0.132}$	$58757.967^{+0.124}_{-0.143}$	
$\Omega$ [deg]	0.0	$-0.87^{+0.39}_{-0.27}$	
$i_{\text{mut}}$ [deg]	$1.26^{+0.41}_{-0.60}$		
mass ratio [ $q = m_{\text{sec}}/m_{\text{pri}}$ ]	$0.984^{+0.005}_{-0.004}$	$0.573^{+0.013}_{-0.015}$	
$K_{\text{pri}}$ [ $\text{km s}^{-1}$ ]	$106.1^{+2.2}_{-1.6}$	$32.4^{+1.3}_{-1.1}$	
$K_{\text{sec}}$ [ $\text{km s}^{-1}$ ]	$107.8^{+2.4}_{-1.7}$	$56.2^{+0.9}_{-0.5}$	
stellar parameters			
	Aa	Ab	B
Relative quantities			
fractional radius [ $R/a$ ]	$0.1372^{+0.0010}_{-0.0014}$	$0.1330^{+0.0011}_{-0.0014}$	$0.0198^{+0.0006}_{-0.0005}$
temperature relative to $(T_{\text{eff}})_{\text{Aa}}$	1	$0.9949^{+0.0024}_{-0.0027}$	$0.9977^{+0.0214}_{-0.0425}$
fractional flux [in <i>TESS</i> -band]	$0.2146^{+0.0037}_{-0.0028}$	$0.1987^{+0.0039}_{-0.0025}$	$0.4339^{+0.0362}_{-0.0298}$
fractional flux [in $R_C$ -band]	$0.2321^{+0.0035}_{-0.0033}$	$0.2149^{+0.0033}_{-0.0028}$	$0.4711^{+0.0407}_{-0.0427}$
Physical Quantities			
$m$ [ $M_\odot$ ]	$1.768^{+0.111}_{-0.082}$	$1.740^{+0.108}_{-0.078}$	$2.022^{+0.181}_{-0.139}$
$R$ [ $R_\odot$ ]	$2.014^{+0.054}_{-0.047}$	$1.958^{+0.052}_{-0.056}$	$2.909^{+0.688}_{-0.069}$
$T_{\text{eff}}$ [K]	$7921^{+191}_{-152}$	$7877^{+202}_{-140}$	$7734^{+346}_{-146}$
$L_{\text{bol}}$ [ $L_\odot$ ]	$14.27^{+1.17}_{-1.24}$	$13.21^{+1.07}_{-1.15}$	$27.36^{+8.23}_{-2.53}$
$M_{\text{bol}}$	$1.88^{+0.10}_{-0.09}$	$1.97^{+0.10}_{-0.08}$	$1.18^{+0.10}_{-0.29}$
$M_V$	$1.83^{+0.10}_{-0.09}$	$1.92^{+0.10}_{-0.09}$	$1.12^{+0.11}_{-0.29}$
$\log g$ [dex]	$4.080^{+0.011}_{-0.008}$	$4.099^{+0.010}_{-0.007}$	$3.815^{+0.038}_{-0.031}$
Global system parameters			
$\log(\text{age})$ [dex]	$8.966^{+0.078}_{-0.102}$		
$[M/H]$ [dex]	$0.073^{+0.058}_{-0.240}$		
$E(B - V)$ [mag]	$0.381^{+0.008}_{-0.008}$		
extra light $\ell_4$ [in <i>TESS</i> -band]	$0.152^{+0.030}_{-0.040}$		
extra light $\ell_4$ [in $R_C$ -band]	$0.081^{+0.045}_{-0.039}$		
$(M_V)_{\text{tot}}$	$0.37^{+0.09}_{-0.19}$		
distance [pc]	$2440^{+197}_{-178}$		

*Notes.*  $\tau_0^{\text{inf/sup}}$  denotes the moment of an inferior or superior conjunction of the secondary (Ab) and the tertiary (B) along their inner and outer orbits, respectively. Superior conjunctions are noted with \*.

ing tendency<sup>8</sup> and, incidentally, both kinds of eclipses will disappear at the same time around 2049.

Finally, note that this is the only system in our sample for which Gaia gives an astrometric solution. We compare two parameters,  $e_{\text{out}}$  and  $i_{\text{out}}$  between our photodynamical, and Gaia's astrometric solutions, and note that we did not utilize either of these in our fit. We find  $e_{\text{out}} = 0.463 \pm 0.005$  compared to Gaia's value of  $e_{\text{out}} = 0.458 \pm 0.026$ , and  $i_{\text{out}} = 92.3^\circ \pm 0.08^\circ$  vs. Gaia's value of  $i_{\text{out}} = 92.0^\circ \pm 0.8^\circ$ . These are both in excellent agreement.

<sup>8</sup> In the case of third-body eclipses we can only talk about a tendency instead of a monotonic variation. For example, the forthcoming third-body eclipse that will occur around 21-23 March 2023 is expected to be deeper than the one detected by *TESS*. The reason is that next spring the third star will totally eclipse the hotter primary (i.e. *Aa*) instead of the secondary (*Ab*) of the inner pair.

We find masses and radii for the stars in this system of  $M_{\text{Aa}} = 1.65 M_\odot$ ,  $M_{\text{Ab}} = 1.53 M_\odot$ , and  $M_{\text{B}} = 2.37 M_\odot$ , with an evolved radius for the tertiary of  $11.5 R_\odot$ , which Gaia is not able to provide.

#### 8.1.4 TIC 229785001

As far as the triple-system portion of TIC 229785001 goes, this is a rather flat system viewed nearly edge on, with  $i_{\text{out}} = 89.2^\circ$  and  $i_{\text{mut}} = 3^\circ$ . The three stars combined have the lowest total mass of any of our 9 current systems, with  $M_{\text{Aa}} = 1.3 M_\odot$ ,  $M_{\text{Ab}} = 0.95 M_\odot$ , and  $M_{\text{B}} = 1.6 M_\odot$ .

Perhaps the most interesting thing about this system is that the ETV curve (see Fig. 8) clearly reveals that the triple system has another star (or stars) orbiting it with a very long period (likely more than 5 years). This can be inferred from the overall parabolic trend in the ETV curve which is

superposed on the triple orbital period of 165 days. In fact, when this 4th star is introduced into the photodynamical analysis, the formal solution suggests an outermost period of  $\sim 8.9 \pm 0.5$  years (see Table 7; but we note that the actual uncertainty in this period may be substantially larger). If this is indeed a quadruple system with a 2+1+1 configuration, the ratio of the outermost period to the triple’s period could be as low as  $\sim 20$ , and dynamical interactions between the 4th star and the inner triple could be quite significant.

Because of the presence of the fourth body, we thought it would be good to check the full outer orbital solution parameters (of the triple) from Gaia with those from our photodynamical fit, along with the uncertainties:  $P_{\text{out}} = 166.0 \pm 0.5$ ,  $e_{\text{out}} = 0.49 \pm 0.05$ ,  $\omega_{\text{out}} = 15.9^\circ \pm 0.5^\circ$ , and  $K_{\text{ter}} = 34.3 \pm 1.7$  km s $^{-1}$  for Gaia and  $P_{\text{out}} = 165.37 \pm 0.02$ ,  $e_{\text{out}} = 0.46 \pm 0.02$ ,  $\omega_{\text{out}} = 31^\circ \pm 3^\circ$ , and  $K_{\text{ter}} = 40 \pm 0.5$  km s $^{-1}$  from our photodynamical fit. These are in reasonable agreement, but the discrepancies in  $\omega_{\text{out}}$  and that of  $K_{\text{ter}}$  are at the 5 and 3  $\sigma$  levels.

### 8.1.5 TIC 276162169 = V493 Cyg

The TIC 276162169 system may be the most interesting of the current set of 9 triples. From the photodynamical models, which incorporate a somewhat sparsely sampled, but very useful, ETV curve, the outer orbit appears to be retrograde with respect to the inner binary, with a formal value for the mutual inclination angle of  $i_{\text{mut}} = 179.2 \pm 0.5$ . While both orbital inclination angles are within a fraction of a degree of  $90^\circ$ , the photodynamical fit is distinctly superior for a retrograde outer orbit than for a prograde orbit.<sup>9</sup>

The other unique thing about this system, at least among the current set of 9 triples, is that the tertiary star is distinctly lower in mass than either of the two stars in the binary:  $M_{\text{Aa}} = 2.6 \pm 0.2 M_\odot$ ,  $M_{\text{Ab}} = 2.2 \pm 0.1 M_\odot$ , and  $M_{\text{B}} = 1.49 \pm 0.05 M_\odot$ . The system is also relatively young at 300 Myr.

Due to the potentially important finding of an outer retrograde orbit, we would like to see this confirmed with a good set of radial velocity measurements. At  $G = 12$  this should not be particularly challenging.

Finally, we note that before our current analysis, which is based on the high-precision *TESS* observations, this system was misclassified as a semi-detached, classic Algol-type EB with a period of exactly half the actual eclipsing period (see, e. g. Budding et al. 2004; Samus et al. 2017). The origin of this misclassification might have come from the fact that the primary and secondary eclipses have nearly the same depths, which made them largely indistinguishable in the lesser quality ground-based observations. What is more interesting, however, is that in these catalogs, in addition to the 0.5 mag primary eclipse depth, a shallow 0.1 mag secondary eclipse amplitude is also reported. In our interpretation, this

<sup>9</sup> In contrast to TIC 47151245, in this case the ETV curve, which has contributions from both LTTE and dynamical effects that are of the same order of magnitude, clearly reveals that of the two sets of *TESS* observed third-body eclipses, the first one (in Sector 14) occurred during a superior conjunction of the tertiary star, while the second one (in Sector 55) happened around its inferior conjunction. Thus, the type of ambiguity that occurred in the triple system TIC 47151245, does not exist here.

fact might indicate an historical observation of a third-body event which was probably thought to be a secondary eclipse – most likely reported by Eva Ahnert-Rohlfs about 70 years ago (Hoffmeister et al. 1954).

### 8.1.6 TIC 280883908

TIC 280883908 has one of the most robustly determined sets of system parameters among our set of 9 systems thanks to the availability of RV data, a meaningful ETV curve, and the detection of both types of outer eclipses in the archival data. The outer orbital period is 184.2 days, with a medium-level outer eccentricity 0.260. The EB period is 5.4218 days. The tertiary in the system is also one of the two largest among our collection, with  $R_B = 13.2 \pm 0.5 R_\odot$ . The mutual inclination angle is  $i_{\text{mut}} = 2.3^\circ$ , but with uncertainties that make it still consistent with  $0^\circ$ .

The tertiary, with a mass of  $1.78 M_\odot$ , has evolved substantially off the main sequence while the EB primary, at  $1.37 M_\odot$ , is only slightly evolved. The SED fit is in agreement with the full photodynamical fit, and it yields  $R_B = 14.3 \pm 2.3 R_\odot$ , which is quite consistent with the photodynamical analysis value for  $R_B$ . All of the masses deduced from the SED alone are in excellent agreement with the photodynamical results.

Because this system is so well diagnosed, we compare the full outer orbital solution parameters from Gaia with those from our photodynamical fit with the uncertainties:  $P_{\text{out}} = 184.12 \pm 0.07$ ,  $e_{\text{out}} = 0.256 \pm 0.004$ ,  $\omega_{\text{out}} = 142^\circ \pm 1^\circ$ , and  $K_{\text{ter}} = 38.06 \pm 0.17$  km s $^{-1}$  for Gaia and  $P_{\text{out}} = 184.35 \pm 0.02$ <sup>10</sup>,  $e_{\text{out}} = 0.260 \pm 0.001$ ,  $\omega_{\text{out}} = 146.4^\circ \pm 0.3^\circ$ , and  $K_{\text{ter}} = 38.01 \pm 0.05$  km s $^{-1}$  from our photodynamical fit. These are in substantial agreement, but the uncertainties on the photodynamical parameters are several times smaller than for Gaia.

The distance from the full photodynamical fit is  $1183 \pm 40$  pc, and  $1275 \pm 180$  pc from the SED fit alone. These are to be compared to the Gaia distance of  $3072_{-900}^{+2200}$  pc, but Gaia reports a very large RUWE value of 9.8, so we are rather more confident of the photometric distance. The fitted  $E(B - V)$  is close to 0.30, while we had no cataloged working value to start with. The age of the system is found to be 1800 Myr.

### 8.1.7 TIC 294803663

TIC 294803663 is one of two of our systems (along with TIC 280883908) that has a quite evolved tertiary star with  $R_B = 13.4 \pm 0.2 R_\odot$ . The masses are all comparable at:  $M_{\text{Aa}} = 2.24 \pm 0.07 M_\odot$ ,  $M_{\text{Ab}} = 1.93 \pm 0.07 M_\odot$ , and  $M_{\text{B}} = 2.8 \pm 0.1 M_\odot$ . However, the extra few tenths of a solar mass are just sufficient to have allowed the tertiary to become substantially evolved, while the EB stars are still near the main sequence.

The system is quite flat ( $i_{\text{mut}} = 3.1_{-0.7}^{+1.6}$ ) and viewed nearly edge on with  $i_{\text{out}} = 88.7 \pm 0.1$ . The outer orbital eccentricity is fairly small at  $e_{\text{out}} = 0.030 \pm 0.010$ . The outer period of  $153.43 \pm 0.05$  days and the outer eccentricity are in good agreement with the corresponding Gaia values of  $P_{\text{out}} = 153.1 \pm 0.2$  d and  $e_{\text{out}} = 0.047 \pm 0.01$ . However, our value for the outer argument of periastron of  $\omega_{\text{out}} = 313 \pm 14$  is not in complete accord with Gaia’s value of  $\omega_{\text{out}} = 252 \pm 18$ ,

<sup>10</sup> Note that this is the outer eclipsing period (see Table 11)

even given the large uncertainty in the Gaia value. Our photodynamical distance and Gaia’s compare very favorably at  $1739 \pm 26$  pc and  $1770 \pm 55$  pc, respectively.

One of more unusual features of this system, among our collection, is that there are prominent stellar pulsations (see Fig. 12) which we believe are from the giant tertiary star. We reach this conclusion because (i) the EB is completely blocked during the *TESS* third body event and the pulsations are still present, and (ii) the giant tertiary comprises 75% of the system flux, and only this is likely to accommodate the observed large pulsation amplitude.

### 8.1.8 TIC 332521671

TIC 332521671 is the second of our systems with a short outer orbital period of 48.5 days, similar to that of TIC 81525800. But, in this case, the tertiary star is quite evolved with  $R = 8.4 R_{\odot}$ , compared to that of TIC 81525800 where the tertiary star is still only barely evolved away from the MS.

For this system, we have a nicely sampled RV curve with 11 points around the outer orbit, as well as an ETV curve with a reasonable fraction of the outer orbit sampled on each of two occasions separated by two years. The remarkable thing about this system is the extremely small outer orbital eccentricity of  $e_{\text{out}} = 0.004 \pm 0.002$ . It seems likely that the combination of a short outer orbital period and a large radius for the tertiary has led to tidal circularization.

While the mutual inclination angle is small ( $i_{\text{mut}} = 3^{\circ}$ ), i.e., the system is flat, we are actually viewing the outer orbit  $5^{\circ}$  from edge on. It is the large radius of the tertiary which still allows the outer eclipses to be observed.

Here we briefly discuss the reliability of the rapid dynamically-forced apsidal motion that is suggested by our photodynamical solution (see bottom panel of Fig. 13). One should be cautious about accepting this at face value after noticing that during both sections of the ETV curves—where actual observations are available—one does not observe divergent ETV curves, but rather, the primary and secondary ETV curves overlap each other. In order to investigate this issue, we carried out further numerical integrations by setting the osculating inner eccentricity strictly to zero<sup>11</sup> at epoch  $t_0$ . The only parameter that we modified in the different new runs was the apsidal motion parameter ( $k_2$ ) of each star, thereby controlling the magnitude of the tidal contribution to the motion of the stars. This included the ( $k_2 = 0$ ) case as well, which literally means that we omitted the tidal contribution during the integration of the motion of the three stars, considering them to be point masses. What we found is that all MCMC runs converged to solutions with very similar system parameters, and the ETV curves fit well the observed ETV points. But the fits exhibited different kinds of “apsidal motion” behaviour during the non-constrained sections (i.e., where there are no data). Hence, our conclusion is that the apparent low amplitude, but rapid, dynamically-forced apsidal motion is only some numerical artefact which is the

<sup>11</sup> One should keep in mind, however, that for a perturbed triple system the osculating eccentricity cannot remain zero for all times. The same is true for tidally distorted stars and, especially for the present combination of them, as was discussed, e.g., in Kiseleva et al. (1998) and Borkovits et al. (2002).

consequence of the insufficient data coverage in the case of this practically circular eclipsing binary ( $e \simeq 0.003$ ).

### 8.1.9 TIC 356324779

TIC 356324779 yielded one of the two most useful outer orbit folds based on the ASAS-SN and ATLAS archival data (the other being TIC 47151245; see Fig. 4). For TIC 356324779 we clearly see both primary and secondary outer eclipses during the 86.65-day outer orbit. From the eclipse spacing we find that  $e_{\text{out}} \cos \omega_{\text{out}} = 0.22$ . This is in terrific accord with our photodynamical solution of  $e_{\text{out}} = 0.284$  and  $\omega_{\text{out}} = 144^{\circ}$ .

The system is rather flat ( $i_{\text{mut}} = 1.3^{\circ} \pm 0.5^{\circ}$ ) and viewed very close to exactly edge on with  $i_{\text{in}} = 90.1^{\circ}$  and  $i_{\text{out}} = 89.3^{\circ}$ . The masses are all fairly similar, with the tertiary being more massive by only  $0.25 M_{\odot}$ :  $M_{\text{Aa}} = 1.8 M_{\odot}$ ,  $M_{\text{Ab}} = 1.7 M_{\odot}$ , and  $M_{\text{B}} = 2.0 M_{\odot}$ .

## 8.2 Common Properties

The nine triply eclipsing triples we report on here have a number of properties in common, though they differ in some important details. Here we mention briefly some of their shared characteristics and differences.

The outer orbital periods of the 9 triples range from 47.8 days to 604 days, with two shorter than 50 days and two longer than 250 days. The outer orbital eccentricities range from 0.004 to 0.61, with no obvious correlation between  $P_{\text{out}}$  and  $e_{\text{out}}$ . Since the outer orbital semi-major axes range from  $\sim 1/2$  to 2 AU, we consider all of them to be ‘close’ systems, but they are not particularly ‘tight’ in the sense of having a small value of  $P_{\text{out}}/P_{\text{in}}$ , with ratios in the range of 25-230.

All of the 9 triples are observed rather edge-on with respect to the outer orbit with values of  $i_{\text{out}}$  differing from  $90^{\circ}$  by between  $0.2^{\circ}$  and  $4.5^{\circ}$ . The latter, of course, is something of a selection effect since we were searching for outer orbit eclipses. Seven of the nine triples are rather flat, with  $i_{\text{mut}} \lesssim 5^{\circ}$ . However, the remaining two systems have distinctly misaligned orbits with  $i_{\text{m}} = 20^{\circ}, 40^{\circ}$ . One of the flat systems, TIC 276162169, however, presents the exciting possibility of a compact triple with a retrograde outer orbit, as the preferred photodynamical solution gives mutual inclination of  $i_{\text{mut}} = 179^{\circ}$ . Note, while we are fairly certain of this result, we would like to see it confirmed by further measurements of TIC 276162169.

All the tertiary masses lie in the range of 1.4-2.8  $M_{\odot}$ , with a mean of 1.95  $M_{\odot}$ . Four of the tertiary stars are substantially evolved away from the main sequence, with radii of 8, 11, 13, and 13  $R_{\odot}$  with  $T_{\text{eff}}$  in the range of 4700-4950 K<sup>12</sup>. Three other tertiaries are mildly evolved off the MS. In all cases except for TIC 276162169, the tertiary is either the most

<sup>12</sup> In a small minority of our systems, we cannot exclude the possibility that the tertiary might have ascended the RGB and then returned to near the horizontal branch (HB). However, this is possible only in those cases where the tertiary does not overflow its Roche lobe at the tip of the RGB, which is allowed in only three of the four systems where the tertiary happens to be located near the HB. A detailed investigation of this question is outside the scope of this paper, and whether one or more of the tertiaries is actually on the HB is largely inconsequential for the determinations of our stellar and orbital parameters.

massive of three stars, or close to the mass of binary star *Aa*. By contrast, in TIC 276162169, the tertiary mass is only  $1.49 M_{\odot}$ , while the EB stars are considerably more massive at 2.2 and  $2.6 M_{\odot}$ . The fact that a fair fraction of the tertiary stars are evolved is a selection effect in that larger tertiary stars make it more likely to exhibit third-body eclipses, while at the same time the EB stars cannot grow too large without overflowing their Roche lobes.

The range of the 18 stellar masses in the 9 EBs is  $0.95\text{--}2.6 M_{\odot}$ , which is not so different from the range of tertiary masses. However, as mentioned above, in all but one case, the tertiary manages to be the most massive star in the system, even if not by much.

We find that the ages of the 9 triples lie in the range of  $0.3\text{--}2.5$  Gyr, with 7 of the systems older than 1 Gyr. Thus, the systems are nearly as old as is required for the most massive star to start its ascent of the giant branch, thereby enhancing the detection probability, while avoiding Roche lobe overflow in the EB. This is consistent with the intermediate mass stars we are observing.

Finally, we note that eight of the triples in this collection show no evidence for any stars other than the three stellar components of the triple. This includes looking for non-linear behavior in our ETV curves beyond those induced by the tertiary star on the EB, and by checking Gaia for any bound companion over a separation range of  $0.5''$  to  $20''$ , and down to 4 magnitudes fainter than the triple. On the other hand, TIC 229785001 clearly includes at least one other bound star, making this a somewhat rare  $2+1+1$  hierarchical quadruple.

## 9 SUMMARY AND DISCUSSION

In this work we have presented 9 compact triply eclipsing triples with a full evaluation of their system parameters – both stellar and orbital. We found all of these by searching through millions of *TESS* photometric lightcurves looking for third body eclipses in binary systems (see e.g., Kristiansen et al. 2022; Rappaport et al. 2022). While we were carrying out the research for this paper, the outer eclipses in four of them were also found independently by Zasche et al. (2022), but no further analyses of them were carried out in that work. For four of the systems, Gaia has measured the radial velocities of the outer orbit of the tertiary (in three cases), or the photocenter of the system (in one case). No other analyses were done, nor was there any way to use the Gaia data to even know that one of the components in the system was a binary.

We utilized the *TESS* photometric lightcurve, the ETV points derived from the lightcurve, archival SED data, archival photometry from ASAS-SN and ATLAS, and in some cases, ground-based follow up RV observations as well as eclipse photometry. These were combined in a complex photodynamical analysis where we solve for all the system parameters, as well as the distance to the source. Typical uncertainties on the masses and radii are in the range of a couple of per cent to not much more than  $\sim 5$  per cent. Uncertainties on the angles associated with the orbital planes (e.g.,  $i_{\text{out}}$  and  $i_{\text{mut}}$ ) range from a fraction of a degree to about a degree. All of the many system parameters that we have solved for, and the associated uncertainties, are given in Tables 6 through 10.

In Fig. 17 we present a set of correlation plots for some of the physically interesting parameters associated with our collection of triply eclipsing triples. To the nine sources we have studied in this work, we add the six triples from our previous closely related paper (Rappaport et al. 2022), as well as seven triples studied in Borkovits et al. (2019a, 2020b, 2022a,b), and Mitnyan et al. (2020) using largely the same selection criteria and methods of analysis.

The plot of  $P_{\text{in}}$  vs  $P_{\text{out}}$  shows that the bulk of the outer periods range from 48–285 days, while the inner periods span  $\sim 0.8\text{--}7$  days. The dotted diagonal line represents the dynamical stability limit taken from Eqn. (1) for a nominal case where  $e_{\text{out}} \simeq 0.3$ . Most systems stay comfortably away from this limit.

The top middle panel in Fig. 17 shows how  $e_{\text{out}}$  varies with  $P_{\text{out}}$ . In general, there is little correlation, except to note that for the most circular outer orbits, the outer periods tend to be relatively short. The circularization is likely brought about by tidal damping with an evolved tertiary.

The top right panel of Fig. 17 shows the inclination angle of the outer orbit vs. the mutual inclination angle of the inner binary vs. the outer orbit. The fact that most of the values of  $i_{\text{out}}$  hover near  $90^\circ$  is due to selection effects since these triples were discovered by searching for third-body eclipses. To a lesser extent, the same selection also holds for the alignment of the inner binary, otherwise third body eclipses would be somewhat more difficult to detect, but this is mitigated by the smaller values of orbital separations in the EB more so than for the outer orbit. Two of the systems have large enough  $i_{\text{mut}}$  ( $20^\circ$  and  $40^\circ$ ) to undergo serious precession of their orbital planes, where the one with the larger tilt (TIC 47151245) is, in principle, potentially subject to ZLK cycles (but see the discussion in Sect. 8.1.1). Finally, there is one triple (TIC 276162169) in a nearly flat system, but where the outer orbit is *retrograde* with respect to the inner EB. These are rare systems (see Sect. 8.1.5).

The  $q_{\text{in}}$  vs.  $q_{\text{out}}$  plot (lower left panel in Fig. 17) shows two noteworthy features. First, most of the inner EBs have mass ratios not far from unity, with a mean of 0.87. This may say more about the intrinsic mass ratio distribution in EBs, than anything necessarily to do with triple stars. On the other hand, it may be predictable from the accretion scenario for forming triple-star systems (Tokovinin & Moe 2020). Second, and more interesting, is that the ratio of  $q_{\text{out}} \equiv M_{\text{B}}/M_{\text{EB}}$  never exceeds unity (and not just by definition) and has a mean value of 0.66. This strongly favors the accretion formation scenario of triples (see Offner et al. 2022, for a recent review), and is not obviously caused by any selection effects.

The relation between the tertiary mass and its radius is shown in the bottom middle panel of Fig. 17. Some 8 of the stars are fairly well clustered not too far from the main sequence, crudely represented by the  $R = M$  line shown in the figure. However, the other 14 of the tertiary stars are distinctly evolved away from the main sequence. That is due both to an observational selection effect (larger stellar radii lead to more probable third body eclipses), as well as to the physical limitation whereby only the tertiary can grow this large (the EB stars are confined to their Roche lobes in relatively close orbits).

The age distribution of the systems is shown in the bottom right panel of Fig. 17. All but three of the systems have ages between  $1/2$  and 5 Gyr. The biggest exception is TIC

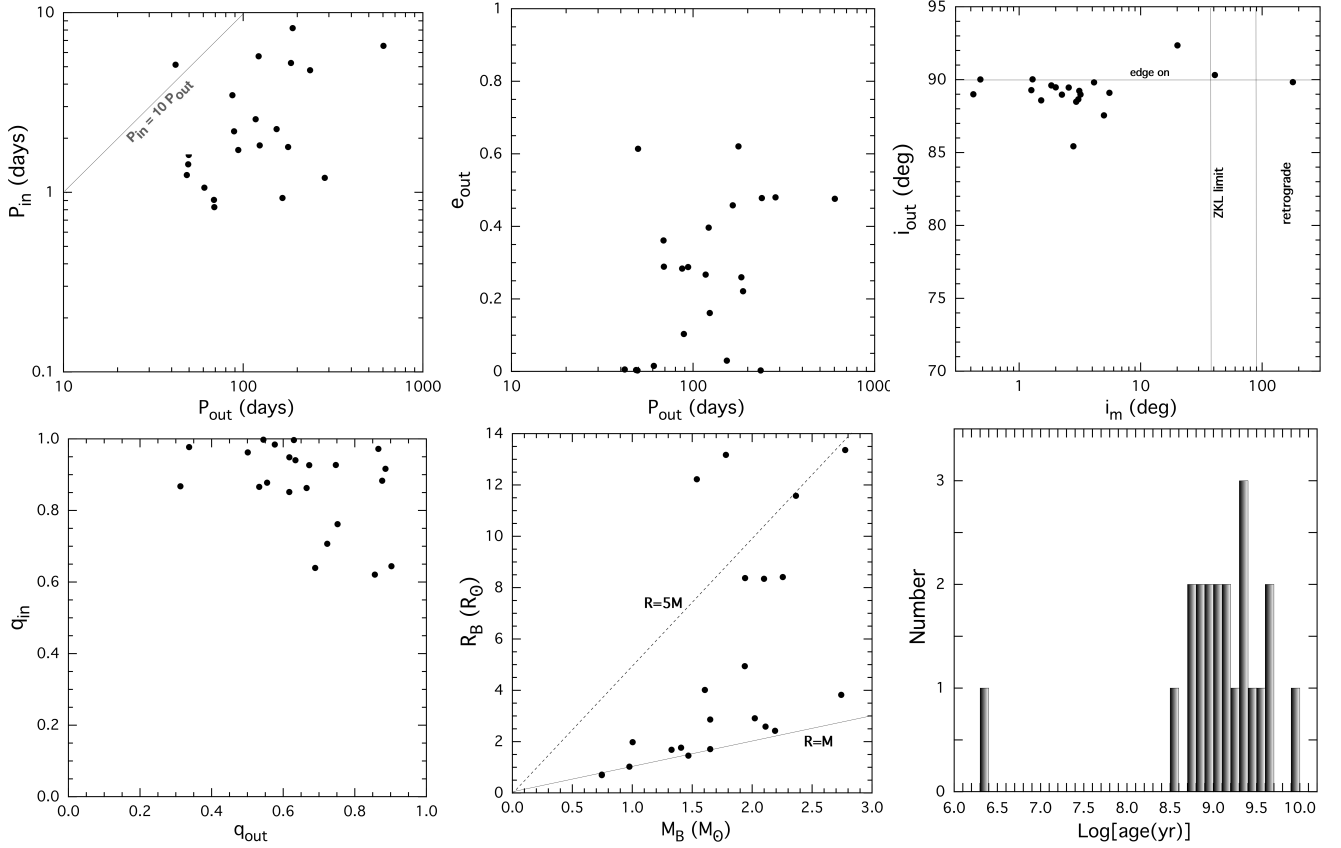


**Figure 17.** Statistical plots for properties of 22 triply eclipsing triples uniformly analyzed (see text for references). *Top-row panels:*  $P_{\text{in}}$  vs.  $P_{\text{out}}$ ,  $e_{\text{out}}$  vs.  $P_{\text{out}}$ , and  $i_{\text{out}}$  vs.  $i_{\text{mut}}$ . The diagonal dotted line in the first plot is a rough estimate of the dividing point between stable and unstable orbits for mildly eccentric outer orbits. In the upper rightmost panel the vertical lines denote the transition to the ZLK cycles, and to retrograde orbits, respectively. *Bottom-row panels:*  $q_{\text{in}}$  vs.  $q_{\text{out}}$ ,  $R_{\text{B}}$  vs.  $M_{\text{B}}$ , and a 1D distribution of log system ages. The sloped dashed lines in the middle panel are for  $R_{\text{B}} = 1 M_{\text{B}}$  and  $= 5 M_{\text{B}}$ , as rough guides of unevolved and quite evolved stars, respectively.

52041148 for which we found only a pre-main-sequence solution (Borkovits et al. 2022a). Thus, 21 of these triples are manifestly long-term dynamically stable and will last until the tertiary overflows its Roche lobe. In principle, the EB stars could also evolve to mass exchange, but the tertiaries in these systems are sufficiently more massive (in all but a couple of cases), so that they will fill their Roche lobes first, before the EB stars have reached Roche-lobe overflow. (The tertiaries’ Roche lobes range in size from 27 to 187  $R_{\odot}$ ). On the other hand just 2/3 of the tertiaries will reach their Roche lobe radii on the ascent of the red giant branch. However, they would all do so on their ascent of the asymptotic giant branch.

Here we briefly follow up on two facts noted above: (i) the mass of all tertiaries is less than the mass of the inner EB, and (ii) in half of the 22 systems, the tertiary stars have evolved to at least twice their main sequence radius. The latter point is something of an observational selection effect since larger stars have a greater probability of eclipsing the other star(s) in a wide orbit. And, the tertiary is more free to expand than the EB stars which are confined in much closer orbits. In our photodynamical analyses we have adopted the assumption that the tertiary star is coeval with the inner EB stars and, more specifically, that no mass has been lost or transferred among the stars. This implicitly includes the assumption that

the tertiary star itself was always a single star, and not the merger product of another binary star, e.g., starting life as a member of a quadruple system, where one of the binaries evolved and merged into a single star.

This scenario can be substantially ruled against by the fact that the mass of the current tertiary star is always (at least in our sample of 22 systems) less than the mass of the inner binary star. This demonstrates that the tertiary is unlikely to be the merger product of a binary that was more massive than the current inner EB<sup>13</sup>. However, there is still the possibility that the tertiary was a merger product of a lower mass binary that evolved to merger first due to magnetic braking (see, e.g., Verbunt & Zwaan 1981); though, the four masses would have to be tuned just right. We might also mention that all but four of the systems in Fig. 17 have outer periods < 200 days. Since there are currently no published papers claiming any

<sup>13</sup> We note, however, that there is actually a small region of parameter space for a binary B to be less massive than its companion binary A, but still contain the most massive star in the system. Example:  $M_{\text{Aa}} = 1.2 M_{\odot}$ ;  $M_{\text{Ab}} = 1.0 M_{\odot}$ ;  $M_{\text{Ba}} = 1.5 M_{\odot}$ ;  $M_{\text{Bb}} = 0.5 M_{\odot}$ . So, while  $M_{\text{A}} > M_{\text{B}}$ , the B binary would still evolve to merger first. In addition, mergers may also result in mass loss, thereby rendering the initially more massive binary, the less massive one.

quadruple with an outer period this short, we conclude that triples arise from a distinct evolutionary channel than that of the quadruples.

Now that the 22 triply eclipsing triples discussed above (see Fig. 17) are known, and their basic parameters determined, the group of them would make for an excellent follow-up ground-based eclipse timing project. This is especially true for modest-size amateur telescopes since the vast majority of the 22 objects have G magnitudes of  $\lesssim 13$ . The ETV data from *TESS* itself was often instrumental in determining some of the parameters found from the photodynamical analyses. Thus, future timing observations of the ordinary EB eclipses in these systems would be quite helpful in significantly improving the parameter determinations. The dynamical delays in these systems as well as the LTTE delays are typically in the minute range, so readily within the realm of amateur observations. There are a sufficient number of these triply eclipsing triples so that anyone interested in pursuing such timing observations would have one of them to observe nearly every night.

For the purpose of predicting accurate timings for future eclipse events, the periods and epochs (conjunction times) given in Tables 6–10, however, cannot be used. The reason, as explained earlier, is that the periods tabulated there are instantaneous, osculating ones that differ substantially from the average eclipsing period. The latter can be deduced, e.g., from ETV curves or the folds of archival data accumulated over nearly a decade. Hence, similar to Table 6 of Rappaport et al. (2022) we give ephemerides for planning future eclipse observation of the nine triples in Table 11.

Finally, we note that Czavalinga et al. (2022) have presented an alternative method for finding substantial numbers of new compact hierarchical triples to the approach taken in this work. They matched known eclipsing binaries with the orbital solutions that Gaia is now including (Babusiaux et al. 2022; Gaia Collaboration 2022) with their distance and kinematic findings. Thus far, this study has already potentially increased the number of compact triples by some 50%. Going forward, this approach is a good complement to the study of triples presented in this work. In addition, the approach present by Czavalinga et al. (2022) can also lead directly to the discovery of new triply eclipsing systems—and indeed three new triply eclipsing systems were reported in that work. And, of course, the outer period is automatically known once a triple has been found by matching known EBs with Gaia orbital solutions.

## DATA AVAILABILITY

The *TESS* data underlying this article were accessed from MAST (Barbara A. Mikulski Archive for Space Telescopes) Portal (<https://mast.stsci.edu/portal/Mashup/Clients/Mast/Portal.html>). The ASAS-SN archival photometric data were accessed from <https://asas-sn.osu.edu/>. The ATLAS archival photometric data were accessed from <https://fallingstar-data.com/forcedphot/queue/>. A part of the data were derived from sources in the public domain as given in the respective footnotes. The derived data generated in this research and the code used for the photodynamical analysis will be shared upon a reasonable request to the corresponding author.

## ACKNOWLEDGMENTS

We thank an anonymous referee for some very insightful comments and suggestions.

We are grateful to Allan R. Schmitt for making his lightcurve examining software tools LcTools freely available.

TB and ZG acknowledge the support of the Hungarian National Research, Development and Innovation Office (NKFIH) grant K-125015, a PRODEX Experiment Agreement No. 4000137122 between the ELTE Eötvös Loránd University and the European Space Agency (ESA-D/SCI-LE-2021-0025), and the support of the city of Szombathely. ZG acknowledges the VEGA grant of the Slovak Academy of Sciences No. 2/0031/22, and the Slovak Research and Development Agency contract No. APVV-20-0148.

VBK is thankful for support from NASA grants 80NSSC21K0351.

AP acknowledges the financial support of the Hungarian National Research, Development and Innovation Office – NKFIH Grant K-138962.

We thank David Latham for facilitating the TRES observations of TIC 280883909 at the F. L. Whipple Observatory. The TRES observations were obtained with the able help of P. Berlind, M. Calkins, and G. Esquerdo. We also thank J. Mink for maintaining the echelle database at the CfA.

The operation of the BRC80 robotic telescope of Baja Astronomical Observatory has been supported by the project “Transient Astrophysical Objects” GINOP 2.3.2-15-2016-00033 of the National Research, Development and Innovation Office (NKFIH), Hungary, funded by the European Union.

T. Mitnyan gratefully acknowledge observing grant support from the Institute of Astronomy and National Astronomical Observatory, Bulgarian Academy of Sciences. We thank Mitko Churalski for obtaining spectra of TIC 99013269 and TIC 280883908 at the NAO Rozhen Observatory.

This paper includes data collected by the *TESS* mission. Funding for the *TESS* mission is provided by the NASA Science Mission directorate. Some of the data presented in this paper were obtained from the Mikulski Archive for Space Telescopes (MAST). STScI is operated by the Association of Universities for Research in Astronomy, Inc., under NASA contract NAS5-26555. Support for MAST for non-HST data are provided by the NASA Office of Space Science via grant NNX09AF08G and by other grants and contracts.

We have made extensive use of the All-Sky Automated Survey for Supernovae archival photometric data. See Shappee et al. (2014) and Kochanek et al. (2017) for details of the ASAS-SN survey.

We also acknowledge use of the photometric archival data from the Asteroid Terrestrial-impact Last Alert System (ATLAS) project. See Tonry et al. (2018) and Heinze et al. (2018) for specifics of the ATLAS survey.

This work has made use of data from the European Space Agency (ESA) mission *Gaia*<sup>14</sup>, processed by the *Gaia* Data Processing and Analysis Consortium (DPAC)<sup>15</sup>. Funding for the DPAC has been provided by national institutions, in particular the institutions participating in the *Gaia* Multilateral Agreement.

This publication utilized data products from the Wide-field

<sup>14</sup> <https://www.cosmos.esa.int/gaia>

<sup>15</sup> <https://www.cosmos.esa.int/web/gaia/dpac/consortium>



**Table 11.** Derived ephemerides for the nine triple systems to be used for planning future observations.

TIC ID	47151245	81525800	99013269	229785001	276162169	280883908	294803663	332521671	356324779
	Inner binary								
$P$	1.201783	1.64935	6.534695	0.92951	2.55018	5.24795	2.246005 2.246025	1.247149	3.47683
$\mathcal{T}_0$	8 627.453	9 475.556	8 717.199	8 683.4830	8 685.522	8 984.923	8 598.513 8 598.543	8 571.352	8 819.194
$\mathcal{A}_{\text{ETV}}$	0.003	0.013	0.012	0.0015	0.003	0.010	0.0025	0.001	0.010
$D$	0.150	0.247	0.327	0.132	0.281	0.252	0.265	0.224	0.278
	Wide binary (third body eclipses)								
$P$	284.90	47.85	604.05	165.25	117.10	184.35	153.20	48.51	86.88
$\mathcal{T}_0^{\text{inf}}$	9 368.4	9 523.7	9 421.0	(9 686.1)	9 813.1	9 629.0	8 629.2	9 335.1:	9 648.9:
$D^{\text{inf}}$	1.1	0.6	2.0	(0.4)	1.6	7.2	4.2	1.6	3.3
$\mathcal{T}_0^{\text{sup}}$	9 294.9:	—	—	9 731.9	8 709.0	9 748.1	9 317.8:	9 310.8	8 837.5
$D^{\text{sup}}$	2.2	—	—	0.8	2.8	5.5	4.1	1.3	1.3

*Notes.* (a) For the inner pairs:  $P$ ,  $\mathcal{T}_0$ ,  $\mathcal{A}_{\text{ETV}}$ ,  $D$  are the period, reference time of a primary minimum, half-amplitude of the ETV curve, and the full duration of an eclipse, respectively.  $\mathcal{T}_0$  is given in BJD  $- 2\,450\,000$ , while the other quantities are in days. As all but one of the inner eccentricities are very small and, hence, the shifts of the secondary eclipses relative to phase 0.5 are negligible (quantitatively, they are much smaller than the full durations of the individual eclipses), the same reference times and periods can be used to predict the times of the secondary eclipses. The only exception is the inner EB of TIC 294803663. For this system we give a separate period and reference time for the secondary eclipses, listing them below the primary ephemerides. (b) For the outer orbits we give separate reference times for the third body eclipses around the inferior and superior conjunctions of the tertiary component. The eclipse durations,  $D$ , of the third-body eclipses do not give the extent of any specific third body events. Rather  $D$  represents the time difference corresponding to the very first and last moments around a given third-body conjunction when the first/last contact of a third-body event may occur).

Double dots (:) call attention to the less certain superior/inferior conjunction times at those types of third-body events (i.e., primary vs. secondary outer eclipses) because they were not observed by either *TESS* or *KELT*. The absence of a reference time at a given type of conjunction indicates the absence of a third-body eclipse at those conjunctions. Note, the superior conjunction data of TIC 229785001, given in parentheses, indicate that only very shallow third-body eclipses may occur which can hardly be observed with ground-based instruments.

Infrared Survey Explorer, which is a joint project of the University of California, Los Angeles, and the Jet Propulsion Laboratory/California Institute of Technology, funded by the National Aeronautics and Space Administration.

This work also utilized data products from the Two Micron All Sky Survey, which is a joint project of the University of Massachusetts and the Infrared Processing and Analysis Center/California Institute of Technology, funded by the National Aeronautics and Space Administration and the National Science Foundation.

We used the Simbad service operated by the Centre des Données Stellaires (Strasbourg, France) and the ESO Science Archive Facility services (data obtained under request number 396301).

Finally, we acknowledge the use of the VizieR catalogue access tool, CDS, Strasbourg, France (DOI : 10.26093/cds/vizieR). The original description of the VizieR service was published in [Ochsenbein et al. \(2000\)](#).

## REFERENCES

Alonso R., Deeg H. J., Hoyer S., Lodieu N., Palle E., Sanchis-Ojeda R., 2015, *A&A*, 584, L8  
 Avvakumova, E. A., Malkov, O. Yu., Kniazev, A. Yu., 2013, *Astron. Nachr.*, 334, 860  
 Babusiaux, C., Fabricius, C., Khanna, S., et al. 2022, arXiv e-prints, arXiv:2206.05989  
 Bailer-Jones, C. A. L., Rybizki, J., Fouesneau, M., Demleitner, M., Andrae, R., 2021, *AJ*, 161, 147  
 Bakos, G., Á., Lázár, J., Papp, I., Sári, P., Green, E. M., 2002, *PASP*, 114, 974  
 Bhattacharya, D., & van den Heuvel, E.P.J., *Phys. Rep.*, 203, 1  
 Bianchi, L., Shiao, B., & Thilker, D. 2017, *ApJS*, 230, 24

Bonev, T., Markov, H., Tomov, T., et al., 2017, *Bulgarian Astronomical Journal*, 26, 67  
 Borkovits, T. 2022, ‘Eclipsing Binaries in Dynamically Interacting Close, Multiple Systems’, *Galaxies*, 10, 9 (arXiv:2201.01243)  
 Borkovits, T., Csizmadia, Sz., Hegedüs, T., Bíró, I. B., Sándor, Zs., Opitz, A., 2002, *A&A*, 392, 895  
 Borkovits, T., Érdi, B., Forgács-Dajka, E., Kovács, T., 2003, *A&A*, 398, 1091  
 Borkovits, T., Csizmadia, Sz., Forgács-Dajka, E., & Hegedüs, T. 2011, *A&A*, 528, 53  
 Borkovits, T., Derekas, A., Kiss, L. L., et al., 2013, *MNRAS*, 428, 1656  
 Borkovits, T., Rappaport, S., Hajdu, T., Sztakovics, J., 2015, *MNRAS*, 448, 946  
 Borkovits, T., Hajdu, T., Sztakovics, J., Rappaport, S., Levine, A., Bíró, I. B., Klagyivik, P., 2016, *MNRAS*, 455, 4136  
 Borkovits, T., Albrecht, S., Rappaport, S., et al. 2018, *MNRAS*, 478, 513  
 Borkovits, T., Rappaport, S., Kaye, T., et al. 2019a, *MNRAS*, 483, 1934  
 Borkovits, T., Sperauskas, J., Tokovinin, A., Latham, D. W., Csányi, I., Hajdu, T., Molnár, L., 2019b, *MNRAS*, 487, 4631  
 Borkovits, T., Rappaport, S., Hajdu, T., et al. 2020a, *MNRAS*, 493, 5005  
 Borkovits, T., Rappaport, S., Tan, T.G., et al. 2020b, *MNRAS*, 496, 4624  
 Borkovits, T., Rappaport, S., Maxted, P. F. L., et al. 2021, *MNRAS*, 503, 3759  
 Borkovits, T., Mitnyan, T., Rappaport, S., et al. 2022a, *MNRAS*, 510, 1352  
 Borkovits, T., Rappaport, S. A., Toonen, S., Moe, M., Mitnyan, T., Csányi, I., 2022b, *MNRAS*, 515, 3773  
 Borucki W. J. et al., 2010, *Science*, 327, 977  
 Bouma, L., Hartman, J., Bhatti, W. 2019, *ApJS*, 245, 13.  
 Bressan, A., Marigo, P., Girardi, L. et al. 2012, *MNRAS*, 427, 127  
 Buchhave, L.A., Bakos, G. A., Hartman, J.D., et al. 2010, *ApJ*,

- 720, 1118, doi: 10.1088/0004-637X/720/2/1118
- Budding, E., Erdem, A., Çiçek, C., et al. 2004, *A&A*, 417, 263
- Carter, J.A., et al., 2011, *Science*, 331, 562
- Castelli F., Kurucz R. L., 2003, in Piskunov, N., Weiss, W.W., Gray D. F., eds, *Proc. IAU Symp. 210, Modelling of Stellar Atmospheres*. p.A20, preprint (astro-ph/0405087)
- Chambers, K.C., Magnier, E.A., Metcalfe, N., et al. 2016, arXiv:1612.05560
- Choi J., Dotter A., Conroy C., Cantiello M., Paxton B., & Johnson B. D., 2016, *ApJ*, 823, 102
- Comerford, T.A.F., & Izzard, R.G. 2020, *MNRAS*, 498, 2957
- Cutri, R.M., Wright, E.L., Conrow, T., et al. 2013, *wise.rept*, 1C.
- Czavalinga, D.R., Mitnyan, T., Rappaport, S., et al. 2022, *A&A*, in press; arXiv:2212.02903
- de Vries, N., Portegies Zwart, S., & Figueira, J. 2014, *MNRAS*, 438, 1909
- Donati, J.-F., Semel, M., Carter, B. D., Rees, D. E., & Collier Cameron, A. 1997, *MNRAS*, 291, 658, doi: 10.1093/mnras/291.4.658
- Dotter A., 2016, *ApJS*, 222, 8
- Eggleton, P.P.E. 2006, *Evolutionary Processes in Binary and Multiple Stars* (Cambridge Astrophysics, Series Number 40), Cambridge University Press
- Fausnaugh, M.M., Burke, C.J., Ricker, G.R., & Vanderspek, R. 2020, *Research Notes of the AAS*, 4, 251
- Ford, E. B., 2005, *AJ*, 129, 1706
- Furesz, G. 2008, PhD thesis, University of Szeged
- Gaia Collaboration, Brown, A. G. A., Vallenari, A., Prusti, T. et al. 2021, *A&A*, 649, A1
- Gaia Collaboration, Vallenari, A., Brown, A. G. A., et al. 2022, arXiv e-prints, arXiv:2208.00211
- Glanz, H., & Perets, H.B. 2021, *MNRAS*, 500, 1921
- Green, G.M., Schlafly, E.F., Zucker, C., Speagle, J.S., & Finkbeiner, D.P. 2019, arXiv:1905.02734
- Gunn, J.E., Carr, M., Rockosi, C., et al. 1998, *AJ*, 116, 3040
- Hammers, A.S., Perets, H.B., Thompson, T.A., & Neunteufel, P. 2022, *ApJ*, 925, 178
- Heinze, A.N., Tonry, J.L., Denneau, L., et al. 2018, *AJ*, 156, 241
- Henden, A. A., Levine, S., Terrell, D., Welch, D. 2015, *American Astronomical Society, AAS Meeting #225*, id.336.16
- Hoffmeister, C., Ahnert-Rohlfs, E., Ahnert, P., Huth, H., Goetz, W. 1954, *Veroeffentlichungen der Sternwarte Sonneberg*, 2, 143
- Howell, S.B., Sobek, C., Hass, M., et al. 2014, *PASP*, 126, 398
- Huang, C.X., Vanderburg, A., Pál, A., et al., 2020, *RNAAS*, 4, 206
- Jenkins, J.M., Twicken, J.D., McCauliff, S., et al. 2016, in: *Software and Cyberinfrastructure for Astronomy IV*, volume 9913. International Society for Optics and Photonics, p. 99133E
- Hillel, S., Schreier, R., & Soker, N. 2017, *MNRAS*, 471, 3456
- Kiseleva, L., G., Eggleton, P. P., Mikkola, S., 1998, *MNRAS*, 300, 292
- Klinglesmith, D. A., Sobieski, S., 1970, *AJ*, 75, 175
- Kochanek, C. S., Shappee, B. J., Stanek, K. Z., et al., 2017, *PASP*, 129, 104502
- Kopal Z., 1959, *Close Binary Systems*. Wiley, New York
- Kostov et al., 2021, *ApJ*, 917, 93
- Kostov, V.B., Powell, B.P., Rappaport, S.A, et al. 2022, *ApJS* in press, arXiv:2202.05790
- Kovács, G., Zucker, S., Mazeh, T., 2002, *A&A*, 391, 369
- Kozai, Y. 1962, *AJ*, 67, 591
- Kristiansen, M.H., Rappaport, S., Vanderburg, A., et al. 2022, *PASP*, 134, 4401
- Latham, D. W., Stefanik, R. P., Torres, G., et al. 2002, *AJ*, 124, 1144
- Lidov, M. L., 1962, *Planetary and Space Science*, 9, 719
- Lucy, L.B. 1967, *Zeitschrift für Astrophysik*, 65, 89
- Mardling R. A., & Aarseth S. J., 2001, *MNRAS*, 321, 398
- Masuda, K., Uehara, S., Kawahara, H, 2015, *ApJ*, 806, L37
- Mikkola S., 2008, in Hubrig S., Petr-Gotzens M., Tokovinin A., eds, *Multiple Stars Across the H-R Diagram*. p. 11, doi:10.1007/978-3-540-74745-1\_2
- Mitnyan, T., Borkovits, T., Rappaport, S., Pál, A., Maxted, P. F. L., 2020, *MNRAS*, 498, 6034
- Muñoz, D.J., Lai, D., Kratter, K., & Miranda, R. 2020. *ApJ*, 889, 114
- Nardiello, D., Borsato, L., Piotto, G., et al. 2019, *MNRAS*, 490, 3806
- Nordström, B., Latham, D. W., Morse, J. A., et al. 1994, *A&A*, 287, 338
- Ochsenbein, F., Bauer, P., & Marcout, J. 2000. *A&AS*, 143, 23
- Oelkers, R.J., & Stassun, K.G. 2018, *AJ*, 156, 132
- Offner, S. S. R., Moe, M., Kratter, K. M., Sadavoy, S. I., Jensen, E. L. N., Tobin, John J., 2022 arXiv:2203.10066
- Paegert, M. et al, 2021, arXiv:2108.04778
- Pál, A., 2012, *MNRAS*, 421, 1825
- Paredes, L. A., Henry, T. J., Quinn, S. N., et al. 2021, *AJ*, 162, 176, doi: 10.3847/1538-3881/ac082a
- Paxton, B., Bildsten L., Dotter A., Herwig F., Lesaffre P., & Timmes F., 2011, *ApJS*, 192, 3
- Paxton, B., et al., 2015, *ApJS*, 220, 15
- Paxton, B., et al., 2019, *ApJS*, 243, 10
- Pepper, J., Pogge, R.W., DePoy, D.L., et al., 2007, *PASP*, 119, 923
- Pepper, J., Kuhn, R.B., Siverd, R., et al., 2012, *PASP*, 124, 230
- Pollacco, D. L., Skillen, I., Collier Cameron, A., et al. 2006, *PASP*, 118, 1407
- Powell, B.P., Kostov, V.B., Rappaport, S., et al. 2021, *AJ*, 161, 162
- Prša, A., & Zwitter, T., 2005, *ApJ*, 628, 426
- Rappaport, S., Deck, K., Levine, A., Borkovits, T., Carter, J., El Mellah, I., Sanchis-Ojeda, R. & Kalomeni, B. 2013, *ApJ*, 768, 33
- Rappaport, S., Kurtz, D, Handler, G., et al. 2021, *MNRAS*, 503, 254
- Rappaport, S., Borkovits, T., Gagliano, R., et al. 2022, *MNRAS*, in press
- Ricker, G.R., Winn, J.N., Vanderspek, R., et al. 2015, *JATIS*, 1, 014003
- Sabach, E., & Soker, N. 2015, *MNRAS*, 450, 1716
- Samus', N. N., Kazarovets, E. V., Durlevich, O. V., Kireeva, N. N., Pastukhova, E. N. 2017, *Astron. Rep.*, 61, 80
- Schmitt, A.R., Hartman, J.D., & Kipping, D.M. 2019, arXiv:1910.08034
- Shappee, B. J., Prieto, J. L., Grupe, D., et al. 2014, *ApJ*, 788, 48
- Skrutskie, M.F., Cutri, R.M., Stiening, R., et al. 2006, *AJ*, 131, 1163
- Smith, K.W, Smartt, S.J., Young, D.R., Tonry, J.L., et al. 2020, *PASP*, 132, 5002
- Soker, N., & Bear, E. 2021, *MNRAS*, 505, 4791
- Sterne T. E., 1939, *MNRAS*, 99, 451
- Talens, G.J.J., Spronck, J.F.P., Lesage, A.-L., Otten, G.P.P.L., Stuik, R., Pollacco, D. & Snellen, I.A.G. 2017, *A&A*, 601, A11
- Tauris, T.M., & van den Heuvel, E.P.J. 2014, *ApJL*, 781, 13
- Tauris, T.M., & van den Heuvel, E.P.J., 2023, *Physics of Binary Star Evolution: From Stars to X-ray Binaries and Gravitational Wave Sources*, Princeton Series and Astrophysics, Princeton University Press, 2023
- Tokovinin, A., Fischer, D.A., Bonati, M., et al. 2013, *PASP*, 2013, 125, 1336
- Tokovinin, A., 2021, *Universe*, 7, 352
- Tokovinin, A., Moe, M., 2020, *MNRAS*, 491, 5158
- Toonen, S., & Nelemans, G. 2013, *A&A*, 557, 87
- Tonry, J.L., Denneau, L., Heinze, A.N., et al. 2018, *PASP*, 130, 4505
- Verbunt, F., & Zwaan, C. 1981, *A&A*, 100, 7
- von Zeipel, 1910, *AN*, 183, 345
- Wolf, C., Onken, C.A., Luvaul, L.C., et al. 2018, *PASA*, 35, 10
- Zasche, P., Henzl, Z., & Mašek, M. 2022, *A&A*, 664, 96

**Table A1.** Measured radial velocities of the tertiary component of TIC 99013269. The date is given as BJD – 2 450 000, while the RVs and their uncertainties are in  $\text{km s}^{-1}$ .

Date	RV <sub>B</sub>	$\sigma_B$	Date	RV <sub>B</sub>	$\sigma_B$
9564.20623 <sup>a</sup>	39.49	0.34	9782.39505 <sup>a</sup>	10.65	0.17
9575.21922 <sup>a</sup>	38.06	0.45	9785.51202 <sup>a</sup>	10.70	0.26
9583.21267 <sup>a</sup>	35.94	0.29	9824.46323 <sup>a</sup>	4.28	0.77
9711.53417 <sup>b</sup>	18.97	0.28	9827.53333 <sup>a</sup>	5.06	0.19
9718.53900 <sup>b</sup>	18.08	0.26	9830.39248 <sup>c</sup>	3.81	0.29
9745.55576 <sup>a</sup>	15.31	0.38	9831.44676 <sup>c</sup>	3.92	0.26
9746.54710 <sup>a</sup>	14.38	0.30	9857.29764 <sup>a</sup>	0.69	0.18
9748.55289 <sup>a</sup>	15.47	0.74	9896.25484 <sup>a</sup>	–4.55	0.22
9749.54329 <sup>a</sup>	13.94	0.16	9897.25350 <sup>a</sup>	–4.98	0.26
9750.54483 <sup>a</sup>	14.16	0.21	9898.25200 <sup>a</sup>	–5.34	0.22

Notes. Instruments: <sup>a</sup> Konkoly; <sup>b</sup> Skalnaté Pleso; <sup>c</sup> Rozhen

**Table A2.** Measured radial velocities of the tertiary component of TIC 280883908. The date is given as BJD – 2 450 000, while the RVs and their uncertainties are in  $\text{km s}^{-1}$ .

Date	RV <sub>B</sub>	$\sigma_B$	Date	RV <sub>B</sub>	$\sigma_B$
9473.008411	–14.43	0.18	9567.743108	–45.90	0.19
9479.909811	–10.02	0.16	9585.735308	–74.11	0.16
9489.986911	–5.21	0.14	9596.41174 <sup>a</sup>	–74.43	0.22
9500.912210	–1.48	0.15	9600.792707	–70.85	0.16
9519.953010	0.12	0.19	9605.803607	–65.95	0.14
9522.827010	–0.30	0.16	9615.820607	–53.68	0.19
9524.803410	–0.37	0.15	9622.745707	–45.20	0.18
9527.826110	–1.58	0.15	9635.636206	–31.53	0.15
9531.770109	–2.87	0.12	9658.648005	–13.66	0.23
9548.802309	–15.56	0.13	9915.745996	–13.94	0.15

Notes. All but one RV data were gathered with TRES spectrograph. The only exception is superscripted with an <sup>a</sup> and was obtained with the 2m Rozhen telescope (Bulgaria). The Rozhen point and the last two TRES RV data were not used for the analysis.

**Table A3.** Measured radial velocities of the tertiary component of TIC 294803663. The date is given as BJD – 2 450 000, while the RVs are in  $\text{km s}^{-1}$ .

Date	RV <sub>B</sub>	Date	RV <sub>B</sub>
9700.700109	–19.367	9742.572900	28.245
9720.616709	15.841	9792.486631	–43.705
9725.621810	21.267	9837.471313	–48.825

Notes. All RV data were obtained with CHIRON instrument.

## APPENDIX A: SUPPLEMENTARY MATERIAL – RV DATA

In this appendix, we tabulate the radial velocity data obtained for four tertiary components out of our nine triples (Tables A1–A4).

**Table A4.** Measured radial velocities of the tertiary component of TIC 332521671. The date is given as BJD – 2 450 000, while the RVs are in  $\text{km s}^{-1}$ .

Date	RV <sub>B</sub>	Date	RV <sub>B</sub>
9650.749645032	–19.111	9692.612050781	25.653
9656.684773510	–58.279	9699.574493482	–21.489
9659.753177934	–70.110	9702.580351819	–42.815
9671.652089117	–36.776	9716.612527877	–58.393
9677.611086097	6.692	9725.529218565	2.654
9684.681348653	40.296		

Notes. All RV data were obtained with CHIRON instrument.

**Table B1.** Times of minima of TIC 047151245 (V726 Sco)

BJD −2 400 000	Cycle no.	std. dev. ( <i>d</i> )	BJD −2 400 000	Cycle no.	std. dev. ( <i>d</i> )	BJD −2 400 000	Cycle no.	std. dev. ( <i>d</i> )	BJD −2 400 000	Cycle no.	std. dev. ( <i>d</i> )
58626.858995	−0.5	0.000927	58640.670145	11.0	0.000923	59362.346333	611.5	0.000186	59377.365321	624.0	0.000232
58627.454056	0.0	0.000550	58641.273052	11.5	0.000366	59362.941691	612.0	0.000181	59377.969436	624.5	0.000315
58628.044977	0.5	0.000816	58641.873918	12.0	0.000757	59363.552102	612.5	0.000298	59378.573030	625.0	0.000249
58628.657908	1.0	0.000442	58642.467826	12.5	0.000371	59364.153877	613.0	0.000173	59379.172045	625.5	0.000186
58629.259583	1.5	0.000660	58643.071932	13.0	0.002422	59364.748281	613.5	0.000160	59379.769220	626.0	0.000215
58629.855647	2.0	0.000322	58643.675185	13.5	0.000377	59365.349327	614.0	0.000133	59380.370227	626.5	0.000253
58630.452281	2.5	0.000427	58644.280322	14.0	0.000396	59365.950090	614.5	0.000148	59380.972185	627.0	0.000224
58631.055809	3.0	0.000635	58644.875586	14.5	0.000445	59366.554975	615.0	0.000187	59381.571831	627.5	0.000190
58631.660888	3.5	0.000318	58645.475734	15.0	0.000231	59367.151077	615.5	0.000200	59382.180707	628.0	0.000212
58632.261229	4.0	0.000303	58646.076274	15.5	0.000243	59367.751895	616.0	0.000293	59382.779057	628.5	0.000174
58632.862539	4.5	0.000992	58646.681454	16.0	0.000473	59369.552257	617.5	0.000215	59383.382126	629.0	0.000160
58633.463997	5.0	0.000637	58647.278175	16.5	0.000719	59370.158760	618.0	0.000271	59383.974453	629.5	0.000167
58634.064271	5.5	0.000466	58647.873841	17.0	0.000595	59370.763342	618.5	0.000209	59384.574699	630.0	0.000251
58634.663548	6.0	0.000384	58648.481128	17.5	0.000873	59371.361877	619.0	0.000216	59385.182889	630.5	0.000182
58635.263601	6.5	0.000258	58649.080925	18.0	0.000281	59371.955891	619.5	0.000145	59385.784996	631.0	0.000182
58635.858739	7.0	0.001194	58649.683572	18.5	0.000348	59372.554606	620.0	0.000124	59386.382147	631.5	0.000213
58636.462802	7.5	0.000472	58650.285116	19.0	0.000405	59373.161933	620.5	0.000242	59386.978846	632.0	0.000366
58637.067212	8.0	0.000284	58650.889930	19.5	0.000220	59373.764538	621.0	0.000241	59387.588274	632.5	0.000319
58637.666892	8.5	0.000579	58651.482170	20.0	0.000437	59374.361204	621.5	0.000220	59388.187764	633.0	0.000257
58638.270496	9.0	0.000676	58652.080462	20.5	0.000676	59376.171568	623.0	0.000172	59388.785941	633.5	0.000182
58638.875073	9.5	0.001690	58652.685782	21.0	0.000577	59376.767020	623.5	0.000170	59389.394389	634.0	0.0003140
58640.064596	10.5	0.006170									

*Notes.* Integer and half-integer cycle numbers refer to primary and secondary eclipses, respectively. All eclipses were observed by the *TESS* spacecraft.

**Table B2.** Times of minima of TIC 81525800

BJD −2 400 000	Cycle no.	std. dev. ( <i>d</i> )	BJD −2 400 000	Cycle no.	std. dev. ( <i>d</i> )	BJD −2 400 000	Cycle no.	std. dev. ( <i>d</i> )	BJD −2 400 000	Cycle no.	std. dev. ( <i>d</i> )
59474.728608	−0.5	0.000097	59496.168409	12.5	0.000064	59515.947921	24.5	0.000084	59534.109947	35.5	0.000079
59475.561386	0.0	0.000147	59496.995804	13.0	0.000068	59516.775969	25.0	0.000077	59534.938437	36.0	0.000062
59476.384883	0.5	0.000132	59497.816054	13.5	0.000060	59517.596762	25.5	0.000075	59535.758567	36.5	0.000080
59477.214604	1.0	0.000112	59498.643803	14.0	0.000152	59518.425218	26.0	0.000089	59536.586067	37.0	0.000053
59478.035069	1.5	0.000130	59500.292489	15.0	0.000100	59519.245915	26.5	0.000058	59537.406589	37.5	0.000055
59478.864782	2.0	0.000072	59501.111780	15.5	0.000078	59520.076806	27.0	0.000070	59540.701995	39.5	0.000099
59479.686456	2.5	0.000123	59501.940707	16.0	0.000073	59520.898701	27.5	0.000089	59541.530918	40.0	0.000076
59480.514630	3.0	0.000083	59502.760496	16.5	0.000128	59521.733515	28.0	0.000089	59542.350962	40.5	0.000133
59481.334270	3.5	0.000067	59503.589225	17.0	0.000092	59522.558936	28.5	0.000090	59543.177903	41.0	0.000084
59482.163152	4.0	0.000123	59504.408612	17.5	0.000077	59523.392680	29.0	0.000150	59544.000072	41.5	0.000105
59487.927633	7.5	0.000090	59505.237353	18.0	0.000087	59524.215125	29.5	0.000094	59544.826385	42.0	0.000142
59488.755518	8.0	0.000073	59506.057493	18.5	0.000054	59526.696148	31.0	0.000077	59545.647454	42.5	0.000126
59489.576054	8.5	0.000077	59506.885072	19.0	0.000069	59527.516676	31.5	0.000090	59546.475183	43.0	0.000125
59490.403986	9.0	0.000096	59507.705012	19.5	0.000116	59528.345502	32.0	0.000071	59547.294525	43.5	0.000105
59491.223891	9.5	0.000103	59508.533063	20.0	0.000090	59529.164904	32.5	0.000065	59548.123617	44.0	0.000112
59492.052730	10.0	0.000061	59509.353087	20.5	0.000085	59529.994265	33.0	0.000059	59548.943165	44.5	0.000111
59492.872334	10.5	0.000086	59510.182320	21.0	0.000078	59530.813470	33.5	0.000102	59549.771502	45.0	0.000096
59493.700441	11.0	0.000069	59511.001228	21.5	0.000128	59531.642213	34.0	0.000105	59550.592030	45.5	0.000252
59494.519885	11.5	0.000077	59514.298752	23.5	0.000091	59532.462766	34.5	0.000072	59660.267838	112.0	0.000032
59495.348309	12.0	0.000059	59515.127021	24.0	0.000064	59533.289512	35.0	0.000066			

*Notes.* Integer and half-integer cycle numbers refer to primary and secondary eclipses, respectively. All but one eclipses were observed by the *TESS* spacecraft. The very last time of minimum was determined from ground-based BAO80 observations.

## APPENDIX B: TABLES OF DETERMINED TIMES OF MINIMA FOR ALL THE NINE SYSTEMS

In this appendix, we tabulate the individual mid-minima times of the primary and secondary eclipses, including mostly *TESS*, and a few ground-based observed ones, for the inner EBs of the triples considered in this study (Tables B1–B9).

The complete Appendix B is available supplementary material to the journal, and also in this arXiv version.

**Table B3.** Times of minima of TIC 99013269

BJD −2 400 000	Cycle no.	std. dev. ( <i>d</i> )	BJD −2 400 000	Cycle no.	std. dev. ( <i>d</i> )	BJD −2 400 000	Cycle no.	std. dev. ( <i>d</i> )	BJD −2 400 000	Cycle no.	std. dev. ( <i>d</i> )
58684.513594	−5.0	0.000208	58720.461635	0.5	0.000136	59426.222237	108.5	0.000082	59801.948299	166.0	0.000064
58687.787001	−4.5	0.000283	58723.724083	1.0	0.000092	59429.487117	109.0	0.000064	59805.219247	166.5	0.000081
58691.048878	−4.0	0.000248	58726.996785	1.5	0.000132	59436.023888	110.0	0.000069	59808.483194	167.0	0.000069
58694.322099	−3.5	0.000277	58730.258331	2.0	0.000109	59439.295332	110.5	0.000073	59811.754445	167.5	0.000078
58697.583534	−3.0	0.000299	58733.532437	2.5	0.000136	59442.559063	111.0	0.000066	59815.017709	168.0	0.000061
58704.118271	−2.0	0.000301	58736.793434	3.0	0.000101	59445.831342	111.5	0.000070	59818.289028	168.5	0.000075
58713.926899	−0.5	0.000126	59422.950663	108.0	0.000064	59798.684472	165.5	0.000076	59821.551830	169.0	0.000079
58717.188773	0.0	0.000107									

*Notes.* Integer and half-integer cycle numbers refer to primary and secondary eclipses, respectively. All eclipses were observed by the *TESS* spacecraft.

**Table B4.** Times of minima of TIC 229785001

BJD −2 400 000	Cycle no.	std. dev. ( <i>d</i> )	BJD −2 400 000	Cycle no.	std. dev. ( <i>d</i> )	BJD −2 400 000	Cycle no.	std. dev. ( <i>d</i> )	BJD −2 400 000	Cycle no.	std. dev. ( <i>d</i> )
58683.483148	0.0	0.000168	58854.049357	183.5	0.000283	58999.054886	339.5	0.000391	59627.400615	1015.5	0.000164
58683.947729	0.5	0.000304	58854.514901	184.0	0.000157	58999.519334	340.0	0.000175	59627.865729	1016.0	0.000077
58684.412838	1.0	0.000164	58856.837483	186.5	0.000391	58999.984097	340.5	0.000366	59628.330658	1016.5	0.000181
58684.876945	1.5	0.000382	58857.303168	187.0	0.000180	59000.448813	341.0	0.000172	59628.795175	1017.0	0.000091
58685.342210	2.0	0.000129	58857.767945	187.5	0.000375	59000.913961	341.5	0.000376	59629.259757	1017.5	0.000162
58685.806781	2.5	0.000301	58858.232903	188.0	0.000131	59001.378173	342.0	0.000139	59629.724858	1018.0	0.000087
58686.271941	3.0	0.000154	58858.697463	188.5	0.000290	59001.843326	342.5	0.000318	59630.189057	1018.5	0.000177
58686.735998	3.5	0.000309	58859.162303	189.0	0.000154	59002.308079	343.0	0.000145	59630.654159	1019.0	0.000086
58687.201490	4.0	0.000164	58859.626531	189.5	0.000315	59002.772751	343.5	0.000373	59631.118773	1019.5	0.000178
58687.665706	4.5	0.000312	58860.091584	190.0	0.000145	59003.237541	344.0	0.000211	59631.583873	1020.0	0.000092
58688.130588	5.0	0.000161	58860.556299	190.5	0.000506	59003.702621	344.5	0.000314	59632.048345	1020.5	0.000170
58688.595073	5.5	0.000344	58861.021963	191.0	0.000161	59004.167090	345.0	0.000224	59632.513456	1021.0	0.000091
58689.060191	6.0	0.000123	58861.485586	191.5	0.000250	59004.631877	345.5	0.000275	59632.977459	1021.5	0.000187
58689.524898	6.5	0.000327	58861.950452	192.0	0.000155	59005.096672	346.0	0.000136	59633.442885	1022.0	0.000085
58689.989626	7.0	0.000139	58862.415476	192.5	0.000271	59005.561357	346.5	0.000338	59633.907241	1022.5	0.000155
58690.454079	7.5	0.000324	58862.879798	193.0	0.000146	59006.025978	347.0	0.000151	59634.372443	1023.0	0.000094
58690.919415	8.0	0.000134	58863.344507	193.5	0.000289	59006.490901	347.5	0.000345	59634.836806	1023.5	0.000176
58691.383605	8.5	0.000375	58863.809392	194.0	0.000142	59006.955894	348.0	0.000139	59635.301866	1024.0	0.000087
58691.848613	9.0	0.000146	58864.273148	194.5	0.000364	59007.420508	348.5	0.000280	59635.766457	1024.5	0.000169
58692.312737	9.5	0.000288	58864.738428	195.0	0.000160	59007.884898	349.0	0.000144	59637.625980	1026.5	0.000218
58692.778186	10.0	0.000143	58865.203737	195.5	0.000336	59008.350454	349.5	0.000298	59638.090554	1027.0	0.000141
58693.242668	10.5	0.000281	58865.667840	196.0	0.000226	59008.814472	350.0	0.000145	59638.555535	1027.5	0.000189
58693.707711	11.0	0.000158	58866.133375	196.5	0.000431	59009.278515	350.5	0.000998	59639.019790	1028.0	0.000090
58694.171868	11.5	0.000318	58866.597741	197.0	0.000135	59010.673185	352.0	0.000153	59639.484447	1028.5	0.000197
58694.637308	12.0	0.000154	58867.062430	197.5	0.000334	59011.138626	352.5	0.000350	59639.949463	1029.0	0.000088
58695.567564	13.0	0.000206	58867.526764	198.0	0.000247	59011.602899	353.0	0.000143	59640.414051	1029.5	0.000181
58696.030653	13.5	0.000316	58867.992175	198.5	0.000318	59012.067486	353.5	0.000336	59640.878945	1030.0	0.000093
58697.425720	15.0	0.000152	58868.456411	199.0	0.000145	59012.532417	354.0	0.000209	59641.343543	1030.5	0.000165
58697.889616	15.5	0.000327	58870.780051	201.5	0.000274	59012.997470	354.5	0.000267	59641.808471	1031.0	0.000091
58698.354981	16.0	0.000200	58871.245001	202.0	0.000128	59013.461788	355.0	0.000140	59642.273757	1031.5	0.000156
58698.819491	16.5	0.000308	58871.709566	202.5	0.000358	59013.927415	355.5	0.000317	59642.737974	1032.0	0.000080
58699.284522	17.0	0.000211	58872.173858	203.0	0.000146	59014.391484	356.0	0.000157	59643.202795	1032.5	0.000164
58699.749617	17.5	0.000506	58872.639640	203.5	0.000304	59014.856353	356.5	0.000416	59643.667742	1033.0	0.000073
58700.213857	18.0	0.000137	58873.103515	204.0	0.000154	59015.321065	357.0	0.000146	59644.132037	1033.5	0.000173
58700.678706	18.5	0.000267	58873.568535	204.5	0.000389	59015.785830	357.5	0.000338	59644.597093	1034.0	0.000083
58701.143542	19.0	0.000142	58874.033111	205.0	0.000145	59016.250488	358.0	0.000188	59645.061808	1034.5	0.000192
58701.608114	19.5	0.000447	58874.498532	205.5	0.000327	59016.714957	358.5	0.000311	59645.526730	1035.0	0.000078
58702.072890	20.0	0.000206	58874.962572	206.0	0.000135	59017.179935	359.0	0.000172	59645.991425	1035.5	0.000160
58702.537542	20.5	0.000306	58875.427697	206.5	0.000286	59017.644839	359.5	0.000340	59646.456079	1036.0	0.000088
58703.002128	21.0	0.000149	58875.892222	207.0	0.000147	59018.109076	360.0	0.000157	59646.920915	1036.5	0.000149
58703.466972	21.5	0.000284	58876.357382	207.5	0.000292	59018.574232	360.5	0.000390	59647.385541	1037.0	0.000068
58703.931714	22.0	0.000435	58876.821463	208.0	0.000162	59019.038993	361.0	0.000126	59647.849987	1037.5	0.000149
58704.396371	22.5	0.000436	58877.286510	208.5	0.000293	59019.503423	361.5	0.000307	59648.315196	1038.0	0.000091
58704.860938	23.0	0.000136	58877.750893	209.0	0.000184	59019.968153	362.0	0.000162	59648.779723	1038.5	0.000139
58705.326187	23.5	0.000300	58878.215446	209.5	0.000341	59020.433530	362.5	0.000292	59649.244820	1039.0	0.000079
58705.790823	24.0	0.000131	58878.680800	210.0	0.000148	59020.897667	363.0	0.000142	59649.709654	1039.5	0.000169
58706.255275	24.5	0.000318	58879.145440	210.5	0.000520	59021.362582	363.5	0.000287	59650.174063	1040.0	0.000082
58706.720199	25.0	0.000145	58879.610020	211.0	0.000179	59021.827455	364.0	0.000186	59651.568506	1041.5	0.000182
58707.185513	25.5	0.000281	58880.074768	211.5	0.000296	59022.221611	365.5	0.000340	59652.033663	1042.0	0.000097
58707.649634	26.0	0.000153	58880.539681	212.0	0.000145	59022.685930	366.0	0.000155	59652.497824	1042.5	0.000177
58708.114174	26.5	0.000272	58881.003947	212.5	0.000345	59023.150644	366.5	0.000373	59652.962862	1043.0	0.000115
58708.579268	27.0	0.000171	58881.468773	213.0	0.000143	59023.615913	367.0	0.000149	59653.427745	1043.5	0.000185
58709.044068	27.5	0.000335	58881.933498	213.5	0.000328	59024.080778	367.5	0.000354	59653.892154	1044.0	0.000095

**Table B4.** (*continued*)

BJD −2 400 000	Cycle no.	std. dev. (d)	BJD −2 400 000	Cycle no.	std. dev. (d)	BJD −2 400 000	Cycle no.	std. dev. (d)	BJD −2 400 000	Cycle no.	std. dev. (d)
58709.508594	28.0	0.000136	58882.398358	214.0	0.000142	59026.010273	368.5	0.000283	59654.357363	1044.5	0.000163
58709.973641	28.5	0.000311	58882.863143	214.5	0.000347	59026.474785	369.0	0.000149	59654.822222	1045.0	0.000080
58711.832077	30.5	0.000474	58883.328108	215.0	0.000149	59026.939800	369.5	0.000302	59655.286938	1045.5	0.000156
58712.297086	31.0	0.000127	58883.792659	215.5	0.000338	59027.404150	370.0	0.000179	59655.751699	1046.0	0.000096
58712.761190	31.5	0.000285	58885.186563	217.0	0.000160	59027.869058	370.5	0.000384	59656.215859	1046.5	0.000155
58713.226529	32.0	0.000132	58885.650874	217.5	0.000365	59028.333843	371.0	0.000165	59656.681111	1047.0	0.000076
58713.690482	32.5	0.000263	58886.116248	218.0	0.000157	59028.798254	371.5	0.000278	59657.145324	1047.5	0.000165
58714.156150	33.0	0.000261	58886.581158	218.5	0.000287	59029.263528	372.0	0.000158	59657.610433	1048.0	0.000079
58714.620743	33.5	0.000359	58887.045449	219.0	0.000135	59029.727974	372.5	0.000319	59658.075008	1048.5	0.000158
58715.085495	34.0	0.000172	58887.510406	219.5	0.000293	59030.192875	373.0	0.000161	59658.540247	1049.0	0.000084
58715.550000	34.5	0.000355	58887.975397	220.0	0.000150	59030.657528	373.5	0.000329	59659.004699	1049.5	0.000143
58716.014949	35.0	0.000154	58888.439443	220.5	0.000384	59031.122359	374.0	0.000156	59659.469817	1050.0	0.000092
58716.479298	35.5	0.000386	58888.904212	221.0	0.000152	59031.586851	374.5	0.000273	59659.933994	1050.5	0.000167
58716.944484	36.0	0.000139	58889.369408	221.5	0.000362	59032.051805	375.0	0.000137	59660.399142	1051.0	0.000078
58717.408969	36.5	0.000297	58889.833862	222.0	0.000172	59032.517241	375.5	0.000320	59660.863182	1051.5	0.000148
58717.873908	37.0	0.000138	58890.298828	222.5	0.000310	59032.982186	376.0	0.000227	59661.328697	1052.0	0.000098
58718.337766	37.5	0.000309	58890.763374	223.0	0.000155	59033.445420	376.5	0.000347	59661.792718	1052.5	0.000166
58718.803221	38.0	0.000136	58891.228762	223.5	0.000420	59033.910985	377.0	0.000146	59662.258140	1053.0	0.000076
58719.267818	38.5	0.000284	58891.692709	224.0	0.000153	59034.375919	377.5	0.000423	59662.722096	1053.5	0.000166
58719.732451	39.0	0.000139	58892.157855	224.5	0.000420	59034.840029	378.0	0.000122	59663.187748	1054.0	0.000088
58720.196663	39.5	0.000334	58892.622468	225.0	0.000143	59390.839939	761.0	0.000089	59663.651924	1054.5	0.000175
58720.662211	40.0	0.000152	58893.086980	225.5	0.000309	59391.305019	761.5	0.000155	59664.117025	1055.0	0.000083
58721.126317	40.5	0.000408	58893.551917	226.0	0.000182	59391.769316	762.0	0.000082	59665.511117	1056.5	0.000181
58721.591200	41.0	0.000162	58894.017001	226.5	0.000315	59392.234425	762.5	0.000172	59665.975943	1057.0	0.000103
58722.056300	41.5	0.000284	58894.481193	227.0	0.000154	59392.698766	763.0	0.000076	59666.439695	1057.5	0.000180
58722.521063	42.0	0.000174	58894.945975	227.5	0.000311	59393.164015	763.5	0.000146	59666.905324	1058.0	0.000090
58722.985364	42.5	0.000336	58895.410803	228.0	0.000181	59393.628259	764.0	0.000081	59667.370718	1058.5	0.000174
58723.450330	43.0	0.000169	58895.875553	228.5	0.000405	59394.093310	764.5	0.000142	59667.835005	1059.0	0.000090
58723.909386	45.0	0.000133	58896.340065	229.0	0.000141	59394.557542	765.0	0.000097	59668.298561	1059.5	0.000213
58725.773724	45.5	0.000359	58896.804677	229.5	0.000291	59395.022755	765.5	0.000197	59668.764481	1060.0	0.000090
58726.238568	46.0	0.000127	58897.269599	230.0	0.000129	59395.487301	766.0	0.000077	59669.229300	1060.5	0.000215
58726.703425	46.5	0.000382	58897.735628	230.5	0.000487	59395.952035	766.5	0.000167	59669.694258	1061.0	0.000090
58727.168204	47.0	0.000230	58899.592983	232.5	0.000287	59396.416854	767.0	0.000073	59670.158607	1061.5	0.000175
58727.632292	47.5	0.000432	58900.058311	233.0	0.000174	59396.881465	767.5	0.000187	59670.623668	1062.0	0.000100
58728.097745	48.0	0.000125	58900.522234	233.5	0.000383	59397.346241	768.0	0.000089	59671.088080	1062.5	0.000190
58728.562378	48.5	0.000412	58900.987516	234.0	0.000152	59397.811215	768.5	0.000155	59671.553162	1063.0	0.000079
58729.027003	49.0	0.000141	58901.452518	234.5	0.000354	59398.275845	769.0	0.000079	59672.017400	1063.5	0.000168
58729.491508	49.5	0.000290	58901.917305	235.0	0.000155	59398.740641	769.5	0.000159	59672.482504	1064.0	0.000090
58729.956533	50.0	0.000151	58902.381909	235.5	0.000325	59399.205340	770.0	0.000075	59672.946835	1064.5	0.000161
58730.421152	50.5	0.000359	58902.846646	236.0	0.000123	59399.669976	770.5	0.000151	59673.412165	1065.0	0.000083
58730.885996	51.0	0.000120	58903.311538	236.5	0.000430	59400.134627	771.0	0.000083	59673.877173	1065.5	0.000151
58731.350579	51.5	0.000332	58903.776092	237.0	0.000144	59400.599542	771.5	0.000170	59674.341649	1066.0	0.000082
58731.815470	52.0	0.000151	58904.241102	237.5	0.000365	59401.064498	772.0	0.000076	59674.806214	1066.5	0.000180
58732.279558	52.5	0.000255	58904.705725	238.0	0.000131	59402.458635	773.5	0.000176	59675.270782	1067.0	0.000080
58732.745066	53.0	0.000195	58905.170023	238.5	0.000293	59402.923313	774.0	0.000089	59675.735541	1067.5	0.000172
58733.209397	53.5	0.000362	58905.635093	239.0	0.000141	59403.388516	774.5	0.000180	59676.200326	1068.0	0.000084
58733.674674	54.0	0.000164	58907.029054	240.5	0.000402	59403.853020	775.0	0.000074	59676.665010	1068.5	0.000161
58734.138564	54.5	0.000296	58907.494344	241.0	0.000162	59404.318175	775.5	0.000161	59677.130037	1069.0	0.000080
58734.603961	55.0	0.000145	58907.959430	241.5	0.000277	59405.711791	777.0	0.000072	59677.594213	1069.5	0.000150
58735.067832	55.5	0.000293	58908.423044	242.0	0.000146	59406.176684	777.5	0.000188	59678.059181	1070.0	0.000081
58735.533310	56.0	0.000131	58908.889151	242.5	0.000307	59406.641412	778.0	0.000084	59678.523763	1071.5	0.000216
58735.998036	56.5	0.000317	58909.353354	243.0	0.000187	59407.106243	778.5	0.000166	59679.918469	1072.0	0.000091
58736.462885	57.0	0.000169	58909.817823	243.5	0.000298	59407.570921	779.0	0.000072	59680.383748	1072.5	0.000171
58736.927318	57.5	0.000313	58910.283061	244.0	0.000164	59408.035729	779.5	0.000162	59680.847457	1073.0	0.000094
58738.786117	59.5	0.002115	58910.747513	244.5	0.000262	59408.500460	780.0	0.000085	59681.312077	1073.5	0.000195
58739.251423	60.0	0.000192	58911.212095	245.0	0.000157	59408.965416	780.5	0.000171	59681.776823	1074.0	0.000075
58739.715435	60.5	0.000302	58911.677303	245.5	0.000302	59409.430144	781.0	0.000095	59682.242072	1074.5	0.000179
58740.181160	61.0	0.000264	58912.141898	246.0	0.000143	59409.894998	781.5	0.000183	59682.706332	1075.0	0.000108
58741.574483	62.5	0.000328	58914.001000	248.0	0.000134	59410.359733	782.0	0.000086	59683.171401	1075.5	0.000185
58742.039986	63.0	0.000133	58914.465245	248.5	0.000294	59410.824071	782.5	0.000149	59683.635948	1076.0	0.000090
58742.505143	63.5	0.000290	58914.930711	249.0	0.000169	59411.289193	783.0	0.000095	59684.101547	1076.5	0.000176
58742.969504	64.0	0.000148	58915.395769	249.5	0.000402	59411.754204	783.5	0.000157	59684.565366	1077.0	0.000085
58743.434060	64.5	0.000272	58915.859749	250.0	0.000163	59412.218614	784.0	0.000073	59685.030250	1077.5	0.000150
58743.898517	65.0	0.000144	58916.324913	250.5	0.000293	59412.683847	784.5	0.000189	59685.495827	1078.0	0.000094
58744.363750	65.5	0.000378	58916.789671	251.0	0.000153	59413.148339	785.0	0.000068	59685.958974	1078.5	0.000163
58744.828378	66.0	0.000129	58917.253837	251.5	0.000308	59413.613252	785.5	0.000155	59686.889409	1079.5	0.000156
58745.292401	66.5	0.000379	58917.718966	252.0	0.000142	59414.077782	786.0	0.000083	59687.354083	1080.0	0.000074
58745.757595	67.0	0.000135	58918.183559	252.5	0.000346	59414.542365	786.5	0.000176	59687.818786	1080.5	0.000183
58746.222938	67.5	0.000298	58918.648370	253.0	0.000142	59415.007453	787.0	0.000079	59688.283379	1081.0	0.000090
58746.687507	68.0	0.000204	58919.113246	253.5	0.000352	59415.472668	787.5	0.000182	59688.747867	1081.5	0.000161

Table B4. (continued)

BJD -2 400 000	Cycle no.	std. dev. (d)	BJD -2 400 000	Cycle no.	std. dev. (d)	BJD -2 400 000	Cycle no.	std. dev. (d)	BJD -2 400 000	Cycle no.	std. dev. (d)
58747.152757	68.5	0.000309	58919.578223	254.0	0.000177	59415.937026	788.0	0.000069	59689.212598	1082.0	0.000094
58747.617051	69.0	0.000127	58920.042914	254.5	0.000309	59416.401202	788.5	0.000170	59689.677076	1082.5	0.000162
58748.082377	69.5	0.000295	58920.507708	255.0	0.000208	59416.866683	789.0	0.000083	59690.142317	1083.0	0.000080
58748.546142	70.0	0.000164	58920.972518	255.5	0.000334	59417.331430	789.5	0.000157	59690.607204	1083.5	0.000174
58749.011152	70.5	0.000292	58921.437214	256.0	0.000219	59417.796065	790.0	0.000082	59691.071731	1084.0	0.000078
58749.476297	71.0	0.000145	58921.901623	256.5	0.000244	59418.260822	790.5	0.000161	59693.395860	1086.5	0.000153
58749.941383	71.5	0.000376	58922.366977	257.0	0.000166	59418.725381	791.0	0.000081	59693.859289	1087.0	0.000114
58751.800341	73.5	0.000393	58922.831785	257.5	0.000349	59420.119722	792.5	0.000219	59694.324725	1087.5	0.000191
58752.265084	74.0	0.000140	58923.296157	258.0	0.000132	59420.584528	793.0	0.000080	59694.789329	1088.0	0.000084
58752.729456	74.5	0.000549	58923.761287	258.5	0.000272	59421.049913	793.5	0.000186	59695.255144	1088.5	0.000164
58753.194779	75.0	0.000139	58924.225943	259.0	0.000150	59421.514347	794.0	0.000090	59695.719313	1089.0	0.000077
58753.658978	75.5	0.000414	58924.690466	259.5	0.000280	59421.979065	794.5	0.000178	59696.183916	1089.5	0.000190
58754.124366	76.0	0.000169	58925.155721	260.0	0.000116	59422.444031	795.0	0.000084	59696.648516	1090.0	0.000096
58754.588290	76.5	0.000262	58925.620560	260.5	0.000268	59422.908511	795.5	0.000157	59697.113738	1090.5	0.000170
58755.053952	77.0	0.000202	58926.084918	261.0	0.000134	59423.373200	796.0	0.000079	59697.577829	1091.0	0.000069
58755.518784	77.5	0.000389	58926.410021	263.5	0.000277	59423.837944	796.5	0.000154	59698.043244	1091.5	0.000181
58755.983272	78.0	0.000149	58928.873616	264.0	0.000153	59424.302864	797.0	0.000090	59698.507517	1092.0	0.000082
58756.447623	78.5	0.000345	58929.338369	264.5	0.000303	59424.767381	797.5	0.000160	59698.972398	1092.5	0.000177
58756.913139	79.0	0.000134	58929.803644	265.0	0.000150	59425.232435	798.0	0.000075	59699.436931	1093.0	0.000085
58757.377375	79.5	0.000372	58930.267767	265.5	0.000301	59425.696965	798.5	0.000164	59699.901957	1093.5	0.000166
58757.842234	80.0	0.000142	58930.732619	266.0	0.000137	59426.161615	799.0	0.000076	59700.366491	1094.0	0.000076
58758.306612	80.5	0.000292	58931.197961	266.5	0.000283	59426.626775	799.5	0.000193	59700.831344	1094.5	0.000159
58758.771994	81.0	0.000176	58931.662487	267.0	0.000144	59427.091187	800.0	0.000081	59701.296003	1095.0	0.000093
58759.235707	81.5	0.000289	58932.127140	267.5	0.000359	59427.556215	800.5	0.000204	59701.760818	1095.5	0.000158
58759.701722	82.0	0.000140	58932.591980	268.0	0.000150	59428.020833	801.0	0.000075	59702.225397	1096.0	0.000082
58760.165808	82.5	0.000411	58933.056765	268.5	0.000350	59428.485630	801.5	0.000180	59702.689960	1096.5	0.000150
58760.631261	83.0	0.000180	58933.521388	269.0	0.000171	59428.950159	802.0	0.000088	59703.154489	1097.0	0.000092
58761.095190	83.5	0.000348	58933.986326	269.5	0.000372	59429.415679	802.5	0.000173	59703.619323	1097.5	0.000157
58761.560943	84.0	0.000155	58934.451255	270.0	0.000126	59429.879550	803.0	0.000088	59704.084083	1098.0	0.000083
58762.024572	84.5	0.000293	58934.915621	270.5	0.000336	59430.344727	803.5	0.000185	59704.549672	1098.5	0.000184
58762.490208	85.0	0.000414	58935.380396	271.0	0.000136	59430.808988	804.0	0.000080	59705.943209	1100.0	0.000092
58762.955053	85.5	0.000328	58935.846259	271.5	0.000324	59431.274524	804.5	0.000186	59706.408083	1100.5	0.000170
58790.840946	115.5	0.000338	58936.310208	272.0	0.000171	59431.738684	805.0	0.000072	59706.872554	1101.0	0.000120
58791.770326	116.5	0.000266	58936.774321	272.5	0.000312	59432.203494	805.5	0.000165	59707.336586	1101.5	0.000181
58792.235281	117.0	0.000151	58937.239619	273.0	0.000151	59434.062703	807.5	0.000171	59707.802161	1102.0	0.000102
58792.700223	117.5	0.000351	58937.704939	273.5	0.000354	59434.527077	808.0	0.000091	59708.266443	1102.5	0.000165
58793.165208	118.0	0.000146	58938.169107	274.0	0.000140	59434.992451	808.5	0.000165	59708.731748	1103.0	0.000085
58793.629442	118.5	0.000273	58938.634248	274.5	0.000317	59435.456443	809.0	0.000077	59709.195698	1103.5	0.000177
58794.094844	119.0	0.000167	58939.098629	275.0	0.000157	59435.921899	809.5	0.000152	59709.660931	1104.0	0.000101
58794.559837	119.5	0.000318	58939.563035	275.5	0.000350	59436.386096	810.0	0.000072	59710.125562	1104.5	0.000180
58795.024323	120.0	0.000154	58940.028393	276.0	0.000176	59436.851114	810.5	0.000159	59710.590181	1105.0	0.000087
58795.488943	120.5	0.000307	58940.492957	276.5	0.000315	59437.315668	811.0	0.000091	59711.054656	1105.5	0.000174
58795.953634	121.0	0.000143	58941.886750	278.0	0.000146	59437.781235	811.5	0.000179	59711.519745	1106.0	0.000093
58796.418514	121.5	0.000392	58942.353207	278.5	0.000409	59438.245154	812.0	0.000084	59711.983762	1106.5	0.000161
58796.883466	122.0	0.000132	58942.817145	279.0	0.000183	59438.710422	812.5	0.000165	59712.449072	1107.0	0.000086
58797.347793	122.5	0.000426	58943.281235	279.5	0.000264	59439.174917	813.0	0.000084	59712.913537	1107.5	0.000153
58797.813238	123.0	0.000129	58943.746624	280.0	0.000146	59439.639739	813.5	0.000176	59713.378738	1108.0	0.000072
58798.277577	123.5	0.000259	58944.210575	280.5	0.000444	59440.104166	814.0	0.000113	59713.843809	1108.5	0.000135
58798.742638	124.0	0.000132	58944.676041	281.0	0.000155	59440.569643	814.5	0.000181	59714.307984	1109.0	0.000085
58799.207127	124.5	0.000329	58945.141066	281.5	0.000343	59441.033787	815.0	0.000076	59714.772277	1109.5	0.000154
58799.672110	125.0	0.000140	58945.605350	282.0	0.000175	59441.499220	815.5	0.000146	59715.237453	1110.0	0.000087
58800.136961	125.5	0.000323	58946.069972	282.5	0.000316	59441.963422	816.0	0.000095	59715.701893	1110.5	0.000164
58800.601568	126.0	0.000194	58946.535213	283.0	0.000142	59442.428648	816.5	0.000190	59716.166853	1111.0	0.000085
58801.066656	126.5	0.000858	58946.999846	283.5	0.000359	59442.893012	817.0	0.000081	59716.631455	1111.5	0.000177
58801.531568	127.0	0.000130	58947.464648	284.0	0.000152	59443.358209	817.5	0.000161	59717.096102	1112.0	0.000077
58801.996297	127.5	0.000300	58947.929005	284.5	0.000311	59443.822531	818.0	0.000080	59718.954906	1114.0	0.000093
58803.855321	129.5	0.000350	58948.394158	285.0	0.000245	59444.287555	818.5	0.000152	59719.420126	1114.5	0.000160
58804.319611	130.0	0.000145	58948.858382	285.5	0.000288	59444.752170	819.0	0.000086	59719.884301	1115.0	0.000084
58804.784801	130.5	0.000313	58949.323540	286.0	0.000122	59445.217589	819.5	0.000174	59720.349552	1115.5	0.000173
58805.249580	131.0	0.000174	58949.788730	286.5	0.000263	59445.681834	820.0	0.000081	59720.813670	1116.0	0.000081
58805.714211	131.5	0.000298	58950.253038	287.0	0.000163	59446.146895	820.5	0.000172	59721.278643	1116.5	0.000163
58806.178900	132.0	0.000143	58950.717966	287.5	0.000366	59579.994722	964.5	0.000227	59721.743541	1117.0	0.000071
58806.643627	132.5	0.000330	58951.182942	288.0	0.000143	59580.458674	965.0	0.000095	59722.208644	1117.5	0.000170
58807.108638	133.0	0.000127	58951.647352	288.5	0.000346	59580.923441	965.5	0.000216	59722.672860	1118.0	0.000075
58807.573416	133.5	0.000274	58952.112170	289.0	0.000172	59581.388528	966.0	0.000098	59723.137340	1118.5	0.000149
58808.038474	134.0	0.000180	58952.577171	289.5	0.000396	59581.853094	966.5	0.000177	59723.602370	1119.0	0.000087
58808.503041	134.5	0.000288	58953.041862	290.0	0.000276	59582.317807	967.0	0.000090	59724.067214	1119.5	0.000168
58808.967621	135.0	0.000140	58953.506019	290.5	0.000538	59582.782463	967.5	0.000165	59724.531975	1120.0	0.000095
58809.432527	135.5	0.000321	58953.971642	291.0	0.000158	59583.247320	968.0	0.000088	59724.995977	1120.5	0.000166
58809.897305	136.0	0.000167	58954.436615	291.5	0.000321	59583.712122	968.5	0.000158	59725.461346	1121.0	0.000076

**Table B4.** (*continued*)

BJD −2 400 000	Cycle no.	std. dev. ( <i>d</i> )	BJD −2 400 000	Cycle no.	std. dev. ( <i>d</i> )	BJD −2 400 000	Cycle no.	std. dev. ( <i>d</i> )	BJD −2 400 000	Cycle no.	std. dev. ( <i>d</i> )
58810.361726	136.5	0.000299	58955.829846	293.0	0.000412	59584.176809	969.0	0.000081	59725.926160	1121.5	0.000155
58810.826899	137.0	0.000128	58956.294921	293.5	0.000306	59584.641670	969.5	0.000185	59726.390665	1122.0	0.000088
58811.291215	137.5	0.000303	58956.759920	294.0	0.000163	59585.106526	970.0	0.000094	59726.855468	1122.5	0.000145
58811.756001	138.0	0.000157	58957.225011	294.5	0.000307	59585.571290	970.5	0.000157	59727.320292	1123.0	0.000075
58812.220792	138.5	0.000297	58957.689301	295.0	0.000197	59586.035968	971.0	0.000086	59727.784840	1123.5	0.000154
58812.685948	139.0	0.000120	58958.154654	295.5	0.000298	59586.500395	971.5	0.000185	59728.249580	1124.0	0.000076
58813.150626	139.5	0.000335	58958.619158	296.0	0.000131	59586.965929	972.0	0.000100	59728.714362	1124.5	0.000185
58813.615513	140.0	0.000156	58959.084043	296.5	0.000358	59587.429827	972.5	0.000200	59729.179143	1125.0	0.000099
58814.080331	140.5	0.000288	58959.548466	297.0	0.000217	59587.895326	973.0	0.000097	59729.643992	1125.5	0.000165
58814.544779	141.0	0.000152	58960.013337	297.5	0.000319	59588.360138	973.5	0.000173	59730.108829	1126.0	0.000091
58815.006787	141.5	0.001016	58960.477862	298.0	0.000184	59588.824821	974.0	0.000099	59731.502645	1127.5	0.000181
58816.404139	143.0	0.000110	58960.943341	298.5	0.000285	59589.289546	974.5	0.000153	59732.897202	1129.0	0.000096
58816.868897	143.5	0.000337	58961.407495	299.0	0.000214	59589.754257	975.0	0.000095	59733.361725	1129.5	0.000184
58817.333770	144.0	0.000163	58961.873270	299.5	0.000373	59590.219210	975.5	0.000174	59733.826898	1130.0	0.000088
58817.798050	144.5	0.000338	58962.336915	300.0	0.000143	59590.684055	976.0	0.000084	59734.290282	1130.5	0.000170
58818.263237	145.0	0.000150	58962.802153	300.5	0.000299	59591.148586	976.5	0.000175	59734.756156	1131.0	0.000080
58818.728040	145.5	0.000269	58963.266616	301.0	0.000363	59591.613691	977.0	0.000094	59735.220649	1131.5	0.000167
58819.192914	146.0	0.000158	58963.731241	301.5	0.000290	59592.077947	977.5	0.000187	59735.685809	1132.0	0.000085
58819.657210	146.5	0.000351	58964.195805	302.0	0.000154	59592.543008	978.0	0.000093	59736.150741	1132.5	0.000197
58820.122614	147.0	0.000205	58964.662377	302.5	0.000341	59593.937666	979.5	0.000261	59736.615145	1133.0	0.000085
58820.586616	147.5	0.000272	58965.125508	303.0	0.000440	59594.401841	980.0	0.000083	59737.079525	1133.5	0.000150
58821.051934	148.0	0.000126	58965.590662	303.5	0.000343	59594.867641	980.5	0.000238	59737.544619	1134.0	0.000083
58821.516489	148.5	0.000279	58966.055235	304.0	0.000132	59595.332010	981.0	0.000099	59738.009380	1134.5	0.000181
58821.981600	149.0	0.000152	58966.520625	304.5	0.000403	59595.795706	981.5	0.000158	59738.474183	1135.0	0.000074
58822.404623	149.5	0.000308	58966.984309	305.0	0.000127	59596.261101	982.0	0.000096	59738.938965	1135.5	0.000148
58822.911390	150.0	0.000196	58967.450271	305.5	0.000320	59596.725458	982.5	0.000178	59739.403834	1136.0	0.000079
58823.375485	150.5	0.000369	58967.914184	306.0	0.000175	59597.190941	983.0	0.000080	59739.868770	1136.5	0.000178
58823.840755	151.0	0.000152	58969.309846	307.5	0.000389	59597.654937	983.5	0.000172	59740.333323	1137.0	0.000075
58824.304936	151.5	0.000299	58969.773225	308.0	0.000163	59598.120563	984.0	0.000087	59740.798091	1137.5	0.000166
58824.770186	152.0	0.000164	58970.238887	308.5	0.000269	59598.584474	984.5	0.000183	59741.262677	1138.0	0.000084
58825.234229	152.5	0.000320	58970.702972	309.0	0.000172	59599.050122	985.0	0.000096	59741.727675	1138.5	0.000182
58825.699820	153.0	0.000141	58971.167828	309.5	0.000319	59599.513998	985.5	0.000182	59742.192307	1139.0	0.000093
58826.164676	153.5	0.000415	58971.632549	310.0	0.000148	59599.979669	986.0	0.000096	59742.657266	1139.5	0.000156
58826.628999	154.0	0.000138	58972.098022	310.5	0.000382	59600.444246	986.5	0.000342	59743.051467	1141.0	0.000086
58827.093354	154.5	0.000313	58972.562352	311.0	0.000125	59600.909022	987.0	0.000099	59744.516337	1141.5	0.000164
58827.559013	155.0	0.000185	58973.027598	311.5	0.000343	59601.373208	987.5	0.000169	59744.980830	1142.0	0.000085
58829.417583	157.0	0.000182	58973.492186	312.0	0.000143	59601.838654	988.0	0.000085	59745.445394	1142.5	0.000172
58829.882301	157.5	0.000403	58973.957346	312.5	0.000318	59602.302689	988.5	0.000189	59745.910378	1143.0	0.000079
58830.347397	158.0	0.000192	58974.421816	313.0	0.000148	59602.768310	989.0	0.000090	59746.374995	1143.5	0.000174
58830.812253	158.5	0.000328	58974.886224	313.5	0.000308	59603.232341	989.5	0.000171	59746.840070	1144.0	0.000090
58831.276449	159.0	0.000156	58975.351475	314.0	0.000182	59603.697908	990.0	0.000090	59747.304989	1144.5	0.000170
58831.741656	159.5	0.000287	58975.815960	314.5	0.000316	59604.161924	990.5	0.000171	59747.769381	1145.0	0.000088
58832.206182	160.0	0.000183	58976.280834	315.0	0.000138	59604.627352	991.0	0.000090	59748.234294	1145.5	0.000164
58832.670054	160.5	0.000323	58976.745773	315.5	0.000322	59605.091242	991.5	0.000163	59748.698896	1146.0	0.000089
58833.135739	161.0	0.000120	58977.210339	316.0	0.000136	59605.556832	992.0	0.000077	59749.163497	1146.5	0.000168
58833.600052	161.5	0.000358	58977.674824	316.5	0.000333	59606.020620	992.5	0.000199	59749.628829	1147.0	0.000065
58834.065223	162.0	0.000139	58978.140238	317.0	0.000160	59606.486345	993.0	0.000079	59750.093261	1147.5	0.000171
58834.529644	162.5	0.000296	58978.604446	317.5	0.000348	59608.345563	995.0	0.000096	59750.558357	1148.0	0.000084
58834.994566	163.0	0.000211	58979.069804	318.0	0.000140	59608.810053	995.5	0.000178	59751.022384	1148.5	0.000152
58835.458987	163.5	0.000403	58979.534737	318.5	0.000333	59609.275281	996.0	0.000095	59751.487762	1149.0	0.000085
58835.924136	164.0	0.000139	58979.999443	319.0	0.000137	59609.739188	996.5	0.000195	59751.952242	1149.5	0.000150
58836.388578	164.5	0.000279	58980.463685	319.5	0.000365	59610.204327	997.0	0.000110	59752.417267	1150.0	0.000088
58836.853657	165.0	0.000165	58980.928918	320.0	0.000240	59610.668757	997.5	0.000170	59752.881371	1150.5	0.000138
58837.318481	165.5	0.000327	58981.392902	320.5	0.000313	59611.134242	998.0	0.000086	59753.347027	1151.0	0.000083
58837.783407	166.0	0.000133	58981.858199	321.0	0.000136	59611.598104	998.5	0.000197	59753.811258	1151.5	0.000173
58838.248228	166.5	0.000301	58983.717505	323.0	0.000122	59612.063719	999.0	0.000090	59754.276671	1152.0	0.000080
58838.712562	167.0	0.000199	58984.182261	323.5	0.000280	59612.528228	999.5	0.000183	59754.740839	1152.5	0.000163
58839.177280	167.5	0.000284	58984.646741	324.0	0.000143	59612.993322	1000.0	0.000097	59755.206403	1153.0	0.000082
58839.642381	168.0	0.000196	58985.111532	324.5	0.000357	59613.457247	1000.5	0.000168	59755.670282	1153.5	0.000181
58840.107112	168.5	0.000485	58985.576607	325.0	0.000165	59613.922570	1001.0	0.000101	59757.065375	1155.0	0.000085
58840.571684	169.0	0.000196	58986.040768	325.5	0.000485	59614.386664	1001.5	0.000163	59757.529707	1155.5	0.000169
58841.035943	169.5	0.001274	58986.505971	326.0	0.000143	59614.852332	1002.0	0.000131	59757.994835	1156.0	0.000079
58842.895409	171.5	0.000296	58986.970941	326.5	0.000319	59615.316437	1002.5	0.000185	59758.459575	1156.5	0.000191
58843.360215	172.0	0.000155	58987.435476	327.0	0.000157	59615.781826	1003.0	0.000088	59758.924039	1157.0	0.000099
58843.825435	172.5	0.000347	58987.900502	327.5	0.000313	59616.246100	1003.5	0.000169	59759.388269	1157.5	0.000173
58844.290089	173.0	0.000172	58988.364997	328.0	0.000140	59616.711347	1004.0	0.000087	59759.853707	1158.0	0.000078
58844.754777	173.5	0.000298	58988.829870	328.5	0.000296	59617.175534	1004.5	0.000158	59760.318411	1158.5	0.000133
58845.219356	174.0	0.000141	58989.294206	329.0	0.000129	59617.641101	1005.0	0.000090	59760.783188	1159.0	0.000078
58845.684149	174.5	0.000322	58989.758984	329.5	0.000306	59618.105164	1005.5	0.000186	59761.247556	1159.5	0.000171



**Table B4.** (continued)

BJD −2 400 000	Cycle no.	std. dev. ( <i>d</i> )	BJD −2 400 000	Cycle no.	std. dev. ( <i>d</i> )	BJD −2 400 000	Cycle no.	std. dev. ( <i>d</i> )	BJD −2 400 000	Cycle no.	std. dev. ( <i>d</i> )
58846.148886	175.0	0.000144	58990.224015	330.0	0.000147	59618.570653	1006.0	0.000078	59761.712551	1160.0	0.000082
58846.614054	175.5	0.000279	58990.688828	330.5	0.000299	59619.034741	1006.5	0.000167	59762.176882	1160.5	0.000147
58847.078816	176.0	0.000154	58991.153144	331.0	0.000134	59619.500094	1007.0	0.000088	59762.642524	1161.0	0.000087
58847.543469	176.5	0.000284	58991.618479	331.5	0.000336	59619.964014	1007.5	0.000178	59763.106835	1161.5	0.000159
58848.007966	177.0	0.000144	58992.082865	332.0	0.000149	59620.429869	1008.0	0.000100	59763.571985	1162.0	0.000082
58848.472845	177.5	0.000276	58992.548056	332.5	0.000298	59620.893937	1008.5	0.000174	59764.036271	1162.5	0.000159
58848.937516	178.0	0.000152	58993.012384	333.0	0.000117	59621.359206	1009.0	0.000080	59764.501228	1163.0	0.000085
58849.401986	178.5	0.000324	58993.477486	333.5	0.000360	59623.217697	1011.0	0.000117	59764.965570	1163.5	0.000168
58849.867241	179.0	0.000137	58993.941821	334.0	0.000141	59623.681692	1011.5	0.000195	59765.430767	1164.0	0.000104
58850.331560	179.5	0.000328	58994.406908	334.5	0.000282	59624.147736	1012.0	0.000102	59765.895220	1164.5	0.000183
58850.796550	180.0	0.000134	58994.871810	335.0	0.000165	59624.612557	1012.5	0.000207	59766.360333	1165.0	0.000094
58851.261464	180.5	0.000344	58995.336468	335.5	0.000312	59625.077145	1013.0	0.000098	59766.824977	1165.5	0.000148
58851.726375	181.0	0.000186	58997.195537	337.5	0.000301	59625.541357	1013.5	0.000169	59767.289846	1166.0	0.000082
58852.190616	181.5	0.000332	58997.660330	338.0	0.000151	59626.007047	1014.0	0.000098	59767.754194	1166.5	0.000164
58852.655777	182.0	0.000140	58998.125360	338.5	0.000392	59626.470962	1014.5	0.000169	59768.219275	1167.0	0.000083
58853.120594	182.5	0.000272	58998.589556	339.0	0.000151	59626.936538	1015.0	0.000088	59768.684300	1167.5	0.000150
58853.585197	183.0	0.000130									

*Notes.* Integer and half-integer cycle numbers refer to primary and secondary eclipses, respectively. All eclipses were observed by the *TESS* spacecraft.

**Table B5.** Times of minima of TIC 276162169 (V493 Cyg)

BJD −2 400 000	Cycle no.	std. dev. ( <i>d</i> )	BJD −2 400 000	Cycle no.	std. dev. ( <i>d</i> )	BJD −2 400 000	Cycle no.	std. dev. ( <i>d</i> )	BJD −2 400 000	Cycle no.	std. dev. ( <i>d</i> )
58684.246260	−0.5	0.000252	58721.222486	14.0	0.000070	59439.097560	295.5	0.000042	59796.122515	435.5	0.000190
58685.521975	0.0	0.000245	58722.496413	14.5	0.000066	59440.373326	296.0	0.000039	59797.399406	436.0	0.000049
58686.796686	0.5	0.000260	58723.772578	15.0	0.000050	59441.648017	296.5	0.000048	59798.673885	436.5	0.000058
58688.072057	1.0	0.000255	58726.322720	16.0	0.000043	59442.923824	297.0	0.000039	59799.949733	437.0	0.000042
58689.346606	1.5	0.000279	58727.596846	16.5	0.000054	59444.198456	297.5	0.000044	59801.224408	437.5	0.000052
58690.622134	2.0	0.000232	58728.873088	17.0	0.000045	59445.474552	298.0	0.000040	59802.500610	438.0	0.000047
58691.896372	2.5	0.000329	58730.147159	17.5	0.000058	59770.620162	425.5	0.000054	59803.775194	438.5	0.000057
58693.172910	3.0	0.000786	58731.423442	18.0	0.000045	59771.896049	426.0	0.000046	59805.051287	439.0	0.000048
58694.446190	3.5	0.000242	58732.697548	18.5	0.000047	59773.170211	426.5	0.000057	59806.326074	439.5	0.000058
58695.721825	4.0	0.000127	58733.973791	19.0	0.000047	59774.446166	427.0	0.000056	59807.601840	440.0	0.000062
58698.271997	5.0	0.000357	58735.247791	19.5	0.000064	59775.720333	427.5	0.000076	59808.876523	440.5	0.000071
58699.545816	5.5	0.000413	58736.523853	20.0	0.000060	59776.996336	428.0	0.000067	59811.427078	441.5	0.000053
58700.821887	6.0	0.000367	59421.245577	288.5	0.000043	59778.270630	428.5	0.000079	59813.977505	442.5	0.000055
58702.096028	6.5	0.000383	59422.521459	289.0	0.000038	59779.546852	429.0	0.000063	59815.253714	443.0	0.000046
58703.371706	7.0	0.000336	59423.795865	289.5	0.000047	59780.820694	429.5	0.000068	59816.527922	443.5	0.000059
58704.646153	7.5	0.000422	59425.071591	290.0	0.000042	59782.096838	430.0	0.000044	59817.804014	444.0	0.000047
58705.921531	8.0	0.000379	59426.345606	290.5	0.000056	59784.647053	431.0	0.000048	59819.078409	444.5	0.000057
58708.471911	9.0	0.000348	59427.621758	291.0	0.000039	59785.921327	431.5	0.000057	59820.354339	445.0	0.000050
58712.296127	10.5	0.000049	59428.895964	291.5	0.000051	59787.197301	432.0	0.000058	59821.628695	445.5	0.000068
58713.571914	11.0	0.000045	59430.172057	292.0	0.000047	59788.471901	432.5	0.000057	59822.904634	446.0	0.000063
58714.846269	11.5	0.000045	59431.446258	292.5	0.000050	59789.747656	433.0	0.000054	59824.179055	446.5	0.000057
58716.122039	12.0	0.000044	59433.996471	293.5	0.000047	59791.023192	433.5	0.000078	59866.254835	463.0	0.000046
58717.396367	12.5	0.000049	59435.272691	294.0	0.000039	59792.298011	434.0	0.000063	59880.278425	468.5	0.000024
58718.672228	13.0	0.000044	59436.547035	294.5	0.000045	59793.573119	434.5	0.000075	59894.304800	474.0	0.000046
58719.946266	13.5	0.000061	59437.822915	295.0	0.000046	59794.848777	435.0	0.000053			

*Notes.* Integer and half-integer cycle numbers refer to primary and secondary eclipses, respectively. Most of the eclipses (cycle nos. −0.5 to 446.5) were observed by the *TESS* spacecraft. The last 3 times of minima were determined from the ground-based GAO80 observations.

**Table B6.** Times of minima of TIC 280883908

BJD −2 400 000	Cycle no.	std. dev. ( <i>d</i> )	BJD −2 400 000	Cycle no.	std. dev. ( <i>d</i> )	BJD −2 400 000	Cycle no.	std. dev. ( <i>d</i> )	BJD −2 400 000	Cycle no.	std. dev. ( <i>d</i> )
58984.913027	0.0	0.000211	59005.904767	4.0	0.000115	59029.532528	8.5	0.000130	59737.995390	143.5	0.000109
58987.539927	0.5	0.000185	59008.531699	4.5	0.000194	59032.154316	9.0	0.000119	59740.617096	144.0	0.000083
58990.160151	1.0	0.000139	59013.781797	5.5	0.000122	59034.782130	9.5	0.000204	59745.865507	145.0	0.000154
58992.785349	1.5	0.000183	59016.403673	6.0	0.000445	59719.626354	140.0	0.000130	59753.742490	146.5	0.000098
58995.408270	2.0	0.000516	59019.031229	6.5	0.000167	59724.873615	141.0	0.000113	59758.993159	147.5	0.000169
58998.034108	2.5	0.000141	59021.655780	7.0	0.000180	59727.499237	141.5	0.000112	59761.616627	148.0	0.000084
59000.656182	3.0	0.000226	59024.283264	7.5	0.000126	59730.120787	142.0	0.002262	59764.245467	148.5	0.000086
59003.283139	3.5	0.000161	59026.905888	8.0	0.000111	59732.748670	142.5	0.000102	59766.867410	149.0	0.000131

*Notes.* Integer and half-integer cycle numbers refer to primary and secondary eclipses, respectively. All eclipses were observed by the *TESS* spacecraft.

**Table B7.** Times of minima of TIC 294803663

BJD	Cycle	std. dev.	BJD	Cycle	std. dev.	BJD	Cycle	std. dev.	BJD	Cycle	std. dev.
−2 400 000	no.	( <i>d</i> )	−2 400 000	no.	( <i>d</i> )	−2 400 000	no.	( <i>d</i> )	−2 400 000	no.	( <i>d</i> )
58597.414393	−0.5	0.001380	58625.464654	12.0	0.000234	59335.199971	328.0	0.000101	59363.308963	340.5	0.000133
58598.511084	0.0	0.000176	58626.612731	12.5	0.000692	59336.353685	328.5	0.000152	59364.399049	341.0	0.000118
58599.661625	0.5	0.000177	58631.108275	14.5	0.000558	59337.443872	329.0	0.000123	59365.554127	341.5	0.000121
58600.759152	1.0	0.000139	58632.204460	15.0	0.000151	59338.600152	329.5	0.000172	59366.646276	342.0	0.000107
58601.907966	1.5	0.000195	58633.353822	15.5	0.000158	59339.690501	330.0	0.000125	59367.800004	342.5	0.000142
58603.004370	2.0	0.000139	58634.448397	16.0	0.000126	59340.844364	330.5	0.000139	59368.891494	343.0	0.000099
58604.152984	2.5	0.000139	58635.598404	16.5	0.000209	59341.935676	331.0	0.000121	59370.047498	343.5	0.000105
58605.249805	3.0	0.000114	58636.695135	17.0	0.000156	59343.091402	331.5	0.000087	59371.138692	344.0	0.000134
58606.399068	3.5	0.000242	58637.845455	17.5	0.000360	59344.183918	332.0	0.000115	59372.293512	344.5	0.000167
58607.496170	4.0	0.000150	58638.941600	18.0	0.000206	59345.338799	332.5	0.000143	59373.383529	345.0	0.000109
58608.646775	4.5	0.000144	58640.091241	18.5	0.000383	59347.585596	333.5	0.000270	59374.540571	345.5	0.000234
58610.891000	5.5	0.000148	58641.188383	19.0	0.000175	59348.674849	334.0	0.000128	59376.785552	346.5	0.000115
58611.990011	6.0	0.000304	58642.337527	19.5	0.000163	59349.830924	334.5	0.000120	59377.877238	347.0	0.000116
58613.138280	6.5	0.000211	58643.432768	20.0	0.000157	59350.921283	335.0	0.000080	59379.033582	347.5	0.000160
58614.234845	7.0	0.000179	58644.582594	20.5	0.000205	59352.075295	335.5	0.000196	59380.122686	348.0	0.000115
58615.382708	7.5	0.000185	58645.677438	21.0	0.000144	59353.168594	336.0	0.000109	59381.278452	348.5	0.000139
58616.480841	8.0	0.000165	58646.825974	21.5	0.000184	59354.324010	336.5	0.000136	59382.367967	349.0	0.000160
58617.630118	8.5	0.000249	58647.924020	22.0	0.000141	59355.415197	337.0	0.000106	59383.524952	349.5	0.000111
58618.727750	9.0	0.000182	58649.074155	22.5	0.000170	59356.569697	337.5	0.000115	59384.614958	350.0	0.000096
58619.876500	9.5	0.000117	58650.170879	23.0	0.000189	59357.660118	338.0	0.000113	59385.770147	350.5	0.000136
58620.973331	10.0	0.000124	58651.321775	23.5	0.000315	59358.818093	338.5	0.000200	59386.861686	351.0	0.000098
58622.122384	10.5	0.000176	58652.416886	24.0	0.000153	59359.907325	339.0	0.000077	59388.016386	351.5	0.000184
58623.217947	11.0	0.000152	59334.109840	327.5	0.000300	59362.152512	340.0	0.000114	59389.106938	352.0	0.000118

*Notes.* Integer and half-integer cycle numbers refer to primary and secondary eclipses, respectively. All eclipses were observed by the *TESS* spacecraft.

**Table B8.** Times of minima of TIC 332521671

BJD	Cycle	std. dev.	BJD	Cycle	std. dev.	BJD	Cycle	std. dev.	BJD	Cycle	std. dev.
−2 400 000	no.	( <i>d</i> )	−2 400 000	no.	( <i>d</i> )	−2 400 000	no.	( <i>d</i> )	−2 400 000	no.	( <i>d</i> )
58571.351631	0.0	0.000622	58585.069584	11.0	0.000222	59307.792721	590.5	0.000260	59322.135649	602.0	0.000194
58571.975838	0.5	0.000425	58585.693745	11.5	0.000435	59308.415519	591.0	0.000166	59322.759532	602.5	0.000309
58572.598164	1.0	0.001552	58586.316751	12.0	0.000219	59309.038454	591.5	0.000211	59323.382946	603.0	0.000199
58573.222659	1.5	0.000853	58586.941261	12.5	0.000305	59309.662771	592.0	0.000161	59324.006946	603.5	0.000272
58573.845601	2.0	0.000566	58587.564477	13.0	0.000462	59312.157410	594.0	0.000156	59324.630096	604.0	0.000198
58574.468385	2.5	0.000672	58588.188971	13.5	0.000476	59312.781035	594.5	0.000154	59325.253236	604.5	0.000263
58575.091272	3.0	0.000546	58588.811087	14.0	0.000410	59313.404621	595.0	0.000143	59325.877443	605.0	0.000205
58575.715892	3.5	0.000501	58589.435507	14.5	0.000545	59314.029562	595.5	0.000184	59326.501064	605.5	0.000386
58576.339810	4.0	0.000222	58590.058024	15.0	0.000608	59314.651956	596.0	0.000146	59327.124807	606.0	0.000195
58576.963020	4.5	0.000494	58590.684609	15.5	0.000988	59315.275733	596.5	0.000189	59327.747916	606.5	0.000295
58577.586810	5.0	0.000228	58591.305798	16.0	0.000727	59315.898475	597.0	0.000169	59328.372530	607.0	0.000188
58578.210367	5.5	0.000288	58591.931201	16.5	0.000520	59316.523146	597.5	0.000224	59328.996838	607.5	0.000240
58578.833296	6.0	0.000404	58592.551918	17.0	0.000459	59317.145740	598.0	0.000159	59329.619213	608.0	0.000227
58579.457494	6.5	0.000289	58593.177603	17.5	0.001006	59317.771546	598.5	0.000169	59330.243983	608.5	0.000280
58580.081628	7.0	0.000684	58593.799764	18.0	0.000369	59318.392716	599.0	0.000144	59330.866206	609.0	0.000178
58580.706401	7.5	0.000744	58594.423612	18.5	0.000395	59320.887888	601.0	0.000222	59331.490457	609.5	0.000246
58581.327611	8.0	0.000715	58595.047571	19.0	0.000251	59321.511843	601.5	0.000258	59332.113758	610.0	0.000165

*Notes.* Integer and half-integer cycle numbers refer to primary and secondary eclipses, respectively. All eclipses were observed by the *TESS* spacecraft.

**Table B9.** Times of minima of TIC 356324779

BJD	Cycle	std. dev.	BJD	Cycle	std. dev.	BJD	Cycle	std. dev.	BJD	Cycle	std. dev.
−2 400 000	no.	( <i>d</i> )	−2 400 000	no.	( <i>d</i> )	−2 400 000	no.	( <i>d</i> )	−2 400 000	no.	( <i>d</i> )
58817.450745	−0.5	0.000204	58826.139648	2.0	0.000254	58834.832035	4.5	0.000417	59542.378549	208.0	0.000066
58819.188471	0.0	0.000287	58827.878404	2.5	0.000463	58836.570878	5.0	0.000577	59587.572095	221.0	0.000059
58820.925547	0.5	0.000243	58829.615688	3.0	0.000493	58838.311296	5.5	0.000534	59596.260941	223.5	0.000063
58822.664508	1.0	0.000233	58831.354344	3.5	0.000496	58840.050670	6.0	0.000582	59615.378465	229.0	0.000084
58824.402098	1.5	0.000229	58833.093073	4.0	0.000516	59535.414985	206.0	0.000074	59662.328637	242.5	0.000111

*Notes.* Integer and half-integer cycle numbers refer to primary and secondary eclipses, respectively. Most of the eclipses (cycle nos. −0.5 to 6.0) were observed by the *TESS* spacecraft. The last 6 times of minima were determined from the ground-based BAO80 (nos. 206, 242.5) and GAO80 (nos. 208 to 229) observations.